Inaugural dissertation

for

obtaining the doctoral degree

of the

Combined Faculty of Mathematics, Engineering and Natural Sciences

of the

Ruprecht - Karls - University

Heidelberg

Presented by

M.Sc. Nora Jamaladdin

Born in: Ras Alain, Syria

Oral examination: 21.11.2023

The role of key pharmacodynamic and pharmacokinetic parameters in drug response prediction of pediatric tumors in the precision oncology study INFORM

Referees: Prof. Dr. Thomas Höfer

Prof. Dr. med. Till Milde

For my parents and brother

"There is no great discoveries and advances,
as long as there is an unhappy child on earth."

— Albert Einstein

Acknowledgements

I consider myself fortunate to have met and learned from such exceptional individuals during my PhD and I would like to express my sincere gratitude to everyone who has been part of my PhD journey.

Prof. Dr. Med. Olaf Witt for giving me the opportunity to do my PhD at the CCU Pediatric Oncology department. Under your leadership, I felt supported and encouraged in a scientific environment that fosters collaboration and growth. Thank you for challenging me and always reminding me to regain focus on the translational potential of my project.

My supervisor **Prof. Dr. Med. Till Milde** for giving me the space to advance both in my scientific persuit as well as my personal development. Words fail to express how much I have learned under your leadership. The moments of laughter and humor will always be special memories for me and I want to genuinely thank you for everything.

I wish to extend my appreciation to the members of my thesis advisory committee (TAC), for their time, effort and valuable feedback. **Prof. Höfer,** thank you for agreeing to be my first examiner, **Dr. Claudia Ball** and **Dr. Roman Tremmel** thank you for your support and fruitful discussions during the TAC meetings.

I would also like to thank **Prof. Dr. Wölfl** and **Prof. Dr. Med. Haefeli** for accepting to be part of my thesis examination committee.

I would like to express special thanks to **Apl. Prof. Dr. Tim Holland Letz** for his feedback and invaluable scientific expertise regarding mathematics and statistics thoughout my PhD. I would also like to thank you for our fun discussions about books, politics and life before we delved into the scientific part of our meeting.

PD Dr. Cornelis van Tilburg, thank you for inspiring me and introducing me to the CCU Pediatric Oncology department.

Though I did most of my PhD during corona and in home office, the B310 research colleagues have been an invaluable aspect of my PhD journey. I would like to thank **PD Dr. Ina Oehme** and **Dr. Heike Peterziel** for their constructive criticism and for always keeping their door open for questions and feedback. **Dr. Romain Sigaud** for his unique and natural ability to inspire and encourage. I will not forget how R programming errors could only be fun during our meetings. I would also like to thank Daniela, Anna, Jonas, Florian, Leo, Isabel, Carina, Simon, Simay, Sara, Sonja, Marta, Coco, Clarissa, Aileen, Alexandra,Till S., Nicola and Natja for the positive influence you had on my PhD journey, each as such remarkable individuals.

I want to express my deepest gratitude to **Dr. Helke Hillebrand** who has been an inspiration in her aim to provide the PhD students at Heidelberg University with everything they need to make the most of their talents and live their dreams towards entering ambitious and responsible careers. Thank you for taking the time to share your journey with me.

Finally, I want to thank my parents and brother**, Maram, Hassan and Beriar** for their unwavering belief in me during my most vulnerable moments and for their unconditional love and support which has enabled me to grow into the woman I am today. **Dr. Friedrich Rippmann**, thank you for being the best mentor I could wish for. It is remarkable how our discussions and your advice have always reminded me that the world is my oyster, especially in the face of adversity. I also want to express my heartfelt appreciation to the amazing people I met in Heidelberg: **Sona, Ma-Lou, Mira, Philipp, Dan, Taviked, Mike and Iska** who have truly made my time here unforgettable. Our shared love for sports, delicious food, music, dancing, and most importantly our ambition to have a transformative impact in the world, led to wonderful friendships, all in their unique ways, that I deeply treasure.

Submission of my PhD thesis was made possible because of the constant support and encouragement from all these wonderful people.

Summary

The first results of the German pediatric precision oncology program INdividualized Therapy FOr Relapsed Malignancies in Childhood (INFORM) showed the significance of high evidence levels for successfully matched targeted therapy based solely on molecular diagnostics. Yet, only a small number of patients (8%, 42/519) (1) actually present with a high evidence target, highlighting an unmet need to improve drug response predictions and clinical treatment recommendations. Therefore, the aim of this thesis is to integrate pharmacodynamic (PD) parameters from Drug Sensitivity Profiling (DSP) with pharmacokinetic (PK) parameters, and improve drug response prediction in high risk pediatric patients.

To achieve this aim, a literature review was conducted, and nine PK parameters focused on the pediatric population were collected for the drugs from the DSP drug library in the INFORM study. In addition, a database of primary patient tumor (PPT) samples (n=68) and a database of positive control cell (PCC) line models (n=7) were generated. The PCC models habor a specific molecular alteration (e.g., BRAF V600E, NTRK fusion) with a clinically proven drug-target relationship. Among the 68 PPT samples, five samples (PPT subgroup I) harbored a very high priorty (INFORM priorty score 1) alteration with a clinically proven drug-target relationship. Both the PPT samples and PCC models underwent DSP using a library of 79 clinically relevant oncology drugs. Hit selection was based on dose-response curves-derived PD parameters and PD-PK integrated parameters. These parameters were evaluated for their predictive value in the PCC models and the PPT subgroup I samples. Subsequently, the parameter with the best predictive value was investigated in the PPT samples without a defined drug-target relationship.

A PK database of 74 drugs and nine PK parameters for each drug focusing on the pediatric population was successfully created and published for the scientific community. When investigating the predictive power of PD parameters, the drug sensitivity score (DSS) z-score showed the best predictive power in identifying the matching drug in the PPT subgroup I samples based on the molecular background. However, the DSS z-score could not capture the patient's clinical history. Conversely, the integrated PD-PK parameter, the DSS Cmax z-score, could effectively capture the patient's clinical history in the PPT subgroup I samples. In the PPT samples without a defined drug target match and no clinical treatment history, the DSS Cmax z-score provided additional insights for 77% (n=53/68) of the patient samples that were not detected by NGS molecular analysis.

In summary, a previously unavailable and comprehensive pediatric PD database was generated and published to serve the scientific community. The PK parameter Cmax was identified and successfully integrated with the DSS, introducing a novel DSP metric for drug response prediction. The groundwork established by testing and describing the DSS Cmax z-score in this thesis serves as a foundation for further investigation in larger datasets with clinical outcomes. This could refine the prediction of drug response for pediatric high-risk patients and improve their treatment selection without relying on time-consuming and costly techniques.

Zusammenfassung

Die ersten Ergebnisse des deutschen pädiatrischen Präzisionsonkologie-Programms INdividualized Therapy FOr Relapsed Malignancies in Childhood (INFORM) haben gezeigt, wie wichtig eine hohe Evidenz für eine erfolgreich abgestimmte zielgerichtete Therapie ist, die allein auf molekularer Diagnostik beruht. Doch nur bei einer kleinen Anzahl von Patienten (8 %, 42/519) (1) liegt tatsächlich eine Zielstruktur mit hoher Evidenz vor, was den ungedeckten Bedarf an verbesserten Vorhersagen zum Ansprechen auf Medikamente und klinischen Behandlungsempfehlungen unterstreicht. Ziel dieser Arbeit ist es daher, pharmakodynamische (PD) Parameter aus dem Drug Sensitivity Profiling (DSP) mit pharmakokinetischen (PK) Parametern zu integrieren und die Vorhersage des Ansprechens auf Medikamente bei pädiatrischen Hochrisikopatienten zu verbessern.

Um dieses Ziel zu erreichen, wurde basierend auf einer Literaturrecherche eine Datenbank mit den wichtigsten neun pädiatrischen PK-Parametern für die Medikamente aus der DSP-Medikamentenbibliothek in der INFORM-Studie erstellt. Zusätzlich wurden eine Datenbank mit Proben von primären Patiententumoren (PPT) (n=68) und eine Datenbank mit Positivkontroll-Zelllinien (PCC) (n=7) erstellt. Die PCC-Modelle weisen eine spezifische molekulare Veränderung (z. B. BRAF V600E, NTRK-Fusion) mit einem klinisch nachgewiesenen prädiktiven Wert für die Therapie mit einer bestimmten Medikamentenklasse auf. Unter den 68 PPT-Proben wiesen fünf Proben (PPT-Untergruppe I) eine Veränderung mit sehr hoher Priorität (INFORM Prioritäts-Score 1) und einer klinisch nachgewiesenen Prädiktivität für Zielstruktur und Medikamentenklasse auf. Sowohl die PPT-Proben als auch die PCC-Modelle wurden mit einer Bibliothek von 79 klinisch relevanten Krebsmedikamenten auf ihre Medikamentensensitivität hin untersucht. Die Auswahl der Treffer erfolgte auf der Grundlage von PD-Parametern und integrierten PD-PK-Parametern, die aus Dosis-Wirkungs-Kurven abgeleitet wurden. Diese Parameter wurden auf ihren Vorhersagewert in den PCC-Modellen und den Proben der PPT-Untergruppe I untersucht. Anschließend wurde der Parameter mit dem besten Vorhersagewert in den PPT-Stichproben ohne definierte Drug-Target-Beziehung untersucht.

Eine PK-Datenbank mit 74 Medikamenten und neun PK-Parametern für jedes Medikament mit Schwerpunkt auf der pädiatrischen Population wurde erfolgreich erstellt und für die wissenschaftliche Gemeinschaft veröffentlicht. Bei der Untersuchung der Vorhersagekraft der PD-Parameter zeigte der Drug Sensitivity Score (DSS) z-score die beste Vorhersagekraft bei der Identifizierung des passenden Arzneimittels in den Proben der PPT-Untergruppe I, verglichen mit der Grundlage des molekularen Hintergrunds. Der DSS z-score konnte jedoch

nicht die klinische Vorgeschichte des Patienten erfassen. Umgekehrt konnte der integrierte PD-PK-Parameter, der DSS Cmax z-score, die klinische Vorgeschichte des Patienten in den Proben der PPT-Untergruppe I effektiv erfassen. In den PPT-Proben ohne definierte Zielstruktur und ohne klinische Behandlungsvorgeschichte lieferte der DSS Cmax z-score zusätzliche Erkenntnisse für 77 % (n=53/68) der Patientenproben, die von der NGS-Molekularanalyse nicht erfasst wurden.

Zusammenfassend wurde eine bisher nicht verfügbare und umfassende pädiatrische PK-Datenbank erstellt und veröffentlicht, um der wissenschaftlichen Gemeinschaft zu dienen. Der PD-Paramter Cmax wurde identifiziert und erfolgreich in den DSS integriert, wodurch eine neuartige DSP-Metrik für die Prädiktion des Ansprechens auf Medikamente eingeführt wurde. Die Grundlagen, die durch das Testen und die Beschreibung des DSS Cmax z-score im Rahmen dieser Arbeit geschaffen wurden, dienen als Grundlage für weitere Untersuchungen in größeren Datensätzen mit klinischen Ergebnissen. Dies könnte die Vorhersage des Ansprechens auf Medikamente für pädiatrische Hochrisikopatienten verfeinern und ihre Behandlungsauswahl verbessern, ohne sich auf zeit- und kostenintensive Techniken zu verlassen.

Abbreviations

4PL	4-parameter logistic
5PL	5-parameter logistic
ABCB1	ATP binding cassette subfamily B member 1
ABL2	Abelson murine leukemia viral oncogene homolog 2
AKT3	AKT serine/threonine kinase 3
ALK	Anaplastic lymphoma kinase
Amin	Horizontal baseline effect
AML	Acute myeloid leukemia
API	Active pharmaceutical ingredient
ATP	Adenosine triphosphate
AUC	Area under the curve
BBB	Blood-brain barrier
BCL2L2	B-cell lymphoma 2 like protein 2
BCR	Breakpoint cluster region
BET	Bromodomain and Extra-Terminal Domain
BRAF	B-Raf proto-oncogene, serine/threonine kinase
BRD3	Bromodomain-containing protein 3
BzCl	Benzothonium chloride
C5	Highest measured concentration of a drug
CAPRIN1	Cell cycle associated protein 1
CCND3	Cyclin D3
CCNE1	Cyclin E1
CDKN2A/B	Cyclin Dependent Kinase Inhibitor 2A/B
CI	Confidence interval
c-KIT	cellular KIT proto-oncogene, receptor tyrosine kinase
Cl	Clearance
Cmax	Maximum plasma concentration
CNS	Central nervous system
CRM1	Chromosome region maintenance 1
CSF1R	Colony-Stimulating Factor 1 Receptor
Css	Steady-state concentration
Ctrough	lowest plasma concentration reached by the drug before the next dose administration
dDSS	Differential drug sensitivity score
DMSO	Dimethyl sulfoxide
DSP	Drug sensitivity profiling
DSS	Drug sensitivity score
DSS0	Drug sensitivity score with Amin 0
EC50	Half maximal response concentration
ECM	Extracellular matrix
EGFR	Epidermal growth factor receptor
EMA	European Medicines Agency
Emax	Maximum effect reached by the drug
EMMA	Ex vivo Mathematical Myeloma Advisor

EPHB2	EPH receptor B2
EPN	Ependymoma
ERBB4	Erb-b2 receptor tyrosine kinase 4
EWS	Ewing sarcoma
EWSR1	Ewing Sarcoma breakpoint region 1/EWS RNA binding protein 1
EZH2	Enhancer of zeste 2
EZHIP	EZH inhibitory protein
FDA	Food and Drug Administration
FGFR	Fibroblast Growth Factor Receptor
FIMM	Institute for Molecular Medicine Finland
FLI1	Friend leukemia integration 1
GI50	Half cell growth inhibition concentration
GR	Growth rate
HGG	High grade glioma
HGNET	High-grade neuroepithelial tumor
IC50	Half maximal inhibitory concentration
IC75	75% inhibitory concentration
IDC	INFORM DSP cohort
IGF1	Insulin like growth factor 1
INFORM	INdividualized Therapy FOr Relapsed Malignancies in Childhood
iTReX	interactive Therapy Response eXploration
KANK1	KN motif and ankyrin repeat domains 1
LGG	Low grade glioma
LRRFIP1	LRR binding FLII interacting protein 1
MATCH	Pediatric Molecular Analysis for Therapeutic Choice
MAX	MYC associated factor X
MCA	Multiplex Cell Line Authentication
McCT	Multiplex Cell Contamination Test
MDM2	Murine double minute 2
MED	Medulloblastoma
MED_SHH	Sonic hedgehog medulloblastoma
MEK1/2	Mitogen-activated protein kinase kinase 1/2
MET	Mesenchymal Epithelial Transition
MTB	Multidisciplinary molecular tumor board
mTOR	Mammalian target of rapamycin
MYC	v-myc avian myelocytomatosis viral oncogene homolog
NBL	Neuroblastoma
NF1	Neurofibromatosis type 1
NGS	Next-generation sequencing
NLM	National Library of Medicine
NTRK	Neurotrophic tyrosine receptor kinase
OS	Overall survival
OSA	Osteosarcoma
PARP	Poly(ADP-ribose) polymerase
PBS	Phosphate buffered saline

PCA	Principal component analysis
PD	Pharmacodynamic
PDGFC	Platelet derived growth factor C
PDGFRA	Platelet-derived growth factor receptor A
PDX	Patient-derived xenograft
PFS	Progression-free survival
PI3K	Phosphoinositide 3-kinase
PI5	Maximum effect at highest measured concentration
PK	Pharmacokinetic
PPB	Plasma protein binding
PPT	Primary patient tumor
PRKCA	Protein kinase C alpha
PTEN	Phosphatase and tensin homolog
QC	Quality control
RAS	Rat sarcoma
RMS	Rhabdomyosarcoma
ROC	Receiver operating characteristic
RT	Rhabdoid tumor
SCST	Ovarian sex cord-stromal tumor
sDSS	Selective drug sensitivity score
SmPc	Summary of Product characteristics
SRMS	Sclerosing and spindle cell rhabdomyosarcoma
T1/2	Plasma half-life
TD	Screen technical detail
TERT	Telomerase Reverse Transcriptase
Tmax	Time point at which maximum concentration is reached
US	United States
Vd	Volume of distribution
VEGFA	Vascular endothelial growth factor A
XPO1	Exportin 1
ZCCP	Zero Childhood Cancer Program

Table of Contents

List of figures

List of supplementary figures

List of tables

List of supplementary tables

List of equations

1   Introduction

1.1   Precision oncology approaches

1.1.1   Genomic precision oncology

Precision oncology is a concept in which the determination of optimal treatment is primarily driven by specific characteristics of an individual patient's tumor (2). Currently, precision oncology is mainly centered on a genomic framework (3). Genomic oncology uses molecular assays to identify genetic alterations such as mutations, amplifications and deletions which are subsequently matched with targeted therapy (4).

Several pediatric precision oncology programs such as the INdividualized Therapy FOr Relapsed Malignancies in Childhood (INFORM) (1) in Europe, Pediatric Molecular Analysis for Therapeutic Choice (MATCH) (5) in the United States (US) and Zero Childhood Cancer Program (ZCCP) (6) in Australia use state-of-the-art molecular assays to find actionable genetic alterations, matching drugs and clinical trials.

In the initial publication of the INFORM study during its pilot phase, a molecular target prioritization algorithm consisting of a 7-step scale was introduced (Figure 1) (7). The algorithm assigns priority scores ranging from "very high" (priority score 1) to "very low" (priority score 7) to classify molecular targets. The classification is based on the following factors: whether the alteration is drugable, whether there is a genetic change or an expression change, the presence of a direct drug target, a pathway activation or the identification of a synthetic lethal/predictive marker, the level of supporting evidence categorized as confirmed, presumed or possible, and whether the alteration is entity specific (7). It is important to highlight that the algorithm primarily focusses on the druggability and biological relevance of a target rather than the clinical evidence of a compound's efficacy (1). Consequently, targets with a very high priority (priority score 1) were defined as: druggable, genetic hits (mutation, rearrangements) directly targetable in specific entities with confirmed evidence (7).

Detected alteration

Druggable?
— yes
— no, but tumorbiologically relevant

Genetic change?
— yes
— no, expression change

Direct drug target?
— yes
— no, pathway activation
— no, synth. lethal/pred. marker

Evidence level?
— confirmed
••• presumed
• • • possible

*   †   ‡

Entity specific?
— yes/not relevant
— no

Score	Very high	High	Moderate	Intermediate	Boderline	Low	Very low	NA
Patients§	7	7	4	8	5	2	6	13
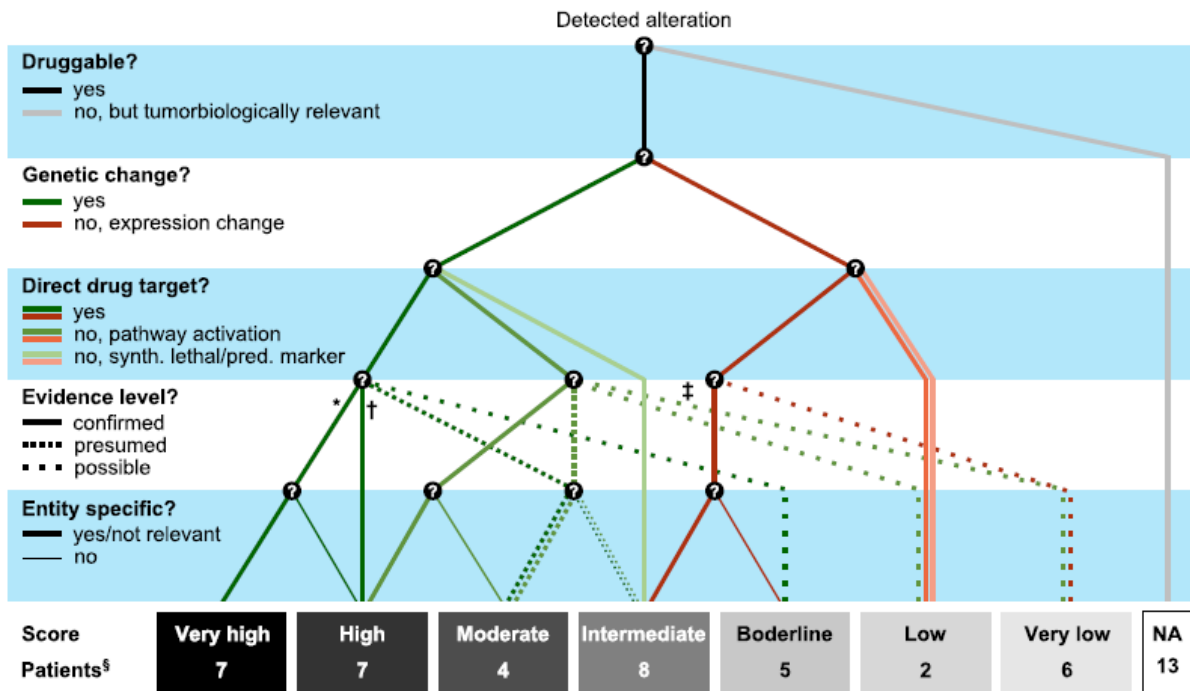
Figure 1. INFORM molecular target prioritization algorithm. Originally published by Worst et al. (2016) (7) showing priority score 1 to 7. Worst et al. outline the following abbreviations: "NA, not applicable; pred., predictive; SNV, single-nucleotide variants; synth. synthetic. '*', included molecular alterations: SNVs, small insertions and deletions (InDel), genomic translocations (fusion genes). '†', Included molecular alterations: focal, high-amplitude copy number variants. '‡', Genetic alterations with some modest literature evidence of possible pathway activation. '§', Number of patients for which this was the highest score in their identified alterations (number for NA includes those patients where no target was identified)" (7).

The INFORM study prospectively investigated the predictive power of the priority score algorithm by conducting a follow-up study to evaluate the clinical benefit. Among the population studied, a very high priority target was identified in n=42/519 (8%) patients (1). Only n=20/42 (47%) patients ultimately received the corresponding treatment with a matching drug. This subgroup of patients, harboring a very high priority score target and receiving the matched targeted therapy, exhibited a progression-free survival (PFS) of 204 (95% CI 99 – N.A.) days and an overall survival (OS) of 354 (95% confidence interval (CI) 165 – N.A.) days (1). In comparison, the remaining n=499/519 (96%) patients (priority score 2 to 7, receiving matching or conventional treatment) had a PFS of 117 (95% CI 106 – 143) days and an OS of 290 (95% CI 256 – 343) days (1). This indicates that only 4% (n=20/519) of the patients demonstrated a doubling of PFS when they harbored a very high priority score target and received the corresponding targeted drug, in comparison to all other patients, harboring priority scores 2 to 7 and either receiving conventional treatments (mostly chemotherapy) or the corresponding targeted drug (1). These findings align with the observations reported in the

ZCCP program, where a therapeutic target was identified for n=176/247 (71%) patients (6). A multidisciplinary molecular tumor board (MTB) recommendation was provided to n=134/201 (67%) patients of which n=112/134 (48%) were categorized as high priority Tier 1 or Tier 2. Of the patients who received the MTB recommendation, n=38/134 (28%) were eligible for follow up of which n=6/38 (15%) were Tier 1. Overall, only 4% (n=11/247) of patients experienced clinical benefit from the matched targeted treatment in the form of complete or partial response (6).

A systematic review conducted by Lee et al. included 21 clinical trials and observational studies, comprising a total of 1408 pediatric patients, focusing on molecular characterization to investigate clinical benefits (8). For n=647/1408 (46%) patients a therapeutic target was identified and n=175/647 (27%) of this group received targeted treatment. The review revealed that while a molecular target was identified for half of the patients, and one third received the targeted treatment, only 5% (n=73/1408) of patient experienced an objective response of which n=12/1408 (0.9%) patients experienced complete remission (8).

Additionally, the INFORM study compared patients with a very high priority target who received matching targeted treatment to those who did not (1). The group that did not receive targeted treatment exhibited similar PFS compared to all the other patients. In their paper (1), the authors argue that this finding confirms the potential predictive value of targeted treatment; however, it does not establish them as prognostic markers for improved outcomes.

Overall, the fraction of patients with high-evidence molecular targets, receiving the corresponding targeted treatment remains low at around 2 - 4%, which contributes to the majority of patients not benefiting clinically from diagnostic programs solely based on molecular analysis.

1.1.2 Functional precision oncology

Functional precision oncology is defined as a strategy in which the response of tumor cells obtained from an individual patient is evaluated when direct administration of drug treatments is applied to these cells. Compared to genomic precision oncology, functional precision oncology does not use a static method to determine treatment recommendations. Instead, it presents the possibility of exposing primary patient tumor cells to a variety of drugs. Additionally, functional precision oncology enables the assessment of multiple drug combinations.

Improving clinical treatment recommendations within precision medicine has become a crucial mission. Functional precision medicine, has emerged as an approach to expose primary patient tumor (PPT) samples obtained through biopsy or surgery, to various treatments. This is done either by cultivating them in animal models or employing them *in vitro* cell culture models. Functional precision oncology was started in hematological cancers, as biopsies within this cancer type are less invasive as compared to solid tumors (9,10).

Over the past six decades, functional assays, including drug DSP techniques, have emerged as valuable tools in precision oncology (11). These approaches, starting with the pioneering work of Wright et al. on chemotherapy-based DSP (11), aim to identify therapeutic sensitivity within PPT samples. By analyzing drug responses in PPT samples, DSP techniques provide insights into the specific sensitivities of tumors, possibly facilitating the identification of effective treatment options. Just as in genomic precision oncology, this information aims to assist physicians in choosing appropriate and safe treatments for individual patients. A notable advantage of this approach is its ability to evaluate a wide range of drugs, including those without clear biomarkers (12). Additionally, DSP provides insights into the effectiveness of potential combination treatments (12). Nevertheless, there are challenges in fully understanding and translating these *ex vivo* experimental results into clinical responses. These challenges have hindered the successful validation and integration of DSP approaches within the clinical setting. Consequently this has led to a lack of supporting evidence in the predictive value of DSP, particularly in the form of prospective correlations.

1.1.2.1 Tissue and cell culture models in drug sensitivity profiling

The utilization of cell culture models derived from PPT samples presents several limitations. Short-term monoculture generation has a low success rate, reducing its feasibility for DSP applications (12). Alternatively, establishing long-term cell lines, a conventional approach with

demonstrated efficacy in various instances, involves selecting clones from the sample that are most responsive to successful culturing (12). However, this selection process leads to a homogenous cell population, deviating from the heterogeneous nature of PPT.

Using PPT samples in patient-derived xenograft (PDX) models is to this day crucial in preclinical research (13). This strategy allows the formation of a tumor microenvironment that may play an important role in drug response, mimicking the in-patient situation. Nevertheless, an inherent disparity inevitably exists between PDX models and the human system. Furthermore, these models are not suitable for high-throughput drug screening in a clinically relevant turnaround-time, requiring substantial labor, time, and expense (13). Despite the success of these approaches, timely decision-making remains paramount in clinical settings, which makes PDX models less suitable for DSP. Therefore, the focus in the following sections will be on *ex vivo* DSP.

In vitro cell culture models can be divided into 2D and 3D models. Traditional 2D cell culture models, where cells are grown in a mono-layer on a flat surface, offer certain benefits such as rapid expansion, suitability for high-throughput screening options, and cost-effectiveness. However, this model lacks the interactive nature of cells, and does not have the shape nor morphology of cells in a physiological setting (14). Additionally, this model fails to replicate the intricate tumor microenvironment, thereby influencing cellular growth, behavior and drug response (15). In contrast, more advanced 3D cell culture models, including spheroids and organoids, have been developed to enhance the genomic and histopathological accuracy to the primary tumor and, to some extent, mimic the 3D tumor environment and tumor microenvironment (14).

Spheroids are 3D cellular aggregates that preserve crucial tumor characteristics such as cell-cell interactions, contact with the extracellular matrix, and the presence of nutrition, waste, and oxygen gradients (16). They serve as valuable models able to show drug resistance by closely mimicking tumor morphology, as opposed to 2D models (14)(16). The formation of spheroids is primarily facilitated by integrins, which are membrane proteins, and extracellular proteins (16). Various techniques can be applied to generate spheroids, offering a range of complexity in their formation (16). Novel techniques have emerged to enhance the cellular composition, ensuring the presence of stromal and immune cells in spheroids. Alternatively, after resection and dissociation, the choice may be made to preserve all cell types in the tumor sample, resulting in organotypic spheroids that maintain the tumor microenvironment (12,17). Generally, spheroids have a high success rate in culture establishment and a relatively short period of establishment, making them suitable for high-throughput screening.

The first organoid, derived from adult epithelial small intestine and colon cells, was successfully generated and published in 2011 (17). Following the dissociation of PPT samples, cells are seeded onto an extracellular matrix-rich hydrogel, which facilitates their spontaneous growth into 3D structures. Organoids effectively recapitulate aspects of the tumor microenvironment, tumor epithelial histology, and exhibit more stable genetic profiles that capture tumor heterogeneity (3). They harbor both healthy cells as well as tumor cells (18). Notably, a pediatric organoid biobank focusing on pediatric kidney tumors and their corresponding normal organoids has been established by Calandrini et al., encompassing samples from over 50 patients (19). With this comprehensive and well-characterized collection of samples, Calandrini et al. have generated a valuable resource for basic cancer research, drug screening, and personalized medicine. Additionally, organoids offer the advantage of enabling co-culturing with immune cells, allowing for the inclusion of crucial immune components within the tumor microenvironment (15). This enables the generation of an immune microenvironment, a component often absent in traditional cell culture models. This provides a greater degree of experimental options, allowing researchers to explore a wide range of immune-related interactions and investigate various aspects of tumor-immune cell interactions within organoid models. Despite the considerable promise and advantages of organoids, the establishment of these models is time-consuming, labor-intensive, and success rates can vary significantly from for instance 16% in prostate cancer (18) to 100% in colon and liver cancer (12,18,20).

The synergy between the fields of engineering and biology has further advanced DSP culturing methodologies. Organs-on-a-chip serve as innovative bioengineering platforms within microfluidics and engineered microenvironments. These dynamic systems aim to mimic human organs on a miniature scale, with cells cultured on a membrane-like platform that enables precise delivery of drugs, media, and signaling molecules. These systems have been used to study normal physiology such as the blood-brain barrier (BBB) but also several organs on their own such as the liver. Lung cancer, colorectal cancer and breast cancer models in adults have also been studied within these dynamic systems (18). Additionally, within cancer research this method can be used to study the extracellular environment, tumor invasion, migration and metastasis (18). Furthermore, organs-on-a-chip incorporate mechanical parameters such as shear stress and extracellular matrix (ECM) stiffness (3). For instance, a single microfluidic chip can test over 30 conditions in an automated manner using high-density microfluidic droplet arrays for spheroid culturing (12). These devices have the potential to be integrated into broader workflows, including the incorporation of pharmacokinetics. Komen et al. assessed the efficacy of a microfluidic device with a separate drug dosing channel, enabling

the application of an *in vivo*-like drug concentration profile (21). By comparing this dynamic drug exposure on cancer cells to the conventional fixed-dose exposure where the maximum plasma concentration (Cmax) was used, they found that growth inhibition was primarily driven by the dynamic application of pharmacokinetic (PK) profiles (21). In another example, Mazzocchi et al. also used a microfluidic device on organoids derived from two mesothelioma patient samples (22). Drug dosing was applied by continuous flow of media and drug infusion for seven days. Two different treatment combination were compared per patient and a strong correlation was found between the organoid outcome and the clinical response of the patients (22).

To summarize, there is no model that fully represents the tumor-drug interaction in a patient as this is a very complex interaction. Functional precision medicine holds significant promise for enhancing clinical treatment recommendations, given its capacity to subject the patient's tumor cells to a range of drugs and drug combinations for direct assessment of their efficacy. However, several challenges remain to be addressed in the field of DSP. Firstly, generating PPT cell models forms a challenge, particularly in obtaining an adequate quantity of tumor cells for screening purposes, especially in cases of solid tumors where metastasis often leads to biopsies instead of resections (12). Secondly, the timeframe for sample collection to treatment recommendation needs to align with real-time clinical situations. Expanding the tissue before conducting screens has been proposed as a potential solution to improve success rates, albeit at the cost of additional time, which is undesirable in a clinical setting. One potential solution is to collect the sample prior to initiating first line treatment, however, this requires the implementation of precision oncology pipeline, incorporating both molecular and functional aspects, at earlier stages rather than as a last resort. Care must be taken, as tumor characteristics may change during treatment and disease progression. Particularly in cases wherein a tumor sample is sent out for DSP analysis, and until the conclusive results are obtained, a novel course of treatment is administered to the patient. Similarly, in instances in which disease progression occurs subsequent to the submission of the sample for DSP analysis. Given the potential alteration in tumor characteristics under such circumstances, the validity of the DSP outcomes becomes compromised. Additionally, the limited duration of viable tissue preservation further limits the feasibility of this approach.

1.1.2.2 Response prediction models in drug sensitivity profiling

Another aspect of DSP involves determining appropriate outcome measures and translating them into clinical decision making and determining their predictive validity. Currently, the outcome measure for each drug in DSP typically revolves around a parameter describing the percentage of viability inhibition. Consequently, several questions arise:

(I)   What is the optimal outcome measure in DSP?
(II) What threshold of the *ex vivo* outcome measure reflects the drug's clinical efficacy?
(III) How can drugs be ranked based on their predicted efficacy?

Ideally, these questions can be addressed when clinical outcomes are available. By examining specific patients who have actually received the predicted drug, insights from clinical outcomes can refine the answers to these questions.

One strategy that has been employed is comparing *ex vivo* drug screens with *in vivo* models to determine their relevance. However, this approach is not practical in a clinical setting due to time constraints and the need for prompt decision making. Nevertheless, it can be used to validate a particular outcome measure in cases where clinical patient data is not accessible.

To assess the efficacy and potency of drugs, various response metrics have been explored, including IC50 (half maximal inhibitory concentration), EC50 (half maximal response concentration), GI50 (half cell growth inhibition concentration), GR50 (half growth rate inhibition concentration), Emax (maximum effect reached by the drug), and AUC (area under curve) of the dose response curve (23). In oncology research, typically, cell line models or patient-derived cells are exposed to a drug across a range of concentrations, followed by measuring the number of viable cells or adenosine triphosphate (ATP) activity after a specified incubation period. Fallahi et al. proposed an alternative approach in which they moved away from frequently applied metrics such as IC50, EC50, and GI50, which focus on potency at the midpoint of the dose-response curve when distinguishing between the effective from non-effective drugs. Instead, they investigated Emax, hill slope, and AUC of dose-response curves (24).

Their study revealed that IC50, GI50, Emax, and hill slope did not exhibit significant correlation, indicating variability within the drugs and cell models used. Notably, the variation in Emax was independent of the proliferation rate (24). To address the substantial variation observed, the researchers examined the AUC, which represents the cumulative response across a specific concentration range, accounting for both the potency (the amount of drug needed for a desired response) and efficacy (the capacity of a drug to produce a desired

response) of a drug. The AUC demonstrated robustness across experiments when compared for a single drug over the entire cohort or database (24). While Emax and IC50 can be used in comparing different drugs with varying concentration ranges, the Emax appears more informative at higher concentrations, whereas IC50 provides more insight at lower concentration ranges (24).

In an effort to enhance drug response prediction and account for parameters that are independent of potentially interfering factors such as cell division and proliferation rates, Hafner et al. proposed the utilization of normalized growth rate (GR) inhibition parameter by comparing GR in the presence and absence of a drug (25). The researchers concluded that their metric improves DSP by taking differences in cell division rates between tumor types into account. As a result, they report to improve cross-study reproducibility with their metric (25).

Subsequently, Brooks et al. applied the aforementioned metric to assess its applicability. They determined that parameters incorporating the growth rate are best suited for evaluating drug response. This is because cellular growth significantly impacts this response. However, the growth rate dependent metrics cannot be calculated when the steady state growth cannot be reliably determined in first place. This is the case particularly in slow-growing primary patient samples (23). Or in some cases the growth rate cannot be determined a priori. To address this, the authors proposed a decision tree that considers the choice of parameter to be calculated based on the available drug response data (23).

In order to move beyond a representation of drug response involving a single parameter, Yadav et al. undertook the development of a multiparametric algorithm. This algorithm aims to convert a combination of parameters into one unified quantitative score, employing the concept of the area under the dose response curve to characterize drug response in terms of potency and efficacy (26). The drug sensitivity score (DSS1) is determined by integrating the dose range as a continuous function, which includes key parameters such as the IC50 (half-maximal inhibitory concentration), top and bottom asymptotes, slope hill, and a minimum activity level. These elements are incorporated into a nonlinear response model proposed by Yadav et al. To account for drugs that exhibit efficacy only at higher concentrations, in contrast to those displaying efficacy at lower concentrations, an additional normalization step employing the top asymptote is used to generate DSS2. Furthermore, DSS2 is then normalized by the active dose range, resulting in DSS3. Additionally, Yadav et al. developed the differential DSS (dDSS) which takes the effect of the drug on healthy control samples from healthy bone marrow in comparison to the DSS.

In an acute myeloid leukemia (AML) precision medicine tumor board incorporating functional drug screening alongside genomics, transcriptomics, and clinical data, a cohort of AML adult patients was enrolled to receive therapeutic recommendations (27). The functional drug screening outcomes were determined using the selective drug sensitivity score (sDSS, corrected DSS for 17 healthy controls). For a total of 37 patients, treatment recommendations were provided, resulting in a favorable response rate of 59% (27). These promising findings also resulted in the initiation of a randomized controlled clinical trial aimed at validating the therapeutic recommendation approach derived from the clinical tumor board setting. The objective of this trial is to assess the efficacy and reliability of the proposed approach in a larger patient population. Moreover, the authors conducted a comparative analysis between the drug screening results and a genomic-based approach. They observed that the *ex vivo* functional drug screening provided informative outcomes for a greater number of patients and also presented a wider range of treatment options compared to the genomic based approach alone (27). This highlights the potential of the functional drug screening approach in enhancing personalized treatment decisions and expanding the therapeutic possibilities for patients.

1.2 Application of drug sensitivity profiling

1.2.1 Application in diagnostic clinical trials

To date, two prominent study examples in the field of pediatrics have demonstrated the additional benefits of DSP when combined with genomic data. The studies are the TARGET pilot study conducted as part of the Australian ZERO Precision Childhood Cancer Program (28) and the INFORM DSP pilot program as part of the INFORM study (29). Both studies incorporated a tumor board and ensured timely reporting of results. They also both focused on high risk pediatric patients with a poor prognosis, including a range of pediatric solid tumors and brain tumors. Despite differences in sample size, number of drugs tested and outcome measurement, both studies identified a similar fraction of drug hits for 76% (TARGET) (28) and 72% (INFORM) (29) of cases, respectively.

The TARGET study enrolled a total of 56 patients, out of which 7 samples were successfully expanded from the primary tumor sample and subjected to DSP against a library of 111 drugs (28). The selection of drug hits was based on two levels: level 1 criteria required the AUC and IC50 z-score to be equal to or below -2, with the IC50 value being below the Cmax; level 2 criteria focused solely on meeting the AUC and IC50 z-score criteria (28). The clinical impact of DSP was retrospectively evaluated by correlating the patient's clinical response with the

predicted response from DSP. Remarkably, in 4 out of 5 patients, DSP accurately predicted the clinical outcome.

The INFORM study involved 89 patient samples, with successful screening conducted on 69 samples (78%), against a range of 75-78 drugs after passing quality control measures (29). A drug hit was defined based on four criteria: (I) adjusting DSSasym for healthy tissue, (II) a minimum of 75% maximum percentage inhibition by the drug, (III) an IC50 below Cmax, and (IV) a goodness of fit of the curve of at least 0.8. Additionally, the 75th percentile was calculated for each drug across the entire patient cohort, and samples exceeding this threshold were considered to have an above average sensitivity (29).

Clinical follow-up information was available for three patient cases, demonstrating a remarkable alignment with the DSP results. In one case, a high grade glioma (HGG) sample initially harboring the BCR:NTRK2 fusion showed actual resistance to all NTRK inhibitors, consistent with the clinical background of the patient. Furthermore, DSP revealed sensitivity to all MET inhibitors, which was subsequently confirmed by an additional genomic analysis showing MET amplification in the sample. The second case involved an EWSR1:FLI1 positive Ewing sarcoma (EWS) patient who exhibited clinical resistance to the EWING2008 and RIST treatments. This was captured by the DSP findings. The third patient, with a central nervous system high-grade neuroepithelial (CNS_HGNET) tumor, demonstrated clinical resistance as confirmed by a comparative screen of the 3rd and 4th relapse samples which showed a decrease in mean DSSasym values from 5.2 to 2.5 (29).

More complex experimental and mathematical models have been investigated mainly in the adult population to test the drug response prediction and improve the clinical predictivity. Silva et al., have screened 52 patients derived multiple myeloma tumor samples against 31 conventional chemotherapeutics using an image-based readout, where they have measured the effect of the drugs every 30 minutes for a total of four days (30). The Ex vivo Mathematical Myeloma Advisor (EMMA) mathematically incorporates properties for tumor heterogeneity, as well as pharmacodynamic (PD), PK and DSP. Within a period of five days the tool can predict the clinical outcome of a patient over a period of three months. Within the cohort of 52 patients, EMMA has accurately predicted and classified 90% of the patients either in the responders or non-responders group. Additionally, the tool was able to correctly classify 79% of the patients into the specific type of response based on the International Myeloma Working group classification (30).

Although the results showed promise in correlation with clinical outcomes, it is important to note that the data in all of these studies is limited due to the relatively small sample size and

the correlative retrospective nature of the analysis. As a result, there is a need for prospective DSP testing in interventional trials to further investigate its potential in pediatric precision oncology.

1.2.2   Application in interventional or observational clinical trials

In the prospective non-randomized observational clinical trial (NCT03860376, Table 1) involving relapsed and/or refractory pediatric patients with various types of cancer *ex vivo* DSP along with genomic information is incorporated. Acanda De La Rocha et al. reported on the outcome of a single case study from their ongoing trial (31).

The case study involved a 7-year-old girl who was diagnosed with sclerosing and spindle cell rhabdomyosarcoma (SRMS) (31). The patient had undergone first, second, and third-line treatments, but experienced relapses and eventually developed metastasis. Once enrolled in the clinical trial, DSP and genetic profiling were performed, leading to the identification of two drug hits. Interestingly, the patient's clinical history did not correlate with the results obtained from the DSP analysis. Following the application of the DSP-based treatment, the patient exhibited a partial response, including a response of liver and pancreas metastases. The patient achieved a PFS of 24 weeks before succumbing to disease progression in the lungs (31).

In the context of adult prospective observational clinical trials, several studies have incorporated a variety of drug screening components . One of these studies (NCT03133273, Table 1) specifically focuses on metastatic colorectal cancer and evaluates chemotherapy-based treatments using the chemosensitivity assay known as Oncogramme (32). In this clinical trial (NCT03133273), the researchers provided only a concise summary of their findings in a pilot study (33). They reported that in the pilot study involving metastatic colorectal cancer (stage IV), Oncogramme exhibited a predictive value of 84% in determining tumor sensitivity to chemotherapy. This result surpassed the maximum predictive value of 50% achieved when chemotherapy was administered according to the consensus method (NCT03133273). The Oncogramme results correlated with the patient clinical outcomes in n=14/22 (64%) of cases studied. The primary outcome of this clinical trial is to assess the length of progression-free disease after one year of inclusion (33). These future findings which have not been published yet will highlight the potential effectiveness of Oncogramme specifically and DSP generally, as a tool for guiding treatment decisions in metastatic colorectal cancer cases.

Table 1. Summary of observational and interventional clinical trials assessing *ex vivo* drug sensitivity profiling. DSS: drug sensitivity score, DSP: drug sensitivity profiling, PFS: progression free survival, RECIST: Response Evaluation Criteria in Solid Tumours, #: several other secondary objectives, see reference, OS: overall survival.

NCT	Trial type	Population	DSP platform & readout	Parameter	Intervention	Primary objective	Secundary objective	Results DSP
NCT03860376	Observational	Chemorefractory and/or relapsed pediatric cancer patients without alternative treatment options	*Ex vivo* assays Lumi-nescent cell viability assay	DSS adapted from Yadav. et al. (34)	n.a.	Percentage of pediatric cancer patients receiving DSP guided treatment. Trial feasibility success is achieved if 16/25 (64%) of patients have treatment initiation within 4 weeks	Assessment of objective response rate and PFS by comparing DSP guided and DSP non-guided therapy (standard of care)	Not published yet. Case study published (31): PFS 24 weeks based on DSP guided treatment.
NCT03133273	Interventional	Adult patients with metastatic colorectal cancer (stage IV)	*Ex vivo* assay Onco-gramme®	Ratio of 'death percentage in treated cells' to death percentages in untreated cells. Above 75th percentile considered sensitive.	Onco-gramme® based result	Occurrence of patient progression (assessed by RECIST) or mortality within one year of inclusion	First line treatment response and overall survival#	Not published yet. Pilot study results (33): successrate of Oncogramme® application was 97%, predictive value of 84% for sensitivity

NCT	Trial type	Population	DSP platform & readout	Parameter	Intervention	Primary objective	Secundary objective	Results DSP
NCT04470947	Observational	Adult patients with aggressive haematological malignancies	*Ex vivo* assay Pharmaco-scopy	Integrated pharmaco-scopy (i-PCY) score	High throughput image based *in vitro* drug screening and comprehensive genomic profiling	Percentage of patients experiencing a PFS ≥1.3 times greater in pharmacoscopy-guided treatment compared to treatment before study inclusion.	Average pharmacoscopy PFS/PFS ratio of last pre-inclusion treatment, overall response rate, and number of identifiable treatable targets	Not published yet. Interim analysis trial: 12/17 (71%) patients receiving pharmacoscopy-guided treatment achieved a PFS ratio of 1.3 or higher (35)
NCT03389347	Interventional	Adult patients with relapsed or refractory multiple myeloma or plasma cell leukemia	*Ex vivo* assay Lumi-nescent cell viability assay	IC50 and AUC	n.a.	Achieving actionable outcomes from DSP for over 50% of the enrolled patients	Evaluation of the overall response rate of DSP-guided treatment using the criteria set by the International Myeloma Working Group	Of 25 patients, 16 had sufficient plasma cells for actionable DSP-based treatment. Among 13 patients who underwent DSP-guided treatment, 92% achieved stable disease or better

(Continued on following page)

NCT	Trial type	Population	DSP platform & readout	Parameter	Intervention	Primary objective	Secundary objective	Results DSP
NCT03561207	Observational	Adult patients with Ovarian Cancer Glioblastoma Multiforme Anaplastic Astrocytoma	*Ex vivo* assay Lumi-nescent cell viability assay	IC50	EV3D assay	Determination of the correlation between the assay results and reported clinical outcomes in patients.	Assessment of assay implementation, effect of assay on decision making and the patient outcome. Comparison of clinical response (PFS, time to progression) between patients with DSP guided treatment and patients who were not treted according to DSP	Temozolomide responsiveness was accurately predicted in 17/20 (85%) patients. The median OS for patients categorized as responders was 11.6 months, compared to 5.9 months observed in non-responders

Another ongoing clinical trial focuses on evaluating the genomic and functional drug screening profiles of patients with aggressive hematological cancers (NCT04470947, Table 1). In this study, researchers utilize a multiparametric single-cell image-based analysis method they refer to as pharmacoscopy (35). In an interim analysis of the trial, a patient cohort consisting of 48 individuals was prospectively evaluated. Among them, 17 patients met the criteria to receive pharmacoscopy-guided treatment and n=15/17 (88%) had an overall response. The researchers observed that 12 out of these 17 patients (71%), achieved a PFS ratio of 1.3 or higher. Furthermore, the median PFS for this subgroup increased fourfold, from 5.7 weeks to 22.6 weeks (35). These findings indicate the potential of pharmacoscopy-guided treatment in improving patient outcomes in aggressive hematological cancers.

In a clinical trial (NCT03389347, Table 1) combining DSP and genomics for guiding treatment options in multiple myeloma patients, 25 patients were enrolled, of which 16 (64%) had sufficient cells for DSP analysis (36). These cells underwent screening against 170 compounds, and notably, 13 out of 16 patients received the drugs identified through DSP. An additional approach was employed to characterize the overall DSP of each patient. This involved calculating the mean AUC of all 170 drugs tested and comparing it to the 50th percentile based on PSF. A threshold was established, considering AUC values above the 50th percentile as resistant and below as sensitive. Furthermore, an additional filtering step was implemented in the drug response metric. Only drug hits that met the criteria of having an IC50 below 0.2 uM and equal to or less than the Cmax were reported. Among the patients who received the identified drugs based on these criteria, an encouraging outcome was observed, with 92% achieving at least stable disease (36).

In a prospective clinical trial, 3D-PREDICT (NCT03561207, Table 1), Shuford et al. investigated the *ex vivo* drug response on newly diagnosed HGG patients (37). They focused on a panel of 12 HGG relevant treatments. In their assay, which has been validated on newly diagnose ovarian cancer patients (38), they apply two approaches in defining/distinguishing responsive patients from non-responsive patients: (I) a cut off was determined by applying a binary receiver operating characteristic (ROC) analysis in case of a sufficient number of clinical data availability, (II) when clinical data was scarce, they used the IC50 quartile analysis (25th and 75th quartiles) of test data from all patient samples. The second approach resulted in the formation of three categories: responders, moderate responders and non-responders. This assay was able to predict the temozolomide responders from non-responders in n=17/20 (85%) patients. The median OS for the patients classified as responders in the assay was 11.6 months and was clearly longer compared to the non-responders with 5.9 months (37).

As outlined in Table 1, the application of *ex vivo* DSP across a spectrum of cancer types has shown promising results. Diverse readout techniques are used in each clinical trial, such as luminescent cell viability assays, commercial tools like Oncogramme, and microscopy and imaging based approaches. Notably, the parameters and criteria applied to distinguish drug sensitivity from resistance vary across these trials as well. These criteria span from single metrics like the DSS derived from multiparametric algorithms, to more complex approaches involving parameters from immunofluorescence, microscopy, and single-cell image analysis, such as the integrated pharmacoscopy score. Parameters such as IC50, AUC, and ratios between viable and non-viable cells are also applied. Despite using diverse reachout techniques and drug response metrics a consistent trend emerges: the advantage of DSP-guided treatment over conventional treatment.

Incorporating *ex vivo* DSP in clinical trials is expanding to enhance cancer patient treatment. Though the above-mentioned examples represent a small number of what is currently ongoing, they offer promise for proper DSP validation. Several other ongoing clinical trials involve the use of organoids and PDX avatar models (15,18). However, they are beyond the scope of this research.

1.3 Problem statement

Current precision oncology, primarily relying on genomic analysis, faces limitations in effectively selecting optimal treatments and improving patient outcomes. Molecular assays effectively detect genetic alterations, yet a challenge lies in the low frequency of high-priority targets. Additionally, a significant proportion of patients lack actionable targets. Functional precision oncology, which incorporates patient-derived tissue models, such as organoids and spheroids, along with drug sensitivity profiling, offers a promising approach to enhance treatment selection and potentially improve patient outcomes. These models provide a more representative understanding of tumor behavior and drug responses, complementing the genomic approach.

However, there are challenges in generating reliable and representative patient-derived tissue models, determining appropriate outcome measures that align with clinical efficacy, and integrating functional approaches into clinical practice. These challenges contribute to the failure of many drugs during the translational process, spanning from pre-clinical data generation to early and late-phase clinical trials (39). Risk factors for translational failure in later clinical stages include the absence of a biomarker-driven strategy and the failure to establish proof of concept in phase II trials (39). Extensive efforts have been made to improve the preclinical stage by implementing consensus recommendations and utilizing an adequate number of disease-mimicking models (40,41). Another recurring recommendation is the adjustment of preclinical drug testing based on PK parameters derived from clinical studies (40–42). Poor consideration of pharmacokinetics has been identified as a contributing factor to the lack of reproducibility and translational failures in preclinical research (43). These challenges hinder the widespread clinical implementation of functional precision oncology and limit its potential impact on patient care.

Addressing these challenges by determining robust outcome measures aligned with clinical efficacy and incorporating a better understanding of pharmacokinetics in preclinical research is crucial. Therefore, there is a strong unmet need for improving drug response prediction for relapsed high risk pediatric patients by combining functional, pharmacological and genomic information. By doing so, personalized treatment selection can be improved, patient care can be enhanced, and overall treatment outcomes can be significantly advanced in the field of precision oncology.

2 Aim

The aim of this study is to enhance the accuracy of drug response predictions by developing a novel mathematical approach that integrates functional drug screening parameters, pharmacological parameters next to the genomic information. This research focuses on high-risk relapsed pediatric patients enrolled in the INFORM study, who face a poor prognosis. My objective is to bridge the gap between the *ex vivo* direct cell-drug interaction and the in-patient pharmacological effect of the drug by integrating pharmacological parameters with functional drug screening parameters, thus improving the capacity of DSP to predict drug response in patients.

In order to achieve this aim, four objectives were determined:

1. *Building distinct data bases necessary for this study.* These were either unavailable or formatted in an unsuitable manner for data analysis. The first step involved the establishment of a PK database for the INFORM drug library, with a specific focus on the pediatric population, since no descriptions or publications of such a database existed previously. Secondly, the PPT sample data base was generated in a format suitable for data analysis. While the experiments were conducted, the output data was not prepared in an aggregated and computable manner. The PPT samples divided into two subgroups: subgroup I with a clinically defined drug target relationship and subgroup II without a clinically defined drug target relationship. Finally the generation of the PCC model data base was important to provide a dataset which serves as a positive control for testing the different PD and PK parameters.

2. *Analyzing the performance of PD parameters in the PCC models and PPT samples with a defined drug target match.* The PD parameters were assessed to identify the parameter that demonstrates the best performance. Once identified, I further investigated the performance of this optimal PD parameter by applying it to the PPT subgroup I samples. This analysis aimed to provide valuable insights into the effectiveness of the selected parameter in patient samples with a clinically defined drug-target relationship.

3. *Mathematical integration of the best performing PD parameter with the PK parameter of interest and analyzing its performance in PPT samples with a defined drug target match.* After integration, this PD-PK parameter combination was implemented on the PCC models to evaluate its performance within the given dataset. Furthermore, I applied the parameter combination to the PPT subgroup I samples.

4. *Application of the PD-PK parameter to the PPT without a defined drug target match.* Description of the effect of the PD-PK parameter combination on the PPT samples without a defined drug target match.

3 Materials and methods

3.1 Materials

3.1.1 Cell lines and cell culture

Table 2. Positive control cell line (PCC) model characteristics. TDSU: Translational Drug Screening Unit.

Cell line	Origin	Supplier	Molecular alteration
NB1	Neuroblastoma	TDSU, DKFZ Heidelberg, Germany	ALK amplification
LAN5	Neuroblastoma	TDSU, DKFZ Heidelberg, Germany	ALK R1275Q
NCI-H3122	Lung carcinoma	TDSU, DKFZ Heidelberg, Germany	EML4:ALK fusion
BT40	Pleomorphic Xanthoastrocytoma	TDSU, DKFZ Heidelberg, Germany	BRAF V600E
BT278	High grade glioma (H3.3 G34R)	TDSU, DKFZ Heidelberg, Germany	NF1 p.R440X
SJ-GB-M2	High grade glioma	TDSU, DKFZ Heidelberg, Germany	MET fusion
I070_004	Inflammatory myofibroblastic tumor	TDSU, DKFZ Heidelberg, Germany	ETV6:NTRK3 fusion

Table 3. Cell culture media.

Medium	Additives	Cell lines
RPMI 1640	10% FCS, 1% NEAA	I070_004, BT40, NB1, LAN5, NCI-H3122
Dulbecco's Modified Eagle's Medium (DMEM) high glucose	10% FCS, 1% NEAA	SJ-GB-M2
Tumor Stem Medium (TSM) complete	See Table 4	BT278

Table 4. Preparation of tumor stem medium (TSM) complete.

TSM base	TSM complete (TSM base + supplements below)
HEPES Buffer Solution (1M)	10% FBS, 1% NEAA
L-Glutamine solution bioxtra 200 mM	B-27 Supplement Minus Vitamin A (50X)
MEM Non-Essential Amino Acids Solution 10mM (100X)	H-EGF 20 ng/mL
MEM Sodium Pyruvate Solution 100mM (100X)	Heparin Solution, 0.2%
Neurobasal-A Medium, D-MEM/F-12 (1:1)	H-FGF-basic-154 20 ng/mL
Penicillin-streptomycin solution*stabil	H-PDGF-AA 10 ng/mL

Table 5. Cell culture chemicals and reagents.

Article	Cat. nom.	Supplier
B-27	17504044	Gibco, ThermoFisher Scientific Inc., Waltham, MA, USA
CellTiter-Glo (CTG) 2.0	G9243	Promega, Madison, USA
DMEM	41965062	Gibco, ThermoFisher Scientific Inc., Waltham, MA, USA
EGF (20 µg/mL)	C-60170	PromoCell, Heidelberg, Germany
Fetal calf serum (FCS)	F7524	Sigma-Aldrich, St. Louis, MO, USA
FGFb	C-60240	PromoCell, Heidelberg, Germany
Heparin	H3149-100KU	Sigma-Aldrich, Munich, Germany
HEPES Buffer Solution (1 M)	15630049	ThermoFisher Scientific, Waltham, MA, USA
H-PDGF-AA (10 µg/mL)	10013A	Peprotech, Rocky, Hill, NJ, USA
L-Glutamin, 200 mM	G7513	Merck, Darmstadt, Germany
MEM Non-Essential Amino Acids Solution (100X)	11140035	Gibco, ThermoFisher Scientific Inc., Waltham, MA, USA
Neurobasal-A Medium	1088802	ThermoFisher Scientific, Waltham, MA, USA
PBS	D8537	Sigma-Aldrich, St. Louis, MO, USA
Penicillin-streptomycin solution*stabil	P4333	Sigma-Aldrich, St. Louis, MO, USA
RPMI-1640	21875091	Gibco, ThermoFisher Scientific Inc., Waltham, MA, USA

Article	Cat. nom.	Supplier
Sodium pyruvate (100 mM)	11360039	ThermoFisher Scientific, Waltham, MA, USA
Synth-a-Freeze cryopreservation medium	A1254201	ThermoFisher Scientific, Waltham, MA, USA
Trypsin-EDTA Solution (1X)	T3924-100ML	Sigma-Aldrich, St. Louis, MO, USA
Vi-Cell XR Cell Viability AnalyzerTM solutions	B94987	Beckmann Coulter, Krefeld, Germany

3.1.2 Drugs

Table 6. Drugs.

Drug	Solvent	Stock concentration	Cat. nom.	Supplier
A-1155463	DMSO	100mM	HY-19725/CS-5398	Medchem Express, Monmouth Junction, NJ, USA
A-1210477	DMSO	7mM	A-9036	Active Biochem, Maplewood, NJ, USA
A-1331852	DMSO	10mM	CT-A133	ChemieTek, Indianapolis, IN, USA
Afatinib	DMSO	10mM	S1011	Selleckchem, Houston, TX, USA
Alectinib	DMSO	5mM	S2762	Selleckchem, Houston, TX, USA
Alpelisib	DMSO	10mM	HY-15244	Medchem Express, Monmouth Junction, NJ, USA
AMG-232	DMSO	10mM	CT-AMG232	ChemieTek, Indianapolis, IN, USA
APR-246	DMSO	50mM	S7724	Selleckchem, Houston, TX, USA
Axitinib	DMSO	50mM	A-1107	LC Laboratories, Woburn, MA, USA
Benzethonium Chloride	DMSO	100mM	PHR1425	Sigma-Aldrich, St. Louis, MO, USA
Bortezomib	DMSO	10mM	CT-BZ001	ChemieTek, Indianapolis, IN, USA
Busulfan	DMSO	10mM	S1692	Selleckchem, Houston, TX, USA
Cabozantinib	DMSO	10mM	CT-XL184	ChemieTek, Indianapolis, IN, USA
Ceritinib	DMSO	10mM	S7083	Selleckchem, Houston, TX, USA
Chloroquine	H2O	100mM	C6628-46	Sigma-Aldrich, St. Louis, MO, USA

(Continued on the following page)

Drug	Solvent	Stock concentration	Cat. nom.	Supplier
Cisplatin	H2O	1mg/mL = 3,33mM	S7083	Pharmacy
Cobimetinib	DMSO	10mM	HY-13064	Medchem Express, Monmouth Junction, NJ, USA
Crizotinib	DMSO	50mM	S1068	Selleckchem, Houston, TX, USA
Cytarabine	DMSO	100mM	HY-13605	Medchem Express, Monmouth Junction, NJ, USA
Dabrafenib	DMSO	25mM	CT-DABR	ChemieTek, Indianapolis, IN, USA
Dactinomycin	DMSO	10mM	HY-17559	Medchem Express, Monmouth Junction, NJ, USA
Dasatinib	DMSO	10mM	D-3307	LC Laboratories, Woburn, MA, USA
Daunorubicin	DMSO	10mM	HY-13062	Medchem Express, Monmouth Junction, NJ, USA
Decitabine	DMSO	100mM	S1200	Selleckchem, Houston, TX, USA
Doxorubicin	DMSO	10mM	D1515	Sigma-Aldrich, St. Louis, MO, USA
Entinostat	DMSO	100mM	CT-MS275	ChemieTek, Indianapolis, IN, USA
Entrectinib	DMSO	10mM	HY-12678	Medchem Express, Monmouth Junction, NJ, USA
Erdafitinib	DMSO	10mM	HY-18708	Medchem Express, Monmouth Junction, NJ, USA
Erlotinib	DMSO	100mM	HY-50896	Medchem Express, Monmouth Junction, NJ, USA
Etoposide	DMSO	100mM	HY-13629	Medchem Express, Monmouth Junction, NJ, USA
Everolimus	DMSO	10mM	E-4040	LC Laboratories, Woburn, MA, USA
Foretinib	DMSO	10mM	S1111	Selleckchem, Houston, TX, USA
Gemcitabine	DMSO	10mM	HY-B0003	Medchem Express
I-BET-151	DMSO	100mM	CT-BET151g	ChemieTek, Indianapolis, IN, USA
Idasanutlin	DMSO	100mM	HY-15676	Medchem Express, Monmouth Junction, NJ, USA
Imatinib	DMSO	100mM	HY-50946	Medchem Express, Monmouth Junction, NJ, USA
Irinotecan[a]	DMSO	10mM	S2217	Selleckchem, Houston, TX, USA
Lapatinib	DMSO	10mM	L-4804-100mg	LC Laboratories, Woburn, MA, USA

Drug	Solvent	Stock concentration	Cat. nom.	Supplier
Larotrectinib	DMSO	10mM	HY-12866-5mg	Medchem Express, Monmouth Junction, NJ, USA
Lorlatinib	DMSO	100mM	HY-12215-5mg	Medchem Express, Monmouth Junction, NJ, USA
Melphalan	DMSO	10mM	S8266	Selleckchem, Houston, TX, USA
Mercaptopurine	DMSO	100mM	HY-13677	Medchem Express, Monmouth Junction, NJ, USA
Merestinib	DMSO	10mM	HY-15514A	Medchem Express, Monmouth Junction, NJ, USA
Methotrexate	DMSO	50mM	59-05-2	Sigma-Aldrich, St. Louis, MO, USA
Mitoxantrone	DMSO	10mM	HY-13502A	Medchem Express, Monmouth Junction, NJ, USA
Navitoclax	DMSO	100mM	HY-10087	Medchem Express, Monmouth Junction, NJ, USA
Nilotinib	DMSO	50mM	N-8207-250	LC Laboratories, Woburn, MA, USA
Olaparib	DMSO	100mM	O-9201	LC Laboratories, Woburn, MA, USA
Paclitaxel	DMSO	10mM	HY-B0015	Medchem Express, Monmouth Junction, NJ, USA
Palbociclib	H2O	100mM	S1116	Selleckchem, Houston, TX, USA
Panobinostat	DMSO	10mM	P-3703	LC Laboratories, Woburn, MA, USA
Pazopanib	DMSO	100mM	P-6706	LC Laboratories, Woburn, MA, USA
Ponatinib	DMSO	10mM	S1490	Selleckchem, Houston, TX, USA
Rapamycin (Sirolimus)	DMSO	10mM	R-5000	LC Laboratories, Woburn, MA, USA
Ribociclib	DMSO	20mM	S7440	Selleckchem, Houston, TX, USA
Ruxolitinib	DMSO	100mM	INCB018424-2	ChemieTek, Indianapolis, IN, USA
Selinexor	DMSO	100mM	S7252	Selleckchem, Houston, TX, USA
Selitrectinib	DMSO	10mM	HY-101977	Medchem Express, Monmouth Junction, NJ, USA
Selumetinib	DMSO	100mM	HY-50706	Medchem Express, Monmouth Junction, NJ, USA
SN-38	DMSO	10mM	Hy-13704	Medchem Express, Monmouth Junction, NJ, USA

Drug	Solvent	Stock concentration	Cat. nom.	Supplier
Sorafenib	DMSO	10mM	S-8502	LC Laboratories, Woburn, MA, USA
Staurosporine	DMSO	10mM	T6680-	TargetMol, Wellesley Hills, MA, USA
Sunitinib	DMSO	10mM	S-8803	LC Laboratories, Woburn, MA, USA
Talazoparib	DMSO	10mM	HY-16106	Medchem Express, Monmouth Junction, NJ, USA
Tazemetostat	DMSO	100mM	CT-EPZ438	ChemieTek, Indianapolis, IN, USA
Temozolomide[a]	DMSO	100mM	S1237	Selleckchem, Houston, TX, USA
Temsirolimus	DMSO	10mM	T-8040	LC Laboratories, Woburn, MA, USA
Thioguanine	DMSO	100mM	HY-13765	Medchem Express, Monmouth Junction, NJ, USA
Thiotepa	DMSO	500mM	T6069	Sigma-Aldrich, St. Louis, MO, USA
Topotecan	DMSO	100mM	HY-13768A	Medchem Express, Monmouth Junction, NJ, USA
Trametinib	DMSO	35mM	CT-GSK212	ChemieTek, Indianapolis, IN, USA
Valproic acid	H2O	200mM	P4543	Sigma-Aldrich, St. Louis, MO, USA
Vandetanib	DMSO	10mM	V-9402-2,9mg	LC Laboratories, Woburn, MA, USA
Vemurafenib	DMSO	100mM	CT-P4032-2-50mg	ChemieTek, Indianapolis, IN, USA
Venetoclax	DMSO	10mM	CT-A199-2-10mg	ChemieTek, Indianapolis, IN, USA
Vinblastine	DMSO	10mM	HY-13780-10mM	Medchem Express, Monmouth Junction, NJ, USA
Vincristine	DMSO	10mM	S1241	Selleckchem, Houston, TX, USA
Vinorelbine	DMSO	100mM	S4269	Selleckchem, Houston, TX, USA
Vismodegib	DMSO	100mM	V-4050	LC Laboratories, Woburn, MA, USA
Volasertib	DMSO	10mM	CT-BI6727	ChemieTek, Indianapolis, IN, USA
Vorinostat	DMSO	100mM	V-8477	LC Laboratories, Woburn, MA, USA

3.1.3 Consumables

Table 7. Consumables.

Article	Supplier.
Conical tubes, 15 mL and 50 mL	ThermoFisher Scientific, Waltham, MA, USA
Cryovials	Carl Roth, Karlsruhe, Germany
Micropipette 10 µL, 100 µL, 200 µL and 1000 µL	Eppendorf, Hamburg, Germany
Microplates, 384 well plate, round bottom, black with clear bottom	Corning, Wiesbaden, Germany
Pipette filter tips, 20 µL, 100 µL, 200 µL and 1000 µL	Nerbe plus, Winsen/Luhe, Germany
Safe-Lock reaction tubes	Eppendorf, Hamburg, Germany
Safetyspace filter tips 5-300 µL	Sartorius, Göttingen, Germany
Serological pipettes, 5 mL, 10 mL and 25 mL	Sigma-Aldrich, St. Louis, MO, USA
Tissue Culture Flask T25 and T75	Greiner Bio-One GmbH, Frickenhausen, Germany
Vi-CELL® 4 ml Sample Vials	Beckmann Coulter, Brea, CA, USA

3.1.4 Kits

Table 8. Kits.

Article	Supplier.
QIAamp® DNA Mini Kit	Qiagen, Hilden, Germany

3.1.5 Instruments and machines

Table 9. Instruments and machines.

Instrument	Supplier
Benchtop centrifuge Allegra X-12R	Beckmann Coulter, Brea, CA, USA
CellMate® II Serological Pipette	Matrix Technologies Corporation, ThermoFisher Scientific, Waltham, MA, USA
Centrifuge 5810 R	Eppendorf, Hamburg, Germany
Mr. Frosty freezing container (Nalgene)	ThermoFisher Scientific, Waltham, MA, USA
Grant-bio PMS-1000i plate shaker	Grant, Royston, United Kingdom
Light microscope CKX31	Olympus, Hamburg, Germany
Multichannel pipette	Sartorius, Göttingen, Germany
NanoDrop 2000 Spectrophotometer	ThermoFisher Scientific, Waltham, MA, USA
San Francisco StoragePod	Roylan Developments, Fetcham Leatherhead, UK
Tecan Spark plate reader	Tecan, Männedorf, Switzerland
Vi-CELL XR automated cell counter	Beckmann Coulter, Brea, CA, USA
Waterbath SWB20	P-D Industriegesellschaft mbH, Dresden, Germany

3.1.6 Software

Table 10. Software.

Software	Version
Data Warrior	5.5.0
R	4.3.0
R studio	2023.03.1

Table 11. R packages.

R package	Version
base	4.3.0
broom	1.0.5
complexHeatmap	2.16.0
data.table	1.14.8
datawizard	**0.8.0**
dplyr	1.1.2
drc	3.0-1
ggplot2	3.4.2
ggpubr	0.6.0
ggrepel	0.9.3
graphics	4.3.0
grDevices	4.3.0
grid	4.3.0
gtable	0.3.3
gtools	3.9.4
janitor	2.2.0
methods	4.3.0
openxlsx	4.2.5.2
pacman	0.5.1
patchwork	1.1.2
plotly	4.10.2
pROC	1.18.4
RColorBrewer	1.1-3
reshape	0.8.9
reshape2	1.4.4
rlang	1.1.1
scales	1.2.1
stats	4.3.0
tidyverse	2.0.0

(Continued on the following page)

R package	Version
tools	4.3.0
utils	4.3.0
XLConnect	1.0.7
xlsx	0.6.5

3.2 Methods

3.2.1 Data base generation

The text, figures and table of section 3.2.1.1 have been taken from Jamaladdin et al. (44) and were originally written and generated by myself.

3.2.1.1 Pharmacokinetic data base

For the PK data base a total of nine PK parameters: maximum plasma concentration (Cmax), lowest plasma concentration reached by the drug before the next dose administration (Ctrough), steady-state concentration (Css), the integrated area under the plasma concentration-time curve (AUC), plasma half-life (T1/2), clearance (Cl), volume of distribution (Vd), time point at which maximum concentration is reached (Tmax) and plasma protein binding (PPB) were chosen (Table 12), based on their frequency of reporting in the US Food and Drug Administration (FDA) and European Medicines Agency (EMA) documents (44). As this study uses the INFORM *ex vivo* DSP drug library (29), the PK parameters were collected for the library which comprises 79 clinically available anticancer drugs. The library covers 8 relevant drug classes used in pediatric oncology (Supplementary Figure 1a). The majority of the drugs in the library are kinase inhibitors (n=32/79; 41%) followed by conventional chemotherapeutics (n=22/79; 28%), apoptotic modulators (n=9/79; 11%), epigenetic modifiers (n=7/79; 9%), antineoplastic agents (n=4/79; 5%), rapalogs (n=3/79; 4%), an antimalarial agent (n=1/79; 1%), and a differentiating agent (n=1/79; 1%) (44). The majority, 82% (n=65/79) of the drugs is approved by either the US FDA and/or the EMA whereas 13% (n=10/79) of drugs are still in clinical trial phase I–III and 5% (n=4/79) of the drugs are only used in pre-clinical research (Supplementary Figure 1b) (44). Drugs A-1155463, A-1210477, A-1331852 (all apoptotic modulators) and I-BET151 (differentiating agent) were excluded due to their status in preclinical research which lacked PK data. Additionally, selitrectinib was also excluded because of the absence of available PK data. As a result, PK data for a total of 74 drugs were collected. Drugbank, PubChem, FDA drug labels, and EMA Summary of Product characteristics (SmPcs) were used to report on the approval status and characteristics of the drugs (44).

Table 12. List of pharmacokinetic parameters.

PK parameter	Dimension	Unit	Definition
Cmax	Concentration	nM	Maximum plasma concentration
Ctrough	Concentration	nM	Lowest plasma concentration reached by the drug before the next dose
Css	Concentration	nM	Concentration where the rate of drug input is equal to the rate of drug elimination
AUC	Concentration over time	nM h	Total drug concentration as a function of time
T1/2	Time	h	Time where half of the initial dose is eliminated by the body
Cl	Volume over time	L/min/m2 or L/min	The volume of plasma from which a substance is completely removed per unit time
Vd	Volume over mass or surface	L/m2 or L/kg	Apparent volume into which the drug is distributed over tissue
Tmax	Time	h	Time point at which maximum concentration is reached
PPB	Percentage	%	Plasma protein binding

The search for studies reporting on the PK parameters was conducted between September 2020 to June 2021. The search terms "[drug name]" followed by "pharmacokinetics pediatric oncology" or "pediatric oncology phase I and/or phase II trial" were used in PubMed and Google. In cases where relevant information was not found, additional sources such as FDA drug labels, EMA SmPcs, and the US National Library of Medicine (NLM) database Clinicaltrials.gov were consulted (44).

Study selection was carried out based on specific criteria, with a priority given to studies involving the pediatric population, focusing on oncologic indications, and including phase I and II clinical studies (44). Drugs with special formulations, such as those utilizing nanotechnology and liposomes to improve drug delivery, were excluded from the selection process. To accurately represent the clinical scenario PK parameters measured after multiple dosing were selected, when available. In instances where PK data after multiple doses was not available, PK parameters following a single dose were used instead (44).

One publication was selected for each drug. If multiple potential publications existed, preference was given to the one closest to the clinically applied dose (recommended phase II dose or approved dose) (44). In cases where this criterion was not met, the publication that reported on most of the PK parameters was selected. To ensure accuracy and reliability, the chosen publication, parameters, and calculations were subsequently reviewed by a second reviewer. All relevant information was manually extracted and summarized for further analysis (44).

Additionally, the BBB score was calculated for all drugs in the library. This was done by using the calculator sheet published by Gupta et al. (45). It is important to note that this score only models passive diffusion and does not take active diffusion into account. The score reflects the probability of a compound being CNS active. The BBB score's range spans from a low probability (BBB score near 0) to a high probability (BBB score near 6) of a drug being CNS active. Consequently, higher BBB scores indicate a greater likelihood of BBB penetration. In order to calculate the BBB score, seven physicochemical properties were collected for each drug: number of aromatic rings, number of heavy atoms, molecular weight, number of hydrogen bond acceptor atoms, number of hydrogen bond donor atoms, topological polar surface area, and pKa. The pKa values were obtained from Drugbank (www.drugbank.com) and ChEMBL (www.ebi.ac.uk/chembl), while the remaining parameters were collected using the DataWarrior software (version 5.5.0) (44).

3.2.1.2 Primary patient tumor samples

Data from *ex vivo* DSP of primary patient samples was obtained from the INFORM DSP platform. Samples profiled from the 1st of July 2019 to 18th of January 2022 were collected. Until that date 196 patient samples with a variety of tumor entities were submitted for DSP, of which 60% (n=119/196) were successfully screened.

DSP data storage of INFORM patient samples had a diverse infrastructure, with room for improvement to make data analysis possible. Therefore, there was a high need to generate a single computable data base, containing all patient information for data analysis. This was executed in a multiple step approach. First, sub-data bases were assembled manually and merged into one main data base using R programming. The five sub-data bases assembled were as follows: INFORM DSP cohort (IDC), screen technical details (TD), NGS data, DSP output data, and quality control (QC) data.

The IDC and screen TD sub-data bases were manually assembled from three original data sources: (I) sample overview data (excel sheet, 196 patients including 20 different parameters), (II) drug screen data (excel sheet, 249 different sample types including 69 different parameters) and (III) several DSP output documents for each individual patient ("S-drive") (Figure 2). In detail, the content of original data source I was manually transferred to the IDC data base. The parameters not necessary for further analysis were deleted. Information reported in German was translated to English. The INFORM patient screen ID was manually selected from original data source II. Additionally, two extra parameters, INFORM patient screen ID and availability of DSP output data from source III were added resulting in a total of 8 parameters for 196 patient samples.

To minimize data transfer errors introduced by manual data compilation the data was double checked by using the 'VLOOKUP' function in Excel. The screen TD data base was assembled by using the original data source II. After selecting several parameters in the original data source II, the information of 123 screens was transferred to the screen TD data base. The screen ID was double checked again and 56 undesired parameters were deleted which resulted in 13 final parameters in the screen TC data base.

For generating the NGS data base a ready-to-use excel file was provided by the INFORM NGS team, which included 103 patient samples and 29 parameters. The INFORM screen ID was manually added to the file as an extra column, finally resulting in 535 data points (several mutations for each patient) with 30 parameters.

The original data source III was used to generate the DSP output data base and the QC data base (Figure 2). The original data source III contains a variety of folders, in their entirety containing the DSP output data for each patient. Data was extracted manually from each folder, ensuring alignment of all data points with the same algorithm version. Only the excel document summarizing the DSP screen parameters and the HTML file summarizing the QC were selected. After manual curation of each individual DSP file and manual curation as well as conversion of each individual QC HTML file in Excel format, all files were transferred to compile all data output files in one format and one location. This resulted in 119 excel files in the DSP output data folder where each file included all drugs screened varying from 28 to 79 drugs, with 40 corresponding parameters. For the QC data base this resulted in 119 excel files with 6 by 22 parameters each. Depending on the type of analysis the data bases were merged using R programing.
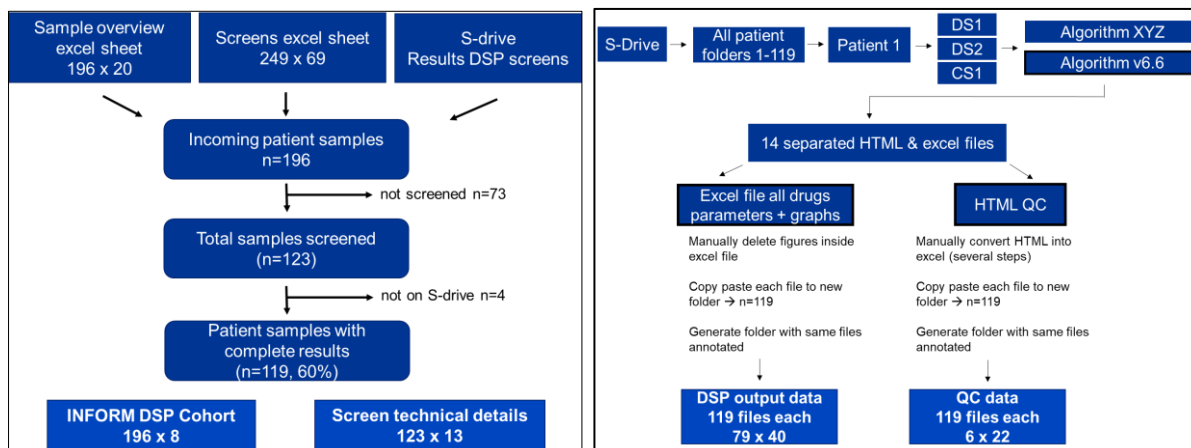
Figure 2. Overview of data bases used to generate one computable data base, in one location, containing all patient information for data analysis. Left: INFORM DSP cohort (IDC) and screen technical details (TD) data bases generated from original data bases sample overview excel sheet, screens excel sheet and S-drive. Right: generating the DSP output and quality control (QC) data from the S-drive.

3.2.1.3 Positive control cell line models

PCC models (both established as well as long-term culture cell lines from INFORM samples) with specific molecular alterations and a clinically proven drug-target relationship (Table 13), were used as a training set to investigate and evaluate the influence and predictive power of different PD and PD-PK parameters. The drugs matching the molecular alteration should show more efficacy in the DSP experiments compared to the other drugs. In total n=7 different cell lines (Table 13), were screened in biological triplicates. A matching drug was defined as a drug with a clinically proven drug-target relationship. Therefore, each cell line has a set of matching and non-matching drugs.

Table 13. Positive control cell line (PCC) models harboring specific molecular alterations with a clinically proven drug-target relationship.

Cell line	Diagnosis	Molecular alteration	Drug class	Matching drug	PMID
NB1	Neuroblastoma	ALK amplification	ALKi	Ceritinib	PMID: 34780709
				Alectinib	PMID: 33010107
				Crizotinib	PMID: 33568345
				Lorlatinib	DOI: 10.1200/JCO.2020.38.15
				Entrectinib	DOI: 10.1200/JCO.2020.38.15
LAN5	Neuroblastoma	ALK R1275Q	ALKi	Ceritinib	PMID: 34780709
				Alectinib	PMID: 33010107
				Crizotinib	PMID: 33568345
				Lorlatinib	DOI: 10.1200/JCO.2020.38.15
				Entrectinib	DOI: 10.1200/JCO.2020.38.15
SJ-GB-M2	High grade glioma	MET fusion	METi	Cabozantinib	PMID: 27825636
				Foretinib	PMID: 27821605
				Merestinib	PMID: 29188469
				Crizotinib	PMID: 33676017

Cell line	Diagnosis	Molecular alteration	Drug class	Matching drug	PMID
BT40	Pleomorphic Xanthoastrocytoma	BRAF V600E	BRAFi	Dabrafenib	PMID: 31811016
				Vemurafenib	PMID: 32523649
				Sorafenib	PMID: 24803676
			MEKi	Selumetinib	PMID: 31151904
				Trametinib	PMID: 36375115
BT278	High grade glioma (H3.3 G34R)	NF1 p.R440X	MEKi	Trametinib	PMID: 33939292
				Selumetinib	PMID: 32187457
				Cobimetinib	PMID: 35715627
NCI-H3122	Lung carcinoma	EML4:ALK fusion	ALKi	Ceritinib	PMID: 34780709
				Alectinib	PMID: 33010107
				Crizotinib	PMID: 33568345
				Lorlatinib	DOI: 10.1200/JCO.2020.38.15
				Entrectinib	DOI: 10.1200/JCO.2020.38.15
I070_004	Inflammatory myofibroblastic tumor	ETV6:NTRK3 fusion	TRKi	Entrectinib	PMID: 31838007
				Larotrectinib	PMID: 32105622
				Selitrectinib	PMID: 28578312

Methods

3.2.2 Cell culture

3.2.2.1 Positive control cell line models

Cell line models were maintained and experiments were conducted under sterile conditions within a laminar flow hood, unless otherwise specified. The specific cell line models used in this study are listed in Table 2 and Table 13. All cell lines were incubated at 37 °C and within controlled environment of 5% CO_2.

Before conducting any experiment, the authenticity and contamination status of the purchased cell line models were investigated. Authentication and contamination testing were performed using the Multiplex Cell Line Authentication test (MCA) (46) and the Multiplex cell Contamination Test (McCT) (46). The QIAmp DNA Mini Kit was used according to the manufacturer's protocol. Multiplexion GmbH (Friedrichshafen, Germany) provided the certification, confirming the absence of bacterial, Mycoplasma, and viral contaminants as well as cross-contamination with other cell lines. Moreover, on a weekly basis, the cell line models were screened for Mycoplasma contamination using the PlasmoTestTM Mycoplasma Detection Kit. Additionally, to ensure optimal conditions, the overall health and confluency of the cell line models were assessed visually using light microscopy every alternate day.

All cell line models were cultured and expanded in T75 (75 cm^2) flasks for adherent cells. Medium was changed for all cell line models every 2-3 days. When the cell confluency reached approximately 80% (one to two times a week), the supernatant was either collected (semi-adherent cell line models) or discarded (adherent cell line models) and the cells in the flask were washed with PBS to remove debris and protein residues. Subsequently, Trypsin was applied for 1-2 minutes at 37 °C to detach the cells from the flask surface. The Trypsin reaction was stopped by adding the respective medium, and the cells were then collected in a 50 mL tube and centrifuged at 1000 rpm for 5 minutes. For the semi adherent cells this was added to the collected supernatant before spinning down in the centrifuge. For cell line model LAN5, the cells were detached using the respective medium. After resuspending the cell pallet, the cells were split in a fixed ratio, fit for the characteristics of each cell line model. The divided cells were then transferred into new flasks for further cultivation. When used for experiments, the cells were counted and seeded according to the specific requirements of each experiment.

3.2.2.2 Freezing of cells

Cells were detached as described in 3.2.2.1 and subsequently counted as described in 3.2.3.1. For each cell line model, a total of 2 million cells were gently resuspended in either 1 mL Synth-a-Freeze cryopreservation medium (BT278, I070_030) or the respective cell medium with the addition of 10% included dimethyl sulfoxide (DSMO) to prevent the formation of cristals, in each cryovial. However, for the cell lines I070_030, NB1, and BT40, 4 million cells were counted per cryovial, whereas for NCI-H3122 and LAN5, 5 million cells were counted per cryovial. The cryovials were first placed in a Mr. Frosty freezing container to ensure a gradual freezing rate (-1°C /min). After 72 hours the cryovials were premanently transferred to the liquid nitrogen tank for long-term storage.

3.2.2.3 Primary patient tumor samples

The preparation of PPT samples followed the protocol described by Peterziel et al. (29). The actual experiments were carried out by the INFORM *ex vivo* DSP team.

3.2.3 Drug response testing

3.2.3.1 Experimental setup metabolic activity assay

The PCC models were prepared for experiments as described in section 3.2.2.1. Subsequently, the cell viability and cell count per 1 mL were assessed using the Vi-Cell XR automatic cell counter. The Vi-Cell XR automatic cell counter distinguishes between living and dead cells, using Trypan blue staining, enabling counting of both viable and non-viable cells. A viability of 65% or higher (29) was considered suitable for further experiments. The PPT sample experiments were conducted by the INFORM *ex vivo* DSP team as described in the work of Peterziel et al. (29).

The PCC models were seeded on ready-to-use 384 round-bottom well plates which were designed at the Institute for Molecular Medicine Finland (FIMM) High Throughput Biomedicine Unit, HiLIFE (University of Helsinki, Finland) (10,27,29). These plates were pre-printed with 75-78 clinically relevant anticancer drugs from the INFORM drug library (29). Additionally the plates DMSO as negative control and benzothonium chloride (BzCl) as positive control. Each drug was pre-printed in duplicate and five different concentrations covering five orders of magnitude (e.g. 1-10000 nM).

Three drug plates were used per experiment to cover the total number of drugs. The plates were stored at room temperature under oxygen and moisture free conditions in a StoragePod (San Francisco StoragePod, Roylan Developments, Fetcham Leatherhead, UK). The same drug plates were used for the PPT samples (29). Additionally, the same experimental set up was used for the PPT samples unless stated otherwise.

A total cell number of 500 cells/well was seeded for PCC models. For the PPT samples, the INFORM *ex vivo* DSP team aimed to seed 1000 cells/well, although this varied between 400 cells/well to 1000 cells/well depending on the received tumor sample and cell viability. For the PCC models the same procedure was followed as done for the PPT samples by the INFORM DSP team (29). The final volume per well was 25 μL of the respective medium. Following seeding, the plates were centrifuged for three minutes at 1200 rpm and subsequently incubated for 72 hours at 37 °C and 5% CO2 (29).

For the Luminescent Cell Viability Assay, 15 μL of CellTiter-Glo 2.0 (Promega, Madison, USA) was added per well, resulting in a total volume of 40 μL per well. In this assay the quantitation of ATP is determined, which serves as an indicator of metabolic active cells. To ensure accurate measurements, the plates were protected from light and shaken for 5 minutes on a plate shaker at 400 rpm. Subsequently, the plates were centrifuged for three minutes at 300 g and then incubated at room temperature for 20 minutes before luminescence was measured using the Tecan Spark plate reader (Tecan, Männedorf, Switzerland). The drug effect was measured as percentage inhibition where the raw data obtained from the metabolic activity essay was normalized to the negative and positive controls as shown in Equation 1 (29).

$$\text{Equation 1} \qquad \% \ inhibition = \frac{mean(DMSO) - (test\ drug)}{mean(DMSO) - mean(BzCl)}$$

3.2.3.2 Pharmacodynamic parameter calculation

PD parameters as shown in Table 14 were collected from the DSP experiments in PCC models and PPT samples and were divided into measured (data measured in the assay) and derived (calculated based on measured data) parameters.

Table 14. List of measured and derived pharmacodynamic (PD) parameters.

Measured PD parameter			
PD parameter	**Dimension**	**Unit**	**Definition**
IC50	Concentration	nM	Half maximal inhibitory concentration
IC75	Concentration	nM	75% inhibitory concentration
PI5	Percentage	%	Maximum effect at highest measured concentration
Derived PD parameter			
PD parameter	**Dimension**	**Unit**	**Definition**
DSS	n.a.	n.a.	Drug Sensitivity Score. Quantitative scoring approach based on continuous model estimation and interpolation to summarize the dose response relationships (26)
DSS0	n.a.	n.a.	Similar calculation DSS but Amin^l = 0 (Horizontal baseline effect)
AUC	n.a.	n.a.	Area under the curve calculated based on the trapezoidal method

The measurement and calculation of all PD parameters was conducted using two distinct algorithms. For the PCC models, analysis was performed using the ShinyApp interactive Therapy Response eXploration (iTReX) (47) while the PPT samples were analyzed using an in-house automated pipeline (29). Both algorithms are based on the Yadav et al. (26) algorithm but have been adapted in certain ways. ElHarouni et al. reported only on one difference in curve fitting between their algorithm and Yadav et al.'s, which is the change from a four-parameter logistic (4PL) model, initially used by Yadav et al., to a five-parameter logistic (5PL) model, used by ElHarouni et al.

The IC50, IC75 (75% inhibitory concentration) and PI5 (maximum effect at highest measured concentration) were measured from the experiments and automatically provided by the algorithms. The DSS is a quantitative single metric derived from the AUC of a dose response

curve using multiple parameters and normalizing for several effects in two steps (26). DSS1 is derived from the integration of the dose range as a continuous function, comprising parameters such as the IC50, top and bottom asymptotes, slope hill, and a minimum activity level (26). In the formula of the DSS1 calculation, a correction is made for the minimum effect level and normalization of data for different scales. To account for drugs with efficacy primarily at higher concentrations, as opposed to those effective at lower concentrations, an extra normalization step is carried out using the upper asymptote, leading to the creation of DSS2. Additionally, DSS2 undergoes further normalization based on the active dose range, resulting in the formation of DSS3 (26). The DSS0 is calculated in the same manner as the DSS, with the exception that the Amin value (representing the horizontal baseline effect) is set to 0, as compared to the standard default of Amin = 10 in the DSS calculation.

The AUC for the PCC models as well as the PPT samples was calculated over the entire concentration range of each drug by applying the trapezoidal rule. For curve fitting a 4PL approach was applied.

3.2.4 Pharmacodynamic pharmacokinetic parameter calculation

3.2.4.1 Drug sensitivity score (DSS) Cmax parameter

In order to incorporate a clinical filtering step and generate a single parameter that excludes drugs that are clinically not achievable, the PD parameter DSS and PK parameter Cmax were implemented together. The distance between the ^{10}log of Cmax and ^{10}log of the IC50 (denoted as X, Equation 2) was calculated for each drug by subtracting these two parameters. A larger distance between these two points indicates a more desirable drug effect, as the half maximum inhibitory concentration is much lower than the maximum concentration which can be reached in the patient.

To address the issue of comparing the effectiveness of different drugs based on the magnitude of the positive X value, a standardization step was implemented, based on the concentration which achieves the maximum possible effect for a given drug. To this end, the distance between parameter the highest measured concentration of a drug (C5) and IC50 was calculated by subtracting the two parameters (denoted as Y, Equation 3) from each other. It should be noted that obtaining the concentration at which the maximum percentage inhibition is 100% was not possible in this study. Instead, C5 was selected under the assumption that the highest concentration measured in the experiment should reasonably well correspond to the highest percentage inhibition achievable.

In cases where X values are negative, indicating that IC50 is higher than the Cmax, the drug would not be clinically attainable at that dose in the patient. Consequently, these drugs were excluded from further calculations. Furthermore, if Y is negative, it suggests that IC50 would be higher than C5. This would result in an unreliable outcome since it is biologically implausible and likely indicates an error in the determination of IC50 by extrapolation of the curve.

Positive X and Y values, were divided resulting in a ratio (Equation 4).

Equation 2 $\qquad \text{Cmax} - \text{IC50} = \text{X}$

Equation 3 $\qquad \text{C5} - \text{IC50} = \text{Y}$

Equation 4 $\qquad X/Y = \text{ratio}$

In situations where the X value exceeds the Y value, resulting in a larger Cmax IC50 distance compared to the IC50 C5 distance, the resulting ratio will be greater than 1. However, in order to maintain consistency with the understanding that the effect of the drug cannot exceed 100%, the ratio was capped at a value of 1. By setting the ratio to 1 in such cases, it ensures that the impact of the drug is not overestimated beyond the maximum achievable effect of 100%. This approach maintains a realistic representation of the drug's efficacy while facilitating straightforward calculations and interpretations in the analysis.

The ratio was then multiplied by the DSS resulting in the DSS Cmax (Equation 5).

Equation 5 $\qquad \text{ratio} \times \text{DSS} = \text{DSS Cmax}$

Thus, the final index penalizes all those drugs where the maximum theoretical effect level cannot be achieved due to Cmax limitations.

3.2.4.2   Area under the curve (AUC) Cmax parameter

The PK parameter Cmax was integrated into the AUC calculation by performing the AUC calculation as previously described, but substituting C5 in the experiment with the Cmax value. This adjustment was made to ensure that the effect remains within the limits of clinically attainable concentrations.

3.2.5   Data analysis and graphics

I used the DataWarrior software (version 5.5.0) to collect physiochemical properties of the drugs included in the PK data generation, see section 3.2.1.1. Data preparation, analysis and graphics were all carried out using R (version 4.3.0). The R packages used are listed in Table 11. For curve fitting and AUC calculation I used the "drc" package. And I generated all graphs using the "ggplot2" package.

3.2.5.1   Z-score calculation

I calculated the z-score for each parameter investigated in this study. This was done on an entire cohort basis meaning that for each drug, the z-score was calculated over all the respective samples included in the calculation. This approach allowed for improved comparison of the different data sets and parameters.

The z-scores for all parameters, except for DSS Cmax, were calculated using the "scale" function in base R. However, for DSS Cmax, a different approach was applied due to specific considerations. For each drug the mean (μ) and standard deviation (σ) as shown in Equation 6 were calculated for the raw DSS values across all samples. Subsequently, the z-score for DSS Cmax was derived by using x as the DSS Cmax value for a specific drug in a given sample, and calculating the z-score (Equation 6) using the previously determined μ and σ values corresponding to the raw DSS data for each respective drug. This approach was applied to address the issue of unfair exclusion of drugs with only one sample (n=1) after clinical filtering steps implementation. As calculating the z-score for a cohort with an n=1 sample is not feasible, this approach ensured that all drugs, even those with limited samples, could be appropriately included in the analysis without compromising the integrity of the results.

$$\text{Equation 6} \qquad Z = \frac{x - \mu}{\sigma}$$

3.2.5.2 Receiver operating characteristics analysis

ROC analysis was carried out to investigate the predictive value of different parameters in finding the matching drug. The AUC of the ROC curve was used to describe this predictive value. The cut off value of each parameter was determined by calculating and maximizing Youden's J as shown in Equation 7. A higher J value indicates a better discriminatory ability within the test, therefore, the cut off value is chosen at the highest J.

$$\text{Equation 7} \qquad J = \text{Sensitivity} + \text{Specificity} - 1$$

4 Results

4.1 Data bases

4.1.1 Pharmacokinetic data base

The text, figures and table in sections 4.1.1.1 and 4.1.1.2 have been taken from Jamaladdin et al. (44) and were originally written and generated by myself.

4.1.1.1 Pharmacokinetic parameter distribution

Data on PK parameters was available for a total of n=74/75 (99%) drugs. Among these, PK parameters were available from pediatric cohorts for n=48/74 (65%) drugs, from cohorts including both children and young adults (maximum age of 24 years) for n=4/74 (5%) drugs, and from adult cohorts for n=22/74 (30%) (Figure 3) (44).

My aim was to report on the Cmax observed during the steady state phase, which occurs during multiple administrations of a drug, for example at the end of a treatment cycle. This phase was selected due to its capacity to provide an optimal representation of PK, given the continuous treatment regimen of drugs administered to patients within the clinical setting. Cmax values during steady state are usually higher when compared to those observed after a single dose, depending on factors such as the drug's half-life and its accumulation in the body. PK parameters were reported following multiple dosing during steady state for n=33/74 (45%) drugs, and after single dosing for n=25/74 drugs (34%) (Figure 4) (44). For n=6/74 (8%) drugs, some PK parameters were reported on during the steady state and others after one dose (Figure 4) (44).
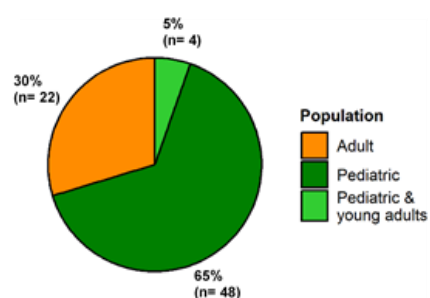
Figure 3. Population distribution across drugs in the pharmacokinetic data base (44).
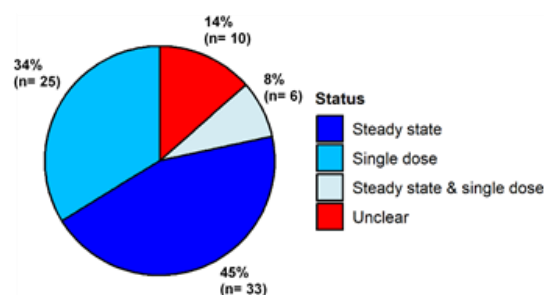
Figure 4. Period at which the pharmacokinetic parameters were measured for each drug (44).

For the remaining 10 (14%) drugs no information on dosing and sampling timepoint, single-dose or steady state, was available (44). The stage at which the PK parameters were measured can be found in the Supplementary Table of Jamaladdin et al. (44). Among the nine PK parameters, information was available for most of the drugs. Specifically the following parameters were reported on for the majority of the drugs: Cmax for n=73/74 (97%), AUC for n=69/74 (92%), PPB for n=66/74 (88%), T1/2 for n=57/74 (76%), Tmax for n=54/74 (72%), Cl for n=52(69%) and Vd for n=37/74 (49%) (Figure 5) (44). Conversely, Ctrough and Css demonstrated comparatively lower reporting frequencies, with 28% (n=21/74) and 5% (n=4/74) of the drugs (Figure 5) (44).
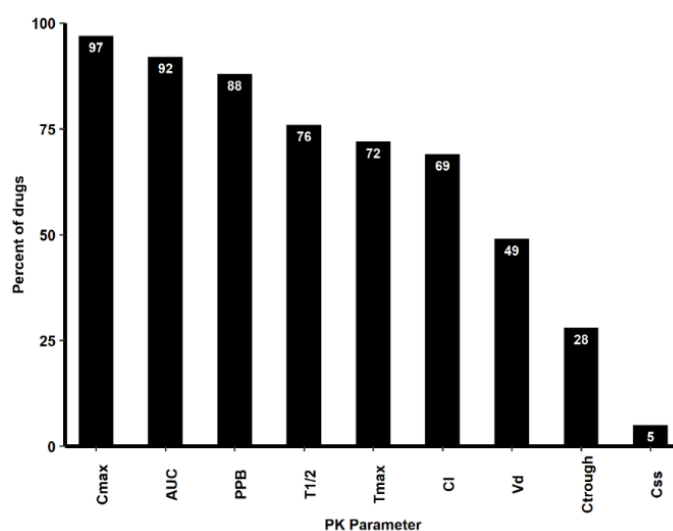
Figure 5. Percentage of drugs found for each pharmacokinetic parameter. Cmax: maximum plasma concentration, AUC: the integrated area under the plasma concentration-time curve, PPB: plasma protein binding, T1/2: plasma half-life, Tmax: time point at which maximum concentration is reached, CL: clearance, Vd: volume of distribution, Ctrough: lowest plasma concentration reached by the drug before the next dose administration, Css: steady-state concentration (44).

An overview of the PK parameters Cmax, Ctrough, Css, AUC, Tmax, T1/2, PPB, Vd, and Cl is listed by active pharmaceutical ingredient (API) generic name of the drugs in Table 15 (44). For each drug, the approval status, the dose, dose unit and route of administration were reported. In order to ensure comparability and applicability of all drugs and PK parameters the dose units reported in various publications were converted to a single unit per parameter. The Cmax, Ctrough, and Css, initially reported in weight/volume units (e.g., ng/mL), were converted to molar concentrations (nM) (Table 15). Similarly, AUC values, originally reported

on in weight time/volume units (ng h/mL), were transformed into molar units (nM h). Additionally, time-related parameters such as Tmax and T1/2 were converted to hours (44).

For intravenous route of administration, the infusion time was added as originally reported on in the publications. Within the drug library, the following five (7%) drugs are prodrugs: decitabine, gemcitabine, irinotecan, mercaptopurine and temozolomide (Table 15) (44). Given that decitabine, gemcitabine, mercaptopurine, and temozolomide do not undergo hepatic conversion, the distinct metabolites of these prodrugs have not been individually listen in Table 15 (44). Temozolomide undergoes conversion under physiological pH, while decitabine, gemcitabine, and mercaptopurine undergo intracellular conversion. The conversion of irinotecan is hepatic and takes place through carboxylesterase enzymes. Therefore its active metabolite SN-38, has been listed separately in Table 15, as both prodrug and active metabolite are relevant for *in vivo* and *in vitro* experiment (44).

Drugs interact with plasma proteins resulting in only the free unbound fraction of a drug to be pharmacologically active in the body. Therefore, the percentage PPB was included in Table 15. In the Supplementary Table of Jamaladdin et al. (44), precise details regarding the specific protein to which the drug binds were also documented. Additionally, information on Ctrough, Css, Vd, Cl, properties of statistical distribution, calculations for unit conversion and drug characteristics was provided in the Supplementary Table of Jamaladdin et al. (44).

4.1.1.2 Blood-Brain Barrier (BBB) Score

The BBB Score, an indicator of a drug's probability to penetrate the BBB, was assessed for all 74 drugs and summarized in Supplementary Table 1. The score determination was based on seven physicochemical properties (45) of the drugs, as detailed in Supplementary Table of Jamaladdin et al. (44). Notably, around 40% (n=30) of the drugs exhibited a BBB Score ranging from 0 to 2 (45), signifying an extremely low predicted chance to be CNS active and 33% (n=25) demonstrated a BBB Score between 2 and 3, indicating very low predictive chance to be CNS active. For 16% (n=12) of the drugs, a BBB Score of 3 to 4 was observed, reflecting a low chance to be CNS active. Furthermore, 5% (n=4) of the drugs carried a BBB Score in the 4 to 5 range, suggesting an intermediate likelihood to be CNS active and 1% (n=1) of the drugs exhibited a BBB Score of 5 to 6, resulting in a high likelihood to be CNS active (44).

Table 15. Overview of key pharmacokinetic parameters for 74 anticancer drugs in the INFORM drug library. p.o: per os, i.v. intra venous, nM: nanomolar, Cmax: maximum plasma concentration, AUC: area under the plasma concentration-time curve, Tmax: time point at which maximum concentration is reached, T1/2: plasma half-life, h: hour, SmPc: Summary of Product characteristics, FDA: Food and Drug Administration. Prodrug[a], active metabolite[b], median[c], range[d], adult[e], pediatric[f], YA: young adults (maximum age of 24 years), PK values are given as a mean unless stated otherwise. NCT01742286[g]. https://doi.org/10.3109/10428199209053588[h] (44).

Generic name	Approval status	Dose	Dose unit	Route	Infusion time (h, min)	Population	Cmax (nM)	AUC (nM h)	Tmax (h)	T1/2 (h)	Protein binding (%)	PMID
Afatinib	Approved[e]	40	mg	p.o.	-	Adult	121	1869	3.0[c]	42.8	95	23161335
Alectinib	Approved[e]	600	mg	p.o.	-	Adult	1401	11189	4.2[c]	-	>99	25153538
Alpelisib	Approved[f]	300	mg	p.o.	-	Adult	6727[c]	75202[c]	4.0[c]	7.5[c]	89	30543347
AMG-232	PhaseI/II	240	mg	p.o.	-	Adult	2498	21634	2.8[c]	14.3	97.5	31359240
APR-246	Phase III	60	mg/kg	i.v.	2h	Adult	278044	1786709	2.4	3.7	-	22965953
Axitinib	Approved[e]	2.4	mg/m2/dose	p.o.	-	Pediatric	123[c]	380[c]	1.5[c]	2.5[c]	>99	30394521
Bortezomib	Approved[e]	1.3	mg/m2	i.v.	Bolus	Pediatric	213	-		14.9	83	18316568
Busulfan	Approved[f]	1	mg/kg	p.o	-	Pediatric	5640	16635	1.2	2.0	32	11833485
Cabozantinib	Approved[f]	40	mg/m2/day	p.o.	-	Pediatric	3376	59839	7.4	79.1	>99.7	29693796
Ceritinib	Approved[e]	500	mg/m2	p.o.	-	Pediatric	1595	28846	5.9[c]	-	97	[g]
Chloroquine	Approved[f]	150	mg	-	-	Pediatric	4470	69401	6.9	-	46-74	18294337
Cisplatin	Approved[f]	75 - 120	mg/m2	i.v.	1, 6 & 72h	Pediatric	5066	44993	-	25.9	90	11599657
Cobimetinib	Approved[e]	60	mg	p.o.	-	Adult	514	8168	2.4[c]	43.6	95	27424159
Crizotinib	Approved[f]	280	mg/m2	p.o.	-	Pediatric	1592	15521	3.8	36.0	91	28032129

(Continued on the following page)

Generic name	Approval status	Dose	Dose unit	Route	Infusion time (h, min)	Population	Cmax (nM)	AUC (nM h)	Tmax (h)	T1/2 (h)	Protein binding (%)	PMID
Cytarabine	Approved[f]	3000	mg/m2	i.v.	3 h	Adult	54400	160200	-	0.8	13	9402329
Dabrafenib	Approved[f]	5.25	mg/kg	p.o.	-	Pediatric	2856	7872[c]	2.1[c]	8.0	99.7	31506385
Dactinomycin	Approved[f]	0.70 - 1.50	mg/m2	i.v. bolus	-	Pediatric	20	35[c]	0.3	0.0	5	16115931
Dasatinib	Approved[f]	65	mg/m2	p.o.	-	Pediatric	318	795[c]	1.0	2.7	96	21263099
Daunorubicin	Approved[f]	1.5	mg/kg	i.v.	10-55 min	Adult	630	1280	-		97	2927175
Decitabine[a]	Approved[e]	20	mg/m2	i.v.	1 h	Pediatric	1288	942	0.8	0.5	<1	29034009
Doxorubicin	Approved[f]	40	mg/m2	i.v.	24 h	Pediatric	116[c]	-			74-76	11979457
Entinostat	Phase III	4	mg/m2	p.o.	-	Pediatric & YA[e]	141[c]	3087	1.0[c]	0.0	-	33438318
Entrectinib	Approved[f]	600	mg	p.o.	-	Adult	2500		4-6[d]	0.0	>99%	28183697
Erdafitinib	Approved[e] FDA	9	mg	p.o.	-	Adult	4519	88650	2.7[c]	53.4	99.8	31088831
Erlotinib	Approved[e]	85	mg/m2	p.o.	-	Pediatric	5134[c]	77267[c]	2.0[c]	9.8[c]	95	18794549
Etoposide	Approved[f]	102	mg/m2	i.v.	242 min	Pediatric	25674[c]	131281[c]	-	0.2[c]	97	8402676
Everolimus	Approved[f]	5	mg/m2	p.o.	-	Pediatric	63[c]	250[c]	1.0[c]	-	74	17947729
Foretinib	Phase II	30	mg	_	-	Adult	76	1181	3.0[c]	-	-	27821605
Gemcitabine[a]	Approved[e]	1200	mg/m3	i.v.	30 min	Pediatric	66490	34068	-	0.2	10	15197207
Idasanutlin	Phase III	400	mg	p.o.	-	Adult	6391	328495	-	31.2	-	31062077

(Continued on the following page)

Results

Generic name	Approval status	Dose	Dose unit	Route	Infusion time (h, min)	Population	Cmax (nM)	AUC (nM h)	Tmax (h)	T1/2 (h)	Protein binding (%)	PMID
Imatinib	Approved[f]	340	mg/m2/day	p.o.	-	Pediatric	5065	80225	3.7	9.2	95	15231574
Irinotecan[a]	Approved[e]	50	mg/m2/day	i.v.	1 h	Pediatric	1237	4476	-	4.7	30-68	17925558
Lapatinib	Approved[e]	900	mg/m2	p.o.	-	Pediatric	10670[c]	94998[c]	5.6[c]	-	>99	20713864
Larotrectinib	Approved[f]	100	mg	p.o.	-	Pediatric	2159	9780	0.9	1.8	70	29606586
Lorlatinib	Approved[e]	100 1dd	mg	p.o.	-	Adult	1400	12462	1.0[c]	-	66	29074098
Melphalan	Approved[f]	80	mg/m2	i.v.	-	Pediatric	9404	6553	-	-	60-90	27092812
Mercaptopurine[a]	Approved[f]	50	mg/m2	p.o.	-	Pediatric	1080	1805[c]	1.0[c]	1.1[c]	19	32519032
Merestinib	Phase II	120	mg	p.o.	-	Adult	726	11203	4.5[c]	9.9	-	30833489
Methotrexate	Approved[f]	5	g/m2	i.v.	24h	Pediatric	72260[c]	1319340[c]	-	-	46.5-54	23187460
Mitoxantrone	Approved[f]	12	mg/m2	i.v.	1 h	Adult	697	1170	-	17.0	78	[h]
Navitoclax	Phase III	315	mg/day	p.o.	-	Adult	6608	93369	5.3	15.1	-	21094089
Nilotinib	Approved[f]	230	mg/m2	p.o.	-	Pediatric	808	10113	2.5[c]	-	98	31676669
Olaparib	Approved[e]	187.5	mg/m2	p.o.	-	Pediatric	18275	76645	1.5[c]	0.0	82	35593736
Paclitaxel	Approved[e]	430	mg/m2	i.v.	24 h	Pediatric & YA[e]	1019	26232	-	10.5	94	17668866
Palbociclib	Approved[e]	75	mg/m2	p.o.	-	Pediatric & YA[e]	313	4958	4.9	15.8	85	33405376

(Continued on the following page)

Results

Generic name	Approval status	Dose	Dose unit	Route	Infusion time (h, min)	Population	Cmax (nM)	AUC (nM h)	Tmax (h)	T1/2 (h)	Protein binding (%)	PMID
Panobinostat	Approved[e]	20	mg/m2	p.o.	-	Pediatric & YA[e]	59[c]	296[c]	-	-	90	32809242
Pazopanib	Approved[e]	450	mg/m2	p.o.	-	Pediatric	136677	900516	3.5	-	>99	23857966
Ponatinib	Approved[e]	45	mg	p.o.	-	Adult	145	2433	4.0	22.0	>99	SmPc Iclusig
Rapamycin (Sirolimus)	Approved[f]	2.5	mg/m2/day	p.o.	-	Pediatric	23	493	3.2	26.6	92	23266742
Ribociclib	Approved[e]	350	mg/m2	p.o.	-	Pediatric	4626	63745	2.1[c]	30-41[d]	70	28432176
Ruxolitinib	Approved[f]	50	mg/m2	p.o.	-	Pediatric	3820	18800	-	3.3	97	25976292
Selinexor	Approved[e] FDA	55	mg/m2	p.o.	-	Pediatric	2202	10437	3.0	8.0	95	27507877
Selumetinib	Approved[f] FDA	25	mg/m2/dose	p.o.	-	Pediatric	1744	4278	1-1.5^	6.2	98.4	FDA report koselugo
SN-38[b]		50	mg/m2	i.v.	1 h	Pediatric	33	214	-	7.6	95	17925558
Sorafenib	Approved[e]	200	mg/m2/dose	p.o.	-	Pediatric	17856	129510	3.4	25-48[d]	99.5	22962440
Sunitinib	Approved[e]	15	mg/m2	p.o.	-	Pediatric	42[c]	2[c]	7.0[c]	38.7[c]	95	21690570
Talazoparib	Approved[e]	600	ug/m2	p.o.	-	Pediatric	47[c]	219[c]	1.0[c]	51.2[c]	74	31724813
Tazemetostat	Approved[f] FDA	800	mg	p.o.	-	Adult	1447	5832	1.1[c]	3.6	88	29650362
Temozolomide[a]	Approved[f]	200	mg/m2	p.o.	-	Adult	82409	180269	0.5	1.7	8-36	10561328

(Continued on the following page)

Generic name	Approval status	Dose	Dose unit	Route	Infusion time (h, min)	Population	Cmax (nM)	AUC (nM h)	Tmax (h)	T1/2 (h)	Protein binding (%)	PMID
Temsirolimus	Approved[e]	75	mg/m2	i.v.	1 h	Pediatric	6095	13491	1.3	30.7	87	22033322
Thioguanine	Approved[e]	60	mg/m2	p.o.	-	Pediatric	520	1500	2.2	1.6	-	11320662
Thiotepa	Approved[f]	300	mg/m2	i.v.	-	Pediatric	10570	-	-	1.3	10 - 30	1525606
Topotecan	Approved[e]	1.4	mg/m2	p.o.	-	Pediatric	15	78	2.6	2.0	35	26714427
Trametinib	Approved[f]	2	mg	p.o.	-	Adult	36	601	1.8[c]	90.2	97.4	22805291
Valproicacid	Approved[f]	120	mg/m2/day	p.o.	-	Adult	1521600	-	2-4[d]	-	81.5 - 90	19318486
Vandetanib	Approved[f]	145	mg/m2	p.o.	-	Pediatric	774	13607[c]	8.5[c]	-	90	20921456
Vemurafenib	Approved[e]	960	mg	p.o.	-	Adult	115731	776031	4.0	51.6	>99%	SmPc Zelboraf
Venetoclax	Approved[f]	240 - 360	mg/m2	p.o.	-	Pediatric	2533	48247	6.0[c]	-	>99%	32171069
Vinblastine	Approved[f]	6	mg/m2	i.v.	Bolus	Pediatric	25 –60[d]	51	-	20.6	98 - 99	22393086
Vincristine	Approved[f]	1.5	mg/m2	i.v.	Bolus	Pediatric	-	190	-	1.4	75	15617994
Vinorelbine	Approved[e]	24 - 37.5	mg/m2	i.v.	20 min	Pediatric	888	868	-	16.5	80- 90	16428494
Vismodegib	Approved[e]	150	mg	p.o.	-	Pediatric	8800[c]	501000[c]	23.5[c]	-	99	24077351
Volasertib	Phase III	300	mg/m2	i.v.	1 h	Pediatric	1745	17646	-	54.8	-	31276318
Vorinostat	Approved[e] FDA	130	mg/m2/day	p.o.	-	Pediatric	1313	4271	2.1	2.2	71	31823832

4.1.2 INFORM patient data base

Data from samples profiled from the 1st of July 2019 to 18th of January 2022 was derived from a diverse infrastructure encompassing various data storage systems and were subsequently combined into a single computable data base. In that timeframe 196 patient samples (Figure 6) with a variety of tumor diagnostic categories were submitted for DSP, of which 60% (119/196) were successfully screened. 82% (98/119) were full screens (entire drug library), of which 89% (87/98) had an intermediate or good QC. NGS was available for 78% (68/87) of the fully screened samples that passed QC. The 68 PPT samples had a total of 268 genetic alterations with varying INFORM priority scores from 1 to 7 (1,7). Five/68 PPT subgroup I samples harbored at least one very high priority (priority score 1) alteration with a clinically proven drug-target relationship (Figure 6, Table 16). In addition, these five samples harbored several lower priority score targets, for a complete overview of the identified targets refer to Table 16.
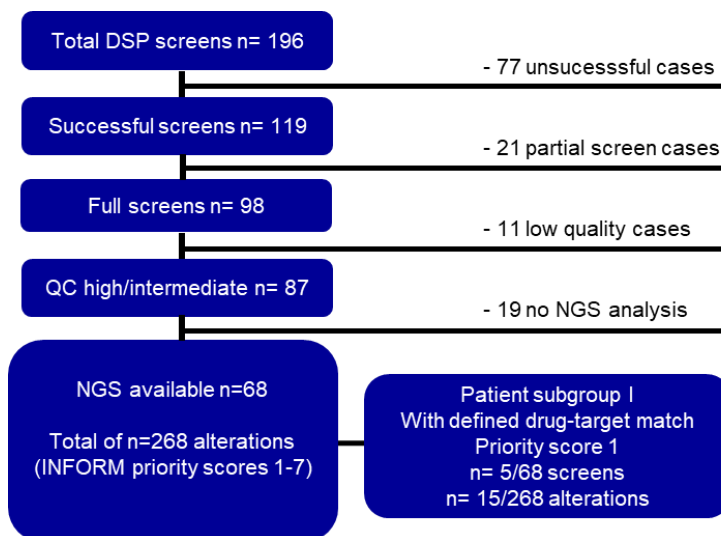
Figure 6. Consort diagram of the INFORM drug sensitivity profiling (DSP) samples.

Table 16. Overview of primary patient tumor (PPT) subgroup I samples, harboring specific molecular alterations with clinically proven drug-target relationship.

Patient ID	Diagnostic category	Genetic alteration	Priority score	Matching drug
P1_KANK1:NTRK3	LGG	KANK1:NTRK3 fusion	1	**NTRK inhibitors**: entrectinib, larotrectinib, selitrectinib
		PRKCA overexpression	5	
		BCL2L2 overexpression	7	
P2_BRAF V600E	HGG	BRAF V600E mutation	1	**BRAF inhibitors**: vemurafenib, dabrafenib, sorafenib, **MEK inhibitors**: trametinib, selumetinib
		CDKN2A/B deletion	3	
		MYC amplification overexpression	4	
		MAP2K1 overexpression	5	
P3_LRRFIP1:ALK	Sarcoma_other	LRRFIP1:ALK fusion	1	**ALK inhibitors**: ceritinib, alectinib, crizotinib, lorlatinib, entrectinib
P4_ ALK R1275Q	NBL	ALK R1275Q mutation	1	**ALK inhibitors**: ceritinib, alectinib, crizotinib, lorlatinib, entrectinib
		AKT3 E17K mutation	2	
		ABL2 overexpression	5	
		BRD3 overexpression	5	
		FGF3 overexpression	6	
P5_BRAF V600E	LGG	BRAF V600E mutation	1	**BRAF inhibitors:** vemurafenib, dabrafenib, sorafenib, **MEK inhibitors:** trametinib, selumetinib

4.1.3 INFORM data base clinical and genomic landscape

The INFORM PPT samples (n=68) were categorized into 13 tumor diagnostic categories (Figure 7) based on the information provided during data entry. Among these diagnostic categories, sarcomas were the most prevalent, accounting for a total of 47% (13% osteosarcoma (OSA), 9% rhabdomyosarcoma (RMS), 9% EWS and 16% other types of sarcomas (sarcoma_other). This was followed by 12% HGG, 9% Wilms tumors, 9% ependymoma (EPN), 6% neuroblastoma (NBL), 4% medulloblastoma (MED) (of which 3% were of the sonic hedgehog molecular group: MED SHH), 3% low grade glioma (LGG), 1% rhabdoid tumor (RT) and 9% comprising a group of mixed rare tumors (other). The male gender constituted the majority (69%, n=47/68) of patients in the cohort (Figure 8, for a per diagnostic category classification refer to Supplementary Figure 2). Specifically, within the diagnostic categories of MED, RT, EPN, and NBL, all patients were male. In contrast, the LGG group comprised only female patients, while the remaining diagnostic categories comprised both male and female patient.
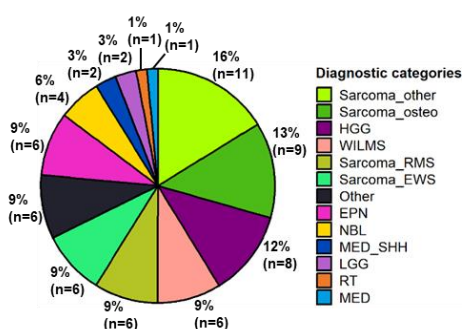
Figure 7. Distribution of tumor diagnostic categories within the INFORM drug sensitivity profiling (DSP) cohort (n=68).
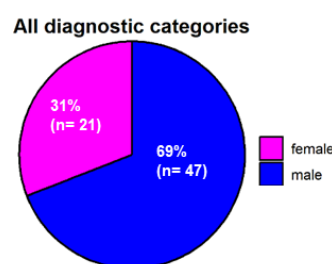
Figure 8. Gender distribution across all diagnostic categories within the INFORM drug sensitivity profiling (DSP) cohort (n=68).

The 68 PPT samples harbored a total of 268 genetic alterations (median: 1, range 1 – 8 genes) of which 157 were unique genes. Within the 268 genetic alterations there were 10 unique alterations (median: 8.5, range: 1 – 158 occurances of alterations) determined by NGS and summarized in Figure 9. The alterations that occurred most frequently were overexpressions, accounting for 59% (n=158/268) of the total number of alterations in the cohort. Following this, mutations were present in 16.8% (n=45/268) and amplifications in 6.7% (n=18/268) of the alterations.
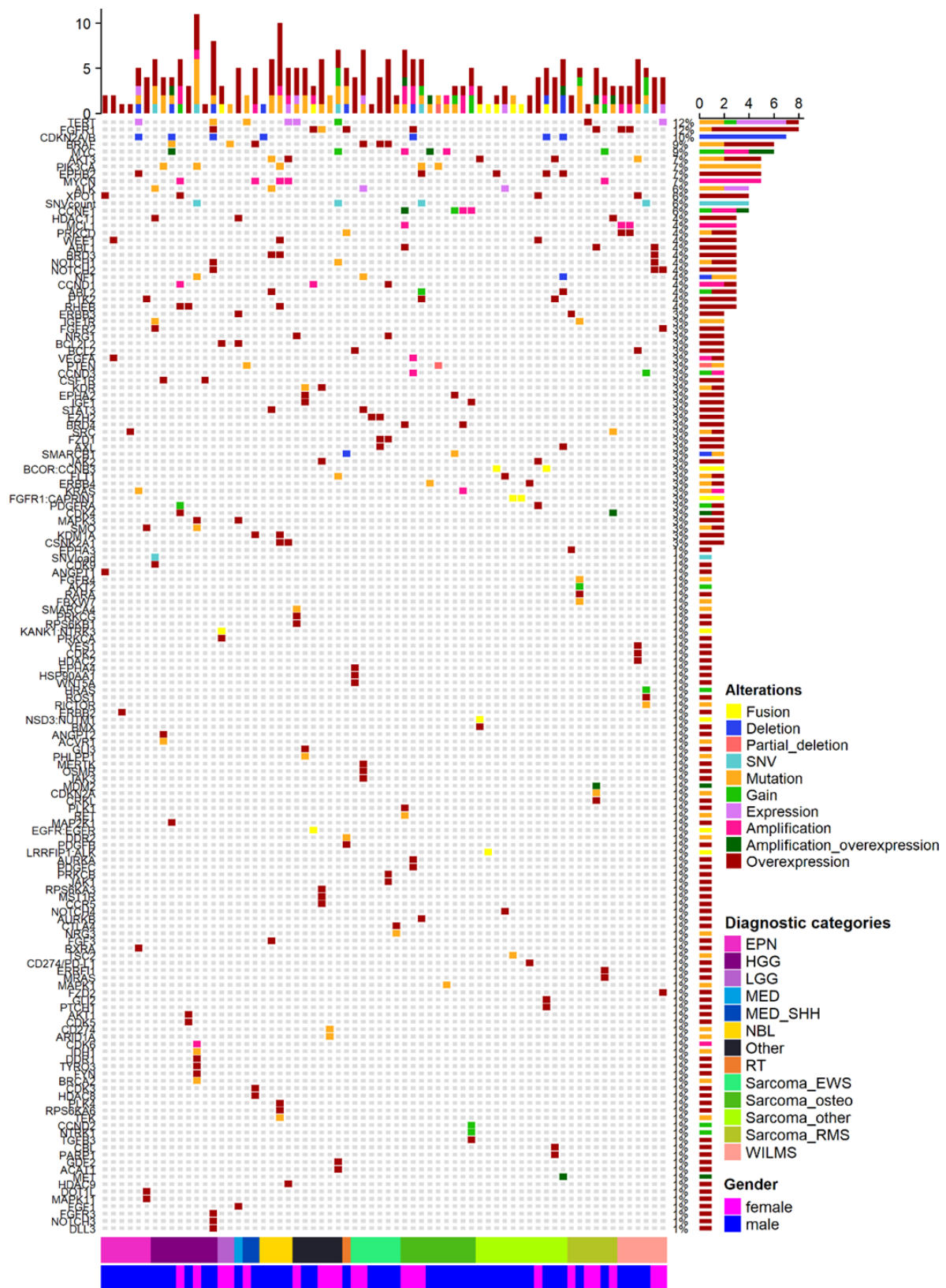
Figure 9. Description of clinical and molecular characteristics of the INFORM patient samples (n=68 screens and n=268 total alterations). Oncoplot summarizing the tumor diagnostic categories, molecular alterations and gender for each primary patient tumor (PPT) sample.

The two most frequently altered genes, occurring in 12% (n=8/68) of the PPT samples (3%, n=8/268 of genetic alterations) were TERT and FGFR1. Four patients harbored a TERT expression, two patients a TERT mutation, one patient a TERT overexpression and one patient a TERT gain. As for FGFR1, seven patients harbored the FGFR1 overexpression and one patient harbored the FGFR1 mutation. Furthermore, 10% (n=7/68) of the PPT samples (2.6%, n=7/268 of genetic alterations) exhibited a deletion in the CDKN2A/B gene, followed by 9% (n=6/68) of the PPT samples (2%, n=6/268 of genetic alterations) showing an alteration in BRAF with four patients having a BRAF overexpression and two patients a BRAF mutation. Additionally, 9% (n=6/68) of the cohort (2%, n=6/268 of genetic alterations) exhibited alterations in MYC, with two patients demonstrating a MYC gain, two patients demonstrating a MYC amplification/overexpression and two patients demonstrating an amplification.

Approximately 63% (99/157) of the unique genetic alterations identified in the PPT samples occurred as singular occurrences in the cohort. The majority, comprising 69% (n=68/99) of these alterations, were overexpressions followed by mutations (16%, n=16/99) and gains (5%, n=5/99). The number of genetic alterations per patient (Figure 9, top column annotation) varied from a minimum of 1 to a maximum of 11 (median: 4). Furthermore, among seven distinct tumor diagnosis categories namely, OSA, other sarcoma types, HGG, Wilms tumors, EWS, a group of mixed rare tumors, and NBL, two or more specific similar genetic alterations were found within their respective diagnostic categories (Figure 10). In the OSA group, 4/9 patient samples exhibited the presence of CCNE1, while MYC alterations were observed in 3/9 patient samples. In the EWS group, 3/6 samples revealed the presence of the BRAF alteration, whereas within the group of several different sarcoma subtypes, the EPHB2 gene alteration was present in 3 out of 11 samples.
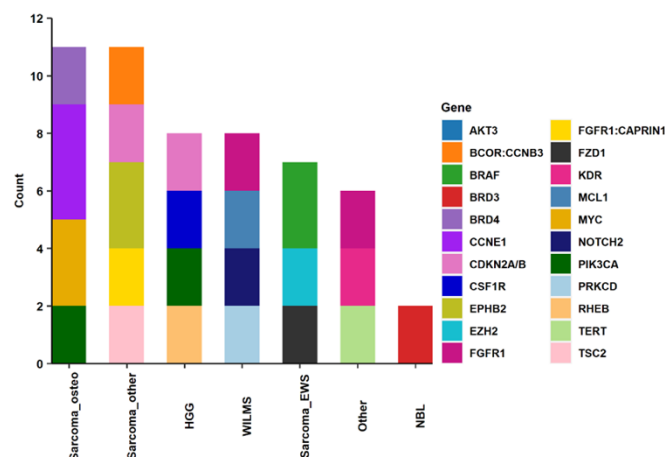
Figure 10. Overview of diagnostic categories with samples sharing two or more identical genetic alterations.

The pie chart in Figure 11 displays the distribution of the INFORM priority scores across the total number of genetic alterations in all patient samples. The majority of genetic alterations were classified as INFORM borderline priority score targets (49%, n=132/268), followed by very low priority (17%, n=45/268), intermediate priority (11%, n=29/268), low priority (8%, n=21/268), moderate priority (8%, n=21/268), high priority (5%, n=13/268) and very high priority (3%, n=7/268) score targets. Notably, the very high priority score targets were predominantly found in the diagnostic categories LGG, MED SHH, NB, HGG, OSA, NBL and a mix of other rare tumor diagnoses (Figure 11, Table 17). As opposed to patients with MED, EWS, Wilms tumor and RT harboring only intermediate, borderline, low and very low priority score targets. HGG and NB patients harbored alterations across all priority levels.
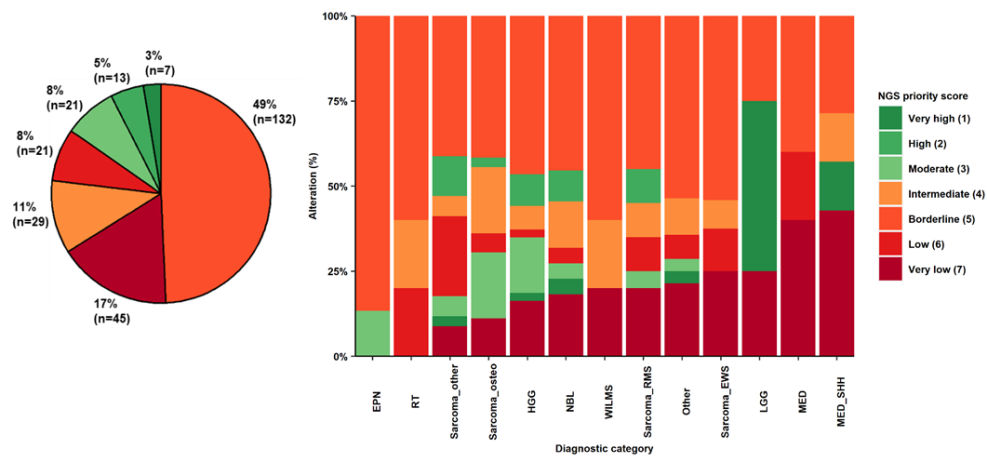
Figure 11. INFORM priority score distribution in the drug sensitivity profiling (DSP) cohort (n=68). Left: overview of priority scores for all alterations (n=268) detected in 68 samples. Right: bar chart illustrating priority scores for all alterations within each tumor diagnostic category.

Table 17. Overview of tumor diagnostic categories and genetic alterations with very high priority (priority score 1) targets. Frequency defined per sample.

Tumor diagnostic category	Gene	Alteration	Frequency gene within diagnostic category	Frequency gene within entire cohort
LGG	KANK1:NTRK3	Fusion	1/2	1/68
LGG	BRAF V600E	Mutation	1/2	2/68
MED SHH	PTEN L325fs	Mutation	1/2	1/68
HGG	BRAF V600E	Mutation	1/8	2/68
Sarcoma_other	LRRFIP1:ALK	Fusion h	1/11	1/68
NBL	ALK .R1275Q	Mutation	1/4	1/68
Other	EGFR:EGFR	Fusion	1/6	1/68

4.2 Technical bias between positive control cell line models and primary patient tumor samples with a defined drug-target match

The DSS calculation for the PCC models and the PPT samples was carried out utilizing two different algorithms, the iTReX application for the PCC models and an automated pipeline for all PPT samples (patient subgroup I included). To address and mitigate any technical bias resulting from the use of two algorithms on the data sets a principal component analysis (PCA) was performed (Figure 12). The analysis of the DSS, revealed a significant discrepancy between the PCC models and the PPT samples (Figure 12a). However, there was an overlap between PPT samples (excluding PPT subgroup I samples) and PPT subgroup I samples (Figure 12a). To further explore and potentially resolve the technical bias, the DSS z-score was implemented to normalize the data sets separately. Following this implementation, the PCA analysis displayed a noticeable overlap between the PCC models, the PPT subgroup I and PTT samples (Figure 12b). This suggested the potential resolution of the technical bias caused by the implementation of two different algorithms. Therefore, the z-score was implemented to all parameters tested.
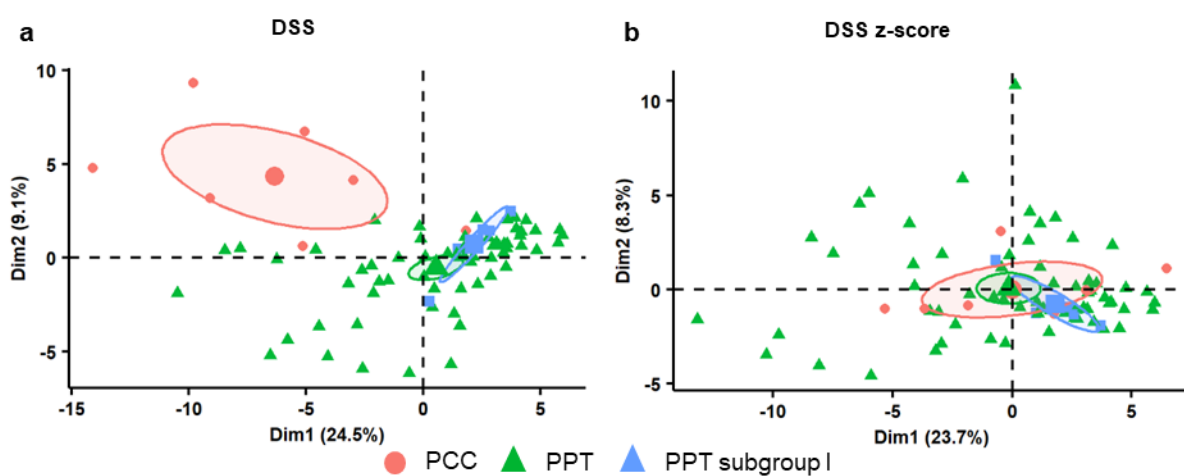
Figure 12. Principal component analysis (PCA) of the positive control cell line (PCC) models (n=7), the primary patient tumor (PPT) subgroup I samples (n=5) and PPT samples (n=63). Application of (a) - the drug sensitivity score (DSS) and (b) - the DSS z-score of all drugs tested within these two data sets.

4.3   Pharmacodynamic parameter analysis

4.3.1   Best performing pharmacodynamic parameter determination in positive control cell line models

In order to investigate the predictive power of the measured and derived PD parameters, seven PCC models were screened against the INFORM drug library. For each PD parameter all PCC models were combined and the drugs were classified into two groups: a drug match group indicating the drugs with a clinically proven drug-target relationship and drug non-match group representing the drugs without a clinically proven drug-target relationship. The classification aimed to evaluate the separation between the two groups (Figure 13). Within these homogenous PCC models, characterized by specific molecular alterations with verified drug-target relationships, the drugs categorized as 'drug match' are anticipated to exhibit evident and preferably superior performance in comparison to the other drugs. Each dot represents one drug for one PCC model. The measured PD parameters (IC50, IC75, PI5) could not distinguish between the drug match and drug non-match group as compared to the derived PD parameters DSS, DSS0 and AUC, where a clear separation is visible. To evaluate the performance of the derived parameters as predictive tools, the z-score and the ROC curves were generated (see sections 3.2.5.1and 3.2.5.1.) The corresponding AUCs are summarized in Table 18. The DSS z-score (AUC ROC 0.8356, cut off -0.22), DSS0 (AUC ROC 0.8295, cut off 0.47) and AUC (AUC ROC 0.8113, cut off 0.21) exhibited similar performance, however the DSS z-score demonstrated the highest performance in identifying the drug matches, as evidenced by the highest AUC ROC value.
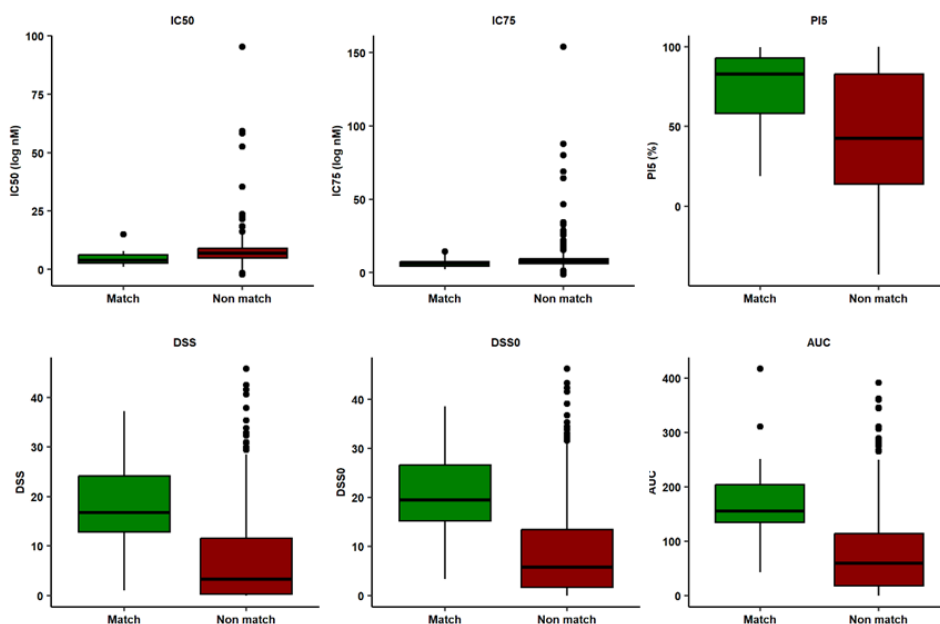
Figure 13. Boxplots of the measured and derived pharmacodynamic (PD) parameters of all positive control cell line (PCC) models combined (n=7). One dot represents one drug of one PCC model. IC50: half maximal inhibitory concentration, IC75: 75% inhibitory concentration, PI5: maximum effect at highest measured concentration, DSS: drug sensitivity score, DSS0: drug sensitivity score with Amin set to 0%, AUC: area under the curve calculated based on the trapezoidal method.

Table 18. Receiver operating characteristic (ROC) analysis of the derived pharmacodynamic (PD) parameters of the positive control cell line (PCC) models combined (n=7). DSS: drug sensitivity score, DSS z-score, DSS0: drug sensitivity score with Amin set to 0%, AUC: area under the curve calculated based on the trapezoidal method.

PD parameter	Best cut off	AUC ROC	95% CI (min – max)
DSS z-score	-0.22	0.8356	0.7798 - 0.8914
DSS$_0$ z-score	0.47	0.8295	0.7697 - 0.8894
AUC z-score	0.21	0.8113	0.7441 - 0.8784

4.3.2 Derived pharmacodynamic parameter DSS z-score able to distinguish between matching and non-matching drug targets in primary patient tumor samples with defined drug target relationship

After determining that the DSS z-score exhibited the best performance in PCC models through ROC analysis, I calculated the DSS z-score for all PPT samples (n=68). Subsequently, the PCC model DSS z-score threshold of -0.22 was set as a threshold to the PPT samples. Samples in which drugs exceeded this threshold were interpreted as exhibiting sensitivity to these drugs, thus implying potential efficacy in the patient. The five PPT subgroup I samples (Table 16) harboring at a very high priority (score 1) genetic alteration with clinically proven drug-target relationship (LRRFIP1:ALK 1/5, ALK R1275Q 1/5, BRAF V600E 2/5, KANK1:NTRK3 1/5) were used to investigate the predictive value of the DSS z-score.

Patient P3_LRRFIP1:ALK harboring the ALK fusion alteration, showed sensitivity for crizotinib, ceritinib and lorlatinib (Figure 14, Table 19) when the DSS z-score was applied. The patient exhibited reduced sensitivity to alectinib and entrectinib as their DSS z-scores fell below the specified threshold. However, this observation, while consistent from a molecular standpoint, did not entirely align with the patient's clinical history (Table 19). The patient had undergone alectinib and lorlatinib treatment during which disease progression was observed. Alectinib was not identified as a drug hit while lorlatinib did surpass the threshold and was identified as a drug hit, which led to a discrepancy in the drug hit outcome.

Figure 14. DSS z-scores for patient P3_LRRFIP1:ALK (black dot) compared with the complete PPT sample set (n=67) (gray dot). Each dot represents a screened drug for an individual sample, with matching drugs denoted by orange arrows. The red line represents the ROC-derived threshold for positive cell line (PCC) models (-0.22).

Table 19. DSS z-score performance in identifying matching drugs for patient P3_LRRFIP1:ALK. Blue: clinical history, red: no hit (DSS z-score below -0.22), green: hit (DSS z-score above -0.22).

P3_LRRFIP1:ALK

	Crizotinib	Ceritinib	Lorlatinib	Alectinib	Entrectinib
DSS z-score					

P4_ALK R1275Q was characterized by a priority score 1 ALK R1275Q mutation, a priority score 2 AKT3 E17K mutation, lower priority score 5 ABL2 and BRD3 overexpression and priority score 6 FGF3 overexpression (Table 20). The sample exhibited sensitivity to all matching drugs (alectinib, lorlatinib, entrectinib and ceritinib), but crizotinib (Figure 15, Table 20). Clinical history, in particular prior and/or post-analysis drug history (i.e. which drug was the patient treated with before and after analysis), was not available to facilitate a direct comparison between the patient's clinical outcome and DSP outcome when applying the DSS z-score as a metric. Essentially, this hindered a direct evaluation of the utility and predictivity of DSP by directly comparing it to the patient's clinical course. The results obtained from a molecular background (LRRFIP1:ALK fusion) were consistent with the DSP outcomes for the corresponding matching drugs.
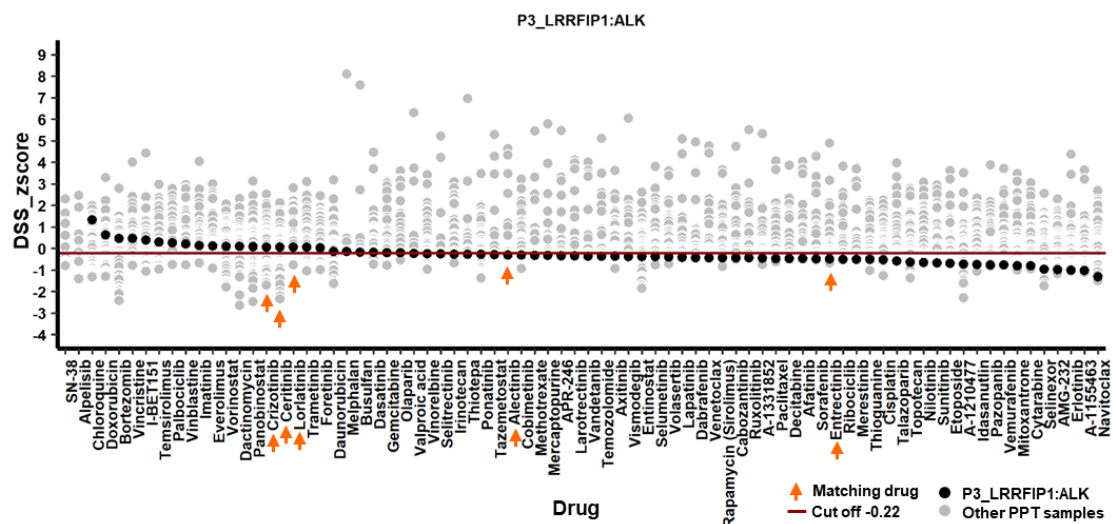

Figure 15. DSS z-scores for patient P4_ALK R1275Q (black dot) compared with the complete PPT sample set (n=67) (gray dot). Each dot represents a screened drug for an individual sample, with matching drugs denoted by orange arrows. The red line represents the ROC-derived threshold for positive cell line (PCC) models (-0.22).

Table 20. DSS z-score performance in identifying matching drugs for patient P4_ALK R1275Q. Blue: clinical history, red: no hit (DSS z-score below -0.22), green: hit (DSS z-score above -0.22).

P4_ALK R1275Q - AKT3 E17K mutation (priority score 2), ABL2 overexpression (priority score 5), BRD3 overexpression (priority score 5) and FGF3 overexpression (priority score 6)

	Alectinib	Lorlatinib	Entrectinib	Ceritinib	Crizotinib
DSS z-score					

Patient P2_BRAF V600E was characterized by a priority score 1 BRAF V600E mutation and BRAF overexpression, a lower priority score 3 CDKN2A/B deletion and priority score 4 MYC amplification and overexpression and priority score 5 MAP2K1 overexpression (Table 21), which have been associated with increased resistance to BRAF and MEK1/2 inhibitors (48). Among the five matching drugs (vemurafenib, trametinib, dabrafenib, sorafenib and selumetinib) only vemurafenib demonstrated sensitivity in the sample (Figure 16, Table 21). All the other matching drugs fell below the threshold value of -0.22. These findings were consistent with the patient's clinical history which involved treatment with trametinib and dabrafenib combination (Table 21). Sampling for DSP was carried out at the onset of temozolomide treatment. Unfortunately, the patient succumbed to the disease before the drug screening process was completed, 21 days into temozolomide treatment. Notably, temozolomide, not a matching drug for this patient sample, showed a DSS z-score below the threshold (-0.36). As the patient succumbed to disease progression 21 days into temozolomide treatment and the sample for DSP was taken at the onset of treatment, this could possibly indicate a predicted resistance towards temozolomide determined through DSP analysis. For this patient case, the clinical history was reflected in the DSS z-score outcome although the efficacy with single treatment vemurafenib might be limited considering the aforementioned treatment and molecular alterations.
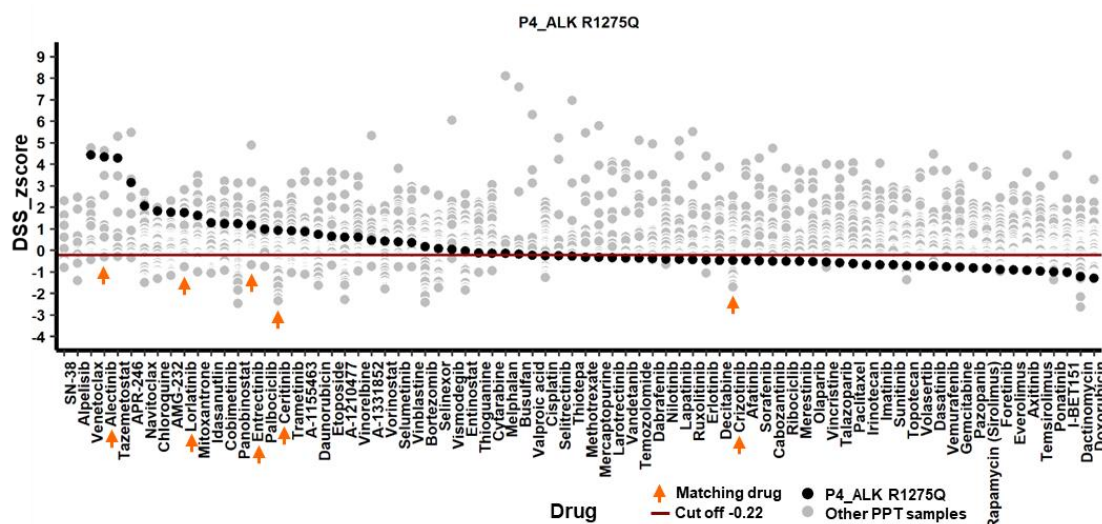

Figure 16. DSS z-scores for patient P2_BRAF V600E (black dot) compared with the complete PPT sample set (n=67) (gray dot). Each dot represents a screened drug for an individual sample, with matching drugs denoted by orange arrows. The red line represents the ROC-derived threshold for positive cell line (PCC) models (-0.22).

Table 21. DSS z-score performance in identifying matching drugs for patient P2_BRAF V600E. Blue: clinical history, red: no hit (DSS z-score below -0.22), green: hit (DSS z-score above -0.22).

P2_BRAF V600E - CDKN2A/B deletion (priority score 3), MYC amplification overexpression (priority score 4) and MAP2K1 overexpression (priority score 5)					
	Vemurafenib	**Trametinib**	**Dabrafenib**	**Sorafenib**	**Selumetinib**
DSS z-score					

Patient P5_BRAF V600E solely harbored a very high priority score 1 BRAF V600E (Table 22), and had received a combination treatment of trametinib and dabrafenib (Table 22) which resulted in disease progression during treatment, prior to sampling for DSP analysis. In the DSS z-score outcome all matching drugs (selumetinib, vemurafenib, trametinib and dabrafenib) surpassed the threshold (Figure 17), except for sorafenib which did not surpass the threshold. Once again, the molecular background (BRAF V600E mutation) appeared to be reflected in the DSS z-score outcome, yet the discrepancy with the patient's clinical history remained.

Figure 17. DSS z-scores for patient P5_BRAF V600E (black dot) compared with the complete PPT sample set (n=67) (gray dot). Each dot represents a screened drug for an individual sample, with matching drugs denoted by orange arrows. The red line represents the ROC-derived threshold for positive cell line (PCC) models (-0.22).

Table 22. DSS z-score performance in identifying matching drugs for patient P5_BRAF V600E. Blue: clinical history, red: no hit (DSS z-score below -0.22), green: hit (DSS z-score above -0.22).

P5_BRAF V600E					
	Selumetinib	**Vemurafenib**	**Trametinib**	**Dabrafenib**	**Sorafenib**
DSS z-score					

For patient P1_KANK1:NTRK3 harboring a priority score 1 KANK1:NTRK fusion, lower priority score 5 PRKCA overexpression and priority score 7 BCL2L2 overexpression (Table 23) the DSS z-score of larotrectinib fell below the threshold, indicating a lack of sensitivity (Figure 18). Selitrectinib and entrectinib exhibited scores above the threshold which aligned with the molecular background (KANK1:NTRK3 fusion). The patient was reported to have previously undergone treatment with untargeted conventional chemotherapeutics with vincristine, etoposide, carboplatin and cyclophosphamide. Interestingly, vincristine and etoposide showed a DSS z-score lower than the threshold (-0.56 and -0.69) which was consistent with the clinical history of the patient. Unfortunately, the two other drugs were not included in the INFORM drug library.
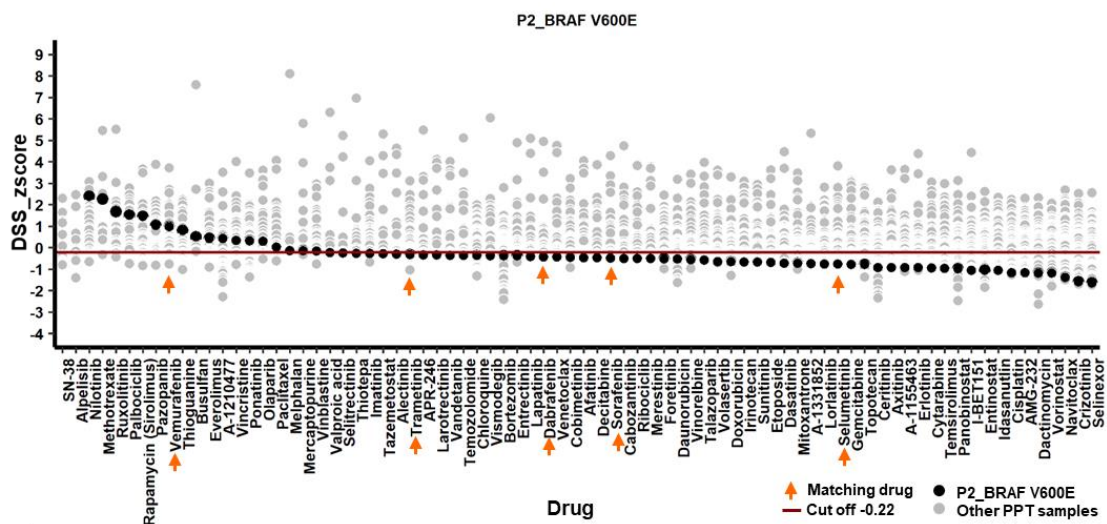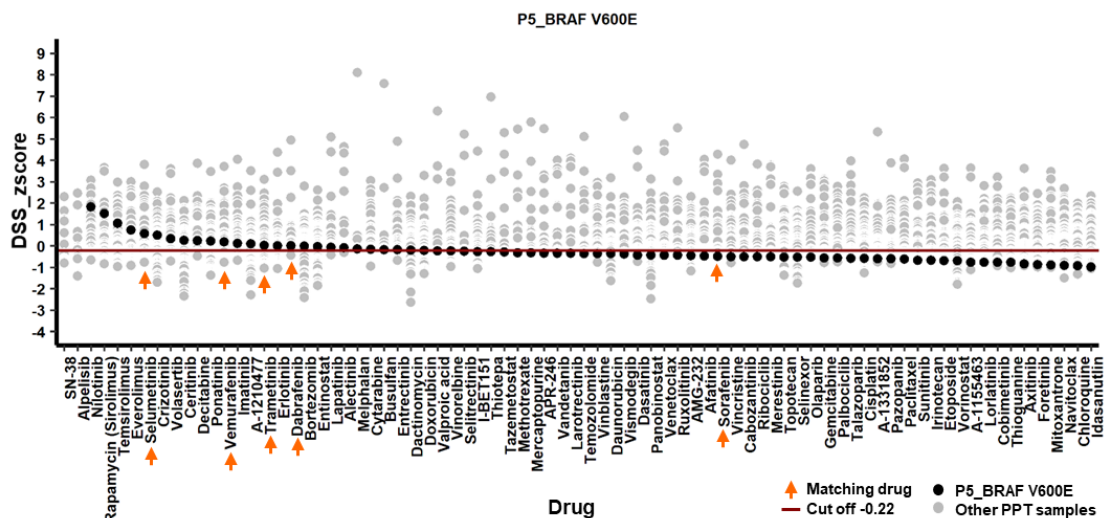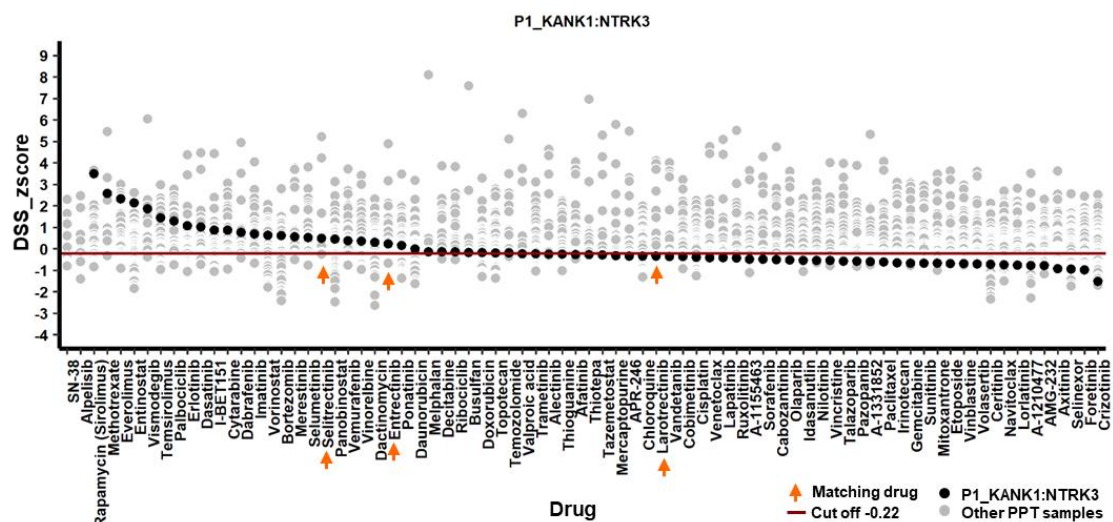

Figure 18. DSS z-scores for patient P1_KANK1:NTRK3 (black dot) compared with the complete PPT sample set (n=67) (gray dot). Each dot represents a screened drug for an individual sample, with matching drugs denoted by orange arrows. The red line represents the ROC-derived threshold for positive cell line (PCC) models (-0.22).

Table 23. DSS z-score performance in identifying matching drugs for patient P1_KANK1:NTRK3. Blue: clinical history, red: no hit (DSS z-score below -0.22), green: hit (DSS z-score above-0.22).

P1_KANK1:NTRK3 - PRKCA overexpression (priority score 5) and BCL2L2 overexpression (priority score 7)			
	Selitrectinib	Entrectinib	Larotrectinib
DSS z-score			

The DSS z-score is able to identify the matching drug for each patient sample based on the molecular background of the samples. Among the four samples P3_LRRFIP1:ALK, P4_ALK R1275Q, P5_BRAF V600E, and P1_KANK1:NTRK3 the DSS z-score was able to identify 60% - 80% of the matching drugs for each sample. For sample P2_BRAF V600E only 20% of the matching drugs were identified, which can be attributed to the presence of additional molecular alterations within the sample's molecular background next to the V600E molecular alteration.

However in terms of the patient's clinical history, the DSS z-score showed limitations in its ability to consistently reflect this aspect across all patient samples. Only in sample P2_BRAF V600E with a molecular background (Table 21) prone to high resistance of the sample, the clinical history of the patient was evident.

4.4 Pharmacokinetic parameter analysis

4.4.1 Selection and rationale of pharmacokinetic parameter Cmax

While the DSS z-score demonstrated high sensitivity in selecting the matching drugs for the majority of the PPT subgroup I samples, several other drugs belonging to different drug classes surpassed the determined threshold as well. These drugs might have held effectiveness in the patient, however, it was crucial to investigate whether these drugs could be administered in a clinically attainable dose. To address this, the IC50 and clinical Cmax values for drugs above the DSS z-score threshold of -0.22 in all PPT samples (n=68) were classified and compared according to diagnostic category (Figure 19). Based on the available PK information for most of the drugs in the INFORM drug library, the PK parameter Cmax was selected for the comparison. Notably, a majority of drugs in the PPT samples exhibited IC50 values higher than the clinically attainable Cmax value, whereas this was not observed in PCC models (Figure 20). Though the percentage of drugs above the DSS z-score threshold with an IC50 above Cmax for MED SHH (45%), Wilms tumors(40%) and NBL (36%) was not higher than the percentage below Cmax, it remains crucial to minimize the percentage of drugs that are clinically unattainable to the greatest extent possible. Given the predominance of drugs with IC50 values that exceeded clinical Cmax values in PPT samples, the implementation of PK parameters as a clinical filtering step could be a potentially effective approach to get closer to identifying effective drugs at the clinically attainable concentrations.
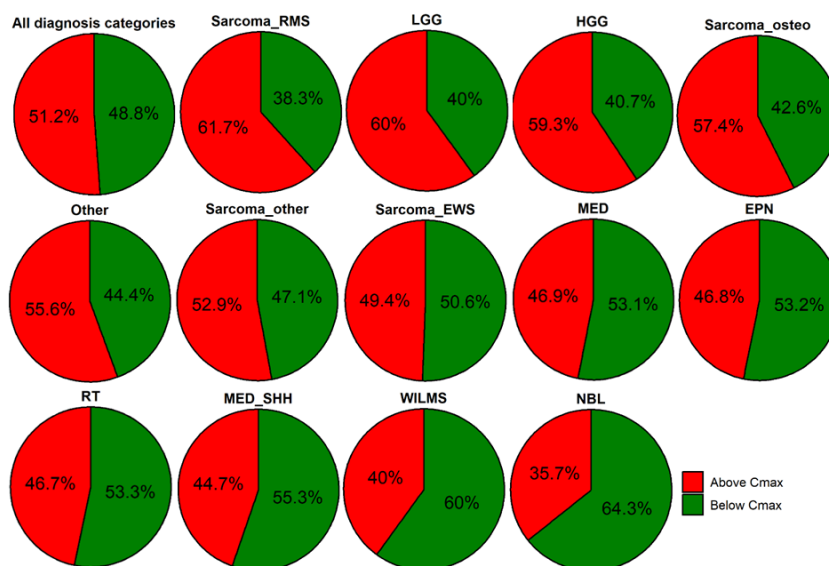
Figure 19. Comaprison of IC50 and Cmax for drugs meeting criteria DSS z-score above -0.22, displayed for all primary patient tumor samples and categorized by tumor diagnostic category.
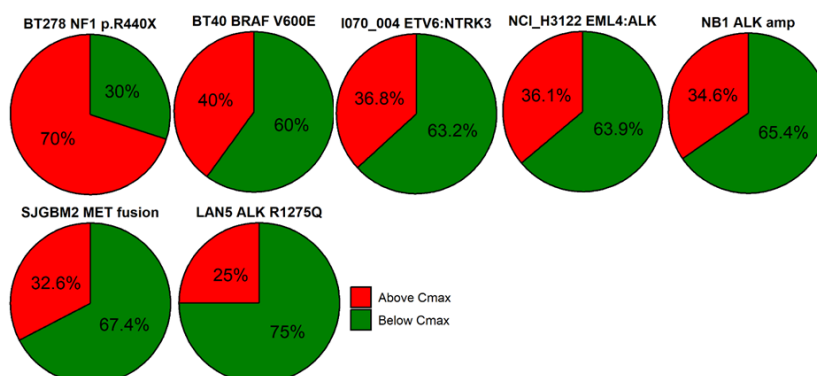

Figure 20. Comaprison of IC50 and Cmax for drugs meeting criteria DSS z-score above -0.22, displayed for all positive control cell line models.

4.4.2 Pharmacodynamic pharmacokinetic parameter DSS Cmax z-score is able to reflect the clinical history in primary patient tumor samples

The best performing PD parameter DSS was combined with the PK parameter Cmax into the DSS Cmax z-score as described in the methods to incorporate a clinical filtering step and generate a single parameter that excludes drug concentrations that are clinically not attainable. The ROC analysis was conducted for the DSS Cmax z-score within the PCC models to assess its predictive capabilities. The AUC ROC was determined to be 0.7391 (95% CI: 0.6349-0.8433) and a cut off value of 0.04 was established. Subsequently, this threshold was used to evaluate the PTT subgroup I samples.

As expected, the application of DSS Cmax z-score led to the exclusion of multiple drugs in the PPT subgroup I sample analysis. The Cmax values for six drugs (A-1155463, A-1210477, A-1331852, I-BET151, selitrectinib and vincristine) utilized in the drug screening process were unavailable (Supplementary Table 2), which made the determination of DSS Cmax z-score unfeasible. In addition, the determination of IC50 was not feasible for several drugs in each sample's screening (Supplementary Table 2).

The decreasing order of missing IC50 values per sample was as follows: P2_BRAF_mix (49%; n=37/76), P4_ALK_R1275Q (41; n=31/76), P3_LRRFIP1:ALK (29%, n=22/76), P1_KANK1:NTRK3 (22%; n=17/76) and P5_BRAF_V600E (14%; n=11/76). For the remaining drugs, the range between Cmax and IC50 was determined from the total number of drugs subtracted by the sum of missing IC50 and Cmax values. The decreasing order of drugs with an IC50 value higher than Cmax per sample was: P1_KANK1:NTRK3 (66%; n=34/53), P2_BRAF_mix (88%; n=29/33), P3_LRRFIP1:ALK (75%; n=36/48), P5_BRAF_V600E (69%; n=41/59), and P4_ALK R1275Q (56%; n=22/39).

Several matching drugs were among those that either lacked a specified IC50 value, exhibited a negative IC50 C5 range or had an unattainable clinical value (negative Cmax IC50 range). Consequently, these drugs were excluded from the DSS Cmax z-score calculation (Supplementary Table 2), after examination of their dose-response curves. Supplementary Table 2 provides a comprehensive list of the excluded matching drugs, along with the corresponding samples and the justification for their exclusion. The observed dose-response curves for these drugs predominantly exhibited a horizontal curve pattern, with a maximum percentage inhibition typically around 25 – 40%. These findings strongly suggested the ineffectiveness of these drugs in inducing cell death.

In the case of the patient sample P3_LRRFIP1:ALK with the ALK fusion, the IC50 of alectinib could not be determined (Table 24). Crizotinib and lorlatinib had IC50 values above the Cmax value and were excluded due to their clinical unattainability in the patient (Figure 21, Table 24). Entrectinib had an IC50 C5 range which was negative and was therefore excluded (Figure 21, Table 24). The DSS Cmax z-score value could only be calculated for ceritinib which did not surrpass the determined threshold (DSS Cmax z-score: -0.5). According to the patient's clinical history, the patient progressed under alectinib and lorlatinib treatment, both excluded from the DSS Cmax z-score calculation as the former showed no IC50 value and the latter was clinically unattainable with an IC50 higher than the Cmax value (Table 24). The clinical history of the patient was well reflected in the DSS Cmax z-score approach. Furthermore, the analysis revealed that this sample exhibited a general resistance to various types of treatment. Temsirolimus was the only drug surpassing the threshold.

Figure 21. DSS Cmax z-scores for patient P3_LRRFIP1:ALK (black dot) compared with the complete PPT sample set (n=67) (gray dot). Each dot represents a screened drug for an individual sample, with matching drugs denoted by orange arrows. The red line represents the ROC-derived threshold for positive cell line (PCC) models (0.04).

Table 24. DSS Cmax z-score performance in identifying matching drugs for patient P3_LRRFIP1:ALK. Blue: clinical history, red: no hit (DSS z-score below 0.04), green: hit (DSS z-score above 0.04), I: no IC50, II: IC50 – C5 range negative, III: Cmax – IC50 range negative.

P3_LRRFIP1:ALK					
	Ceritinib	Alectinib	Crizotinib	Entrectinib	Lorlatinib
DSS_Cmax z-score		I	III	II	III

For the P4_ALK R1275Q sample with an ALK mutation, the IC50 value of lorlatinib could not be determined in the screening (Table 25). Alectinib and entrectinib had an IC50 C5 range which was negative and were therefore excluded. Crizotinib had an IC50 value above the Cmax value, which led to its exclusion as its concentration is clinically unattainable (Table 25). The DSS Cmax z-score could only be calculated for ceritinib in this sample, which surpassed the threshold as shown in Figure 22. Furthermore, it was observed that the patient sample exhibited a consistent and notable sensitivity to drugs belonging to the apoptotic modulators including, venetoclax, APR-264, navitoclax, AMG-232, idasanutlin and selinexor (Figure 22). This observation suggested an in-class effect, indicating a general susceptibility of the patient sample to drugs within this specific drug class. Cobimetinib also surpassed the threshold (Figure 22).
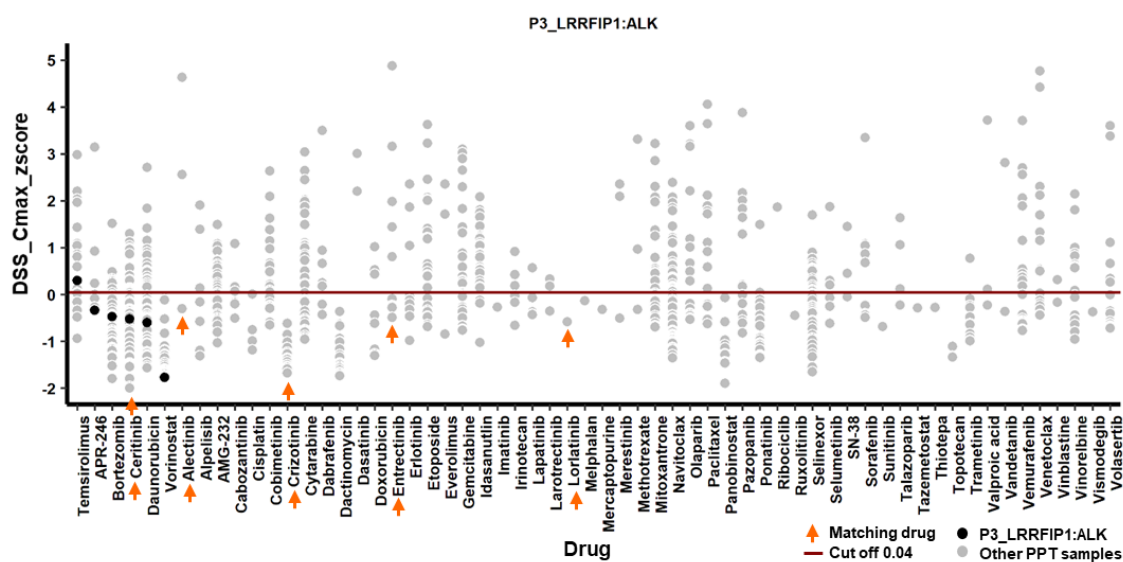

Figure 22. DSS Cmax z-scores for patient P4_ALK R1275Q (black dot) compared with the complete PPT sample set (n=67) (gray dot). Each dot represents a screened drug for an individual sample, with matching drugs denoted by orange arrows. The red line represents the ROC-derived threshold for positive cell line (PCC) models (0.04).

Table 25. DSS Cmax z-score performance in identifying matching drugs for patient P4_ALK R1275Q. Blue: clinical history, red: no hit (DSS z-score below 0.04), green: hit (DSS z-score above 0.04), I: no IC50, II: IC50 – C5 range negative, III: Cmax – IC50 range negative.

P4_ALK R1275Q - AKT3 E17K mutation (priority score 2), ABL2 overexpression (priority score 5), BRD3 overexpression (priority score 5) and FGF3 overexpression (priority score 6)					
	Ceritinib	Alectinib	Crizotinib	Entrectinib	Lorlatinib
DSS_Cmax z-score		II	III	II	I

In the P2_BRAF V600E sample, dabrafenib and sorafenib had no determined IC50 values (Table 26), while selumetinib and trametinib exhibited IC50 values higher than Cmax (Table 26), making them clinically unattainable in the patient. Vemurafenib had an IC50 C5 range which was negative (Table 26) and was therefore excluded. Similarly, for this patient all matching drugs were excluded from the DSS Cmax z-score calculation (Table 26, Figure 23). As stated before, the patient succumbed after treatment with trametinib and dabrafenib combination, while on treatment with temozolomide. Sampling was carried out at the onset of temozolomide treatment and DSP analysis was pending completion at the time of the patient's death. This was reflected in the DSS Cmax z-score outcome enabling this score to confirm the treatment history of the patient (Table 26). Also from a molecular background, it was likely that none of the matching drugs was effective, as the patient carried a CDKN2A/B deletion, MYC amplification overexpression and MAP2K1 overexpression making the sample susceptible to treatment resistance. Furthermore, the sample demonstrated a pronounced overall resistance to all the drugs that were tested in the INFORM drug library.
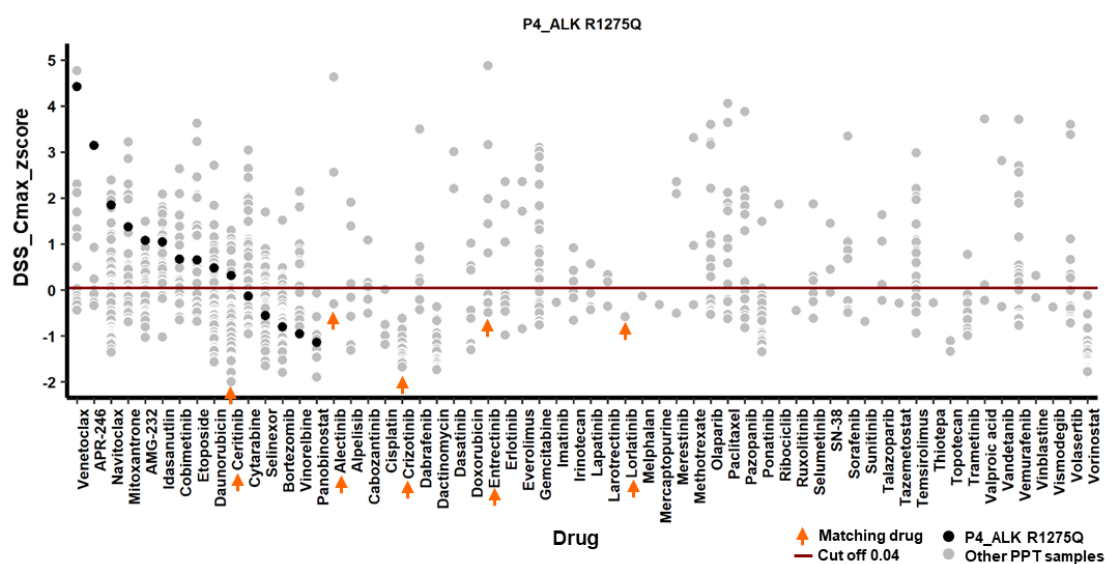

Figure 23. DSS Cmax z-scores for patient P2_BRAF V600E (black dot) compared with the complete PPT sample set (n=67) (gray dot). Each dot represents a screened drug for an individual sample, with matching drugs denoted by orange arrows. The red line represents the ROC-derived threshold for positive cell line (PCC) models (0.04).

Table 26. DSS Cmax z-score performance in identifying matching drugs for patient P2_BRAF V600E. Blue: clinical history, red: no hit (DSS z-score below 0.04), green: hit (DSS z-score above 0.04), I: no IC50, II: IC50 – C5 range negative, III: Cmax – IC50 range negative.

P2_BRAF mix - CDKN2A/B deletion (priority score 3), MYC amplification overexpression (priority score 4) and MAP2K1 overexpression (priority score 5)					
	Dabrafenib	Selumetinib	Sorafenib	Trametinib	Vemurafenib
DSS_Cmax z-score	I	III	I	III	II

In the case of the other sample with a BRAF alteration, P5_BRAF V600E, the IC50 value of all matching drugs could be determined. However, selumetinib and trametinib were excluded (Table 27) due to their IC50 values being higher than the Cmax value, making them clinically unattainable for the patient. The DSS Cmax z-score value could not be calculated for dabrafenib and sorafenib in this sample (Table 27), as their IC50 C5 range was negative. The DSS Cmax z-score value was only calculated for vemurafenib (Table 27, Figure 24), which surpassed the threshold. The mTOR inhibitor temsirolimus and two kinase inhibiters volasertib and ceritinib were found to surpass the established threshold, indicating their potential effectiveness in the patient.
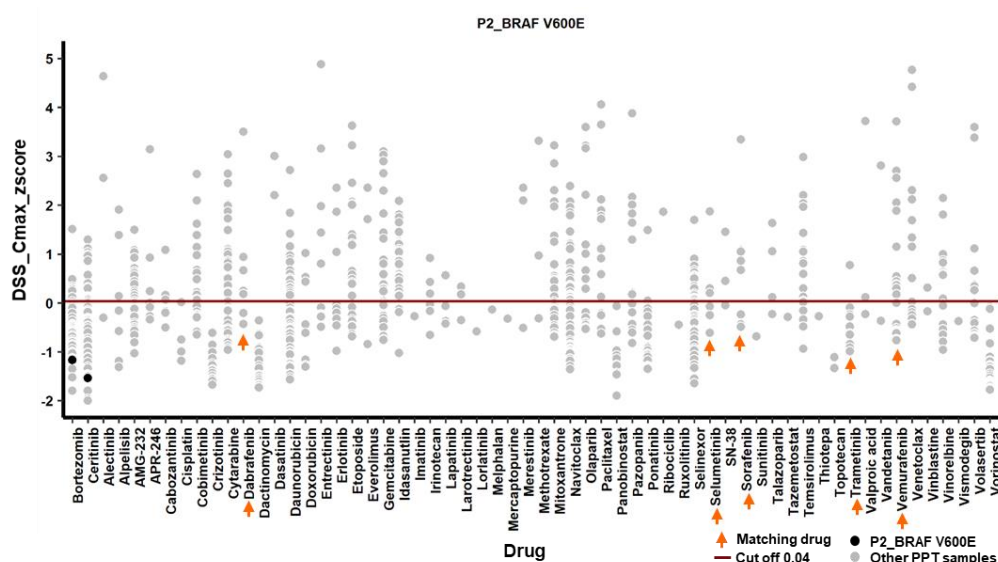

Figure 24. DSS Cmax z-scores for patient P5_BRAF V600E (black dot) compared with the complete PPT sample set (n=67) (gray dot). Each dot represents a screened drug for an individual sample, with matching drugs denoted by orange arrows. The red line represents the ROC-derived threshold for positive cell line (PCC) models (0.04).

Table 27. DSS Cmax z-score performance in identifying matching drugs for patient P5_BRAF V600E. Blue: clinical history, red: no hit (DSS z-score below 0.04), green: hit (DSS z-score above 0.04), I: no IC50, II: IC50 – C5 range negative, III: Cmax – IC50 range negative.

P5_BRAF V600E					
	Vemurafenib	Dabrafenib	Selumetinib	Sorafenib	Trametinib
DSS_Cmax z-score		II	III	II	III

In the P1_KANK1:NTRK3 sample, all matching drugs (larotrectinib, entrectinib and selitrectinib) were excluded (Figure 25, Table 28). For larotrectinib and selitrectinib the IC50 could not be determined. For entrectinib however, the IC50 C5 range was negative and the drug was therefore excluded (Table 28). According to the patient's clinical history, the patient had received vincristine and etoposide and progressed. The Cmax value for vincristine was unavailable, preventing the determination of the DSS Cmax value. Similarly, the DSS Cmax value for etoposide could not be determined as the drug had a negative IC50 C5 value. Interestingly, two of the three mTOR inhibitors, everolimus and temsirolimus and the BRAF inhibitor vemurafenib surpassed the threshold.
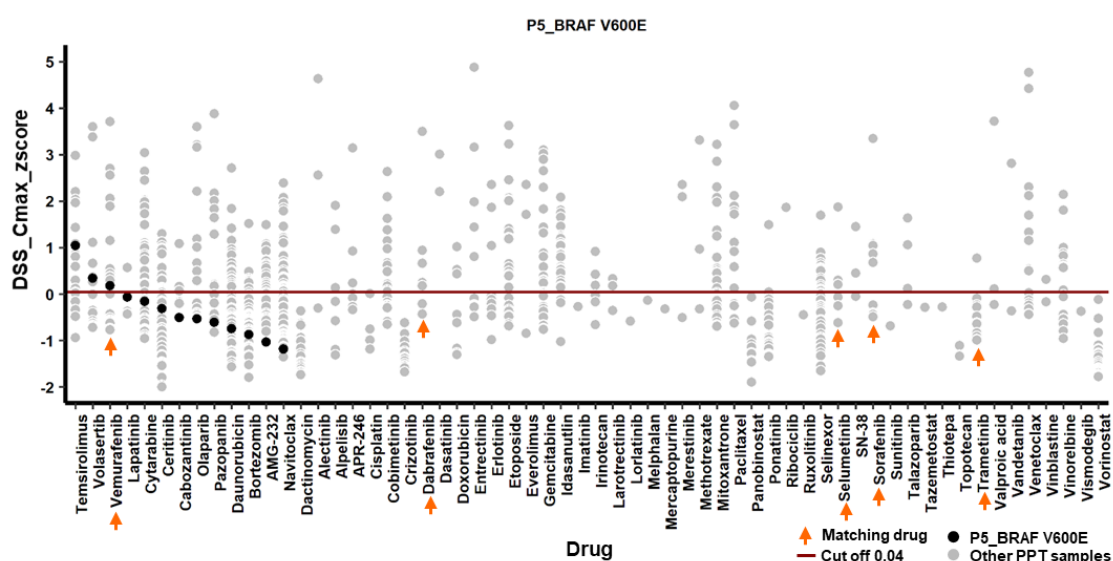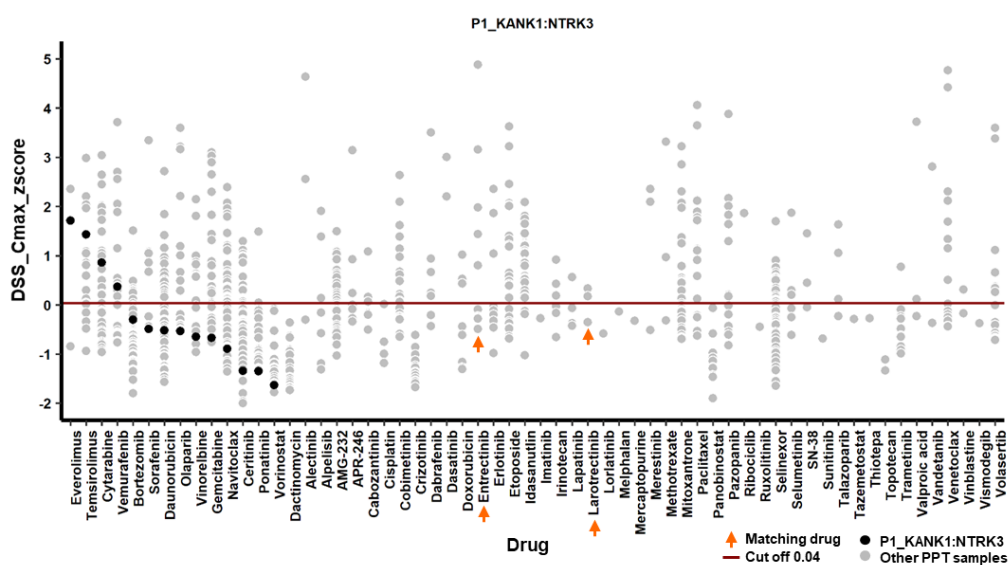

Figure 25. DSS Cmax z-scores for patient P1_KANK1:NTRK3 (black dot) compared with the complete PPT sample set (n=67) (gray dot). Each dot represents a screened drug for an individual sample, with matching drugs denoted by orange arrows. The red line represents the ROC-derived threshold for positive cell line (PCC) models (0.04).

Table 28. DSS Cmax z-score performance in identifying matching drugs for patient P1_KANK1:NTRK3. Blue: clinical history, red: no hit (DSS z-score below 0.04), green: hit (DSS z-score above 0.04), I: no IC50, II: IC50 – C5 range negative, III: Cmax – IC50 range negative.

P1_KANK1:NTRK3 - PRKCA overexpression (priority score 5) and BCL2L2 overexpression (priority score 7)			
	Entrectinib	**Larotrectinib**	**Selitrectinib**
DSS_Cmax z-score	II	I	I / IV

The DSS Cmax z-score is able to reflect the clinical history in each patient sample when information was available. Additionally, for sample P2_BRAF V600E with a molecular background indicating higher resistance of the sample, this was reflected in the DSS Cmax z-score, as none of the drugs in the library exceeded the 0.04 threshold. The DSS Cmax z-score effectively captures the clinical history within the PPT samples with a defined drug target match.

4.5 Additional pharmacodynamic and pharmacokinetic parameters tested

4.5.1 AUC_Cmax z-score demonstrates no difference in predicting the matching drugs and reflecting the clinical history in PPT subgroup I samples compared to AUC z-score

The PD parameters DSS z-score and DSS0 z-score were found to be highly correlated. Consequently, the AUC z-score was chosen as an additional PD parameter to assess its predictive power in identifying matching drugs in PPT subgroup I samples. This was also done for the AUC Cmax z-score. The implementation of the AUC Cmax z-score involved incorporating Cmax with AUC, without performing a pre-check of clinical attainability (as done for DSS Cmax) by excluding specific drugs. Instead, it was assumed that the AUC of clinically unattainable drugs would be smaller than attainable ones since the AUC was calculated up to the Cmax value. As shown in Table 18, the AUC z-score in the PCC models achieved an ROC AUC of 0.8113 (95% CI: 0.7441 - 0.8784) and a threshold value of 0.21 was determined. The ROC analysis of the AUC Cmax in PCC models achieved an ROC AUC of 0.8039 (95% CI: 0.7367-0.8712) and a threshold value of 0.28. Subsequently the AUC z-score and AUC Cmax z-score were calculated for the PPT subgroup I samples and the results were visualized in Figure 26 and Figure 27.

Figure 26. AUC z-score distribution for all drugs across primary patient tumor (PPT) subgroup I samples (n=5), classified by gene alteration. Each dot or triangle symbolizes a screened drug per sample, with dots indicating non-matching drugs and triangles indicating matching drugs. The ROC-derived threshold for positive cell line (PCC) models (0.21) is represented by the red line.
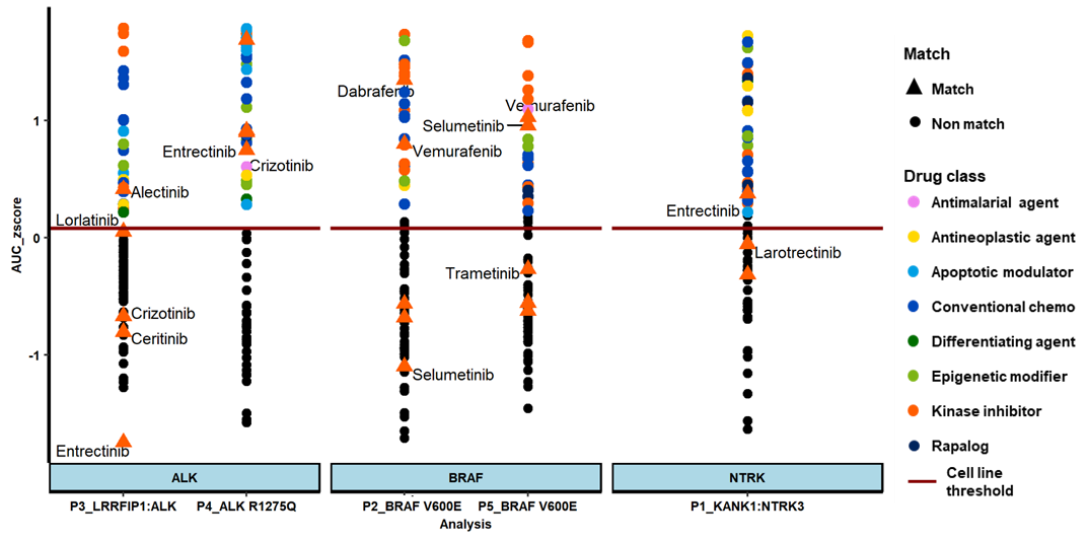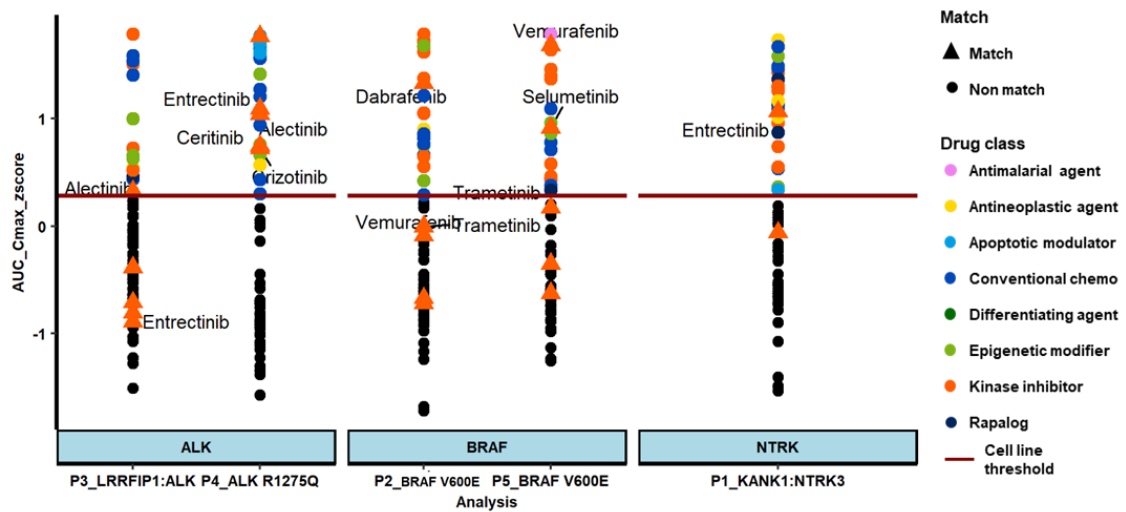

Figure 27. AUC Cmax z-score distribution for all drugs across primary patient tumor (PPT) subgroup I samples (n=5), classified by gene alteration. Each dot or triangle symbolizes a screened drug per sample, with dots indicating non-matching drugs and triangles indicating matching drugs. The ROC-derived threshold for positive cell line (PCC) models (0.28) is represented by the red line.

Applying the AUC z-score yielded insightful findings regarding the drug sensitivities of specific patients. Patient P3_LRRFIP1:ALK, whom harbored the ALK fusion alteration, exhibited sensitivity to only alectinib (Figure 26) while the other ALK inhibitors tested fell below the established threshold. However, this observation did not fully align with the patient's clinical history, as resistance to alectinib and lorlatinib had been observed during treatment progression according to the clinical history. Notably, lorlatinib was on the verge of the threshold, indicating a potential level of sensitivity compared to crizotinib, ceritinib and entrectinib. The AUC Cmax z-score (Figure 27) exhibited identical results to the AUC z-score thereby demonstrating that applying the Cmax correction specifically for the PD parameter AUC in this patient did not yield any discernible difference.

Conversely, for patient P4_ ALK R1275Q with the ALK mutation, all matching drugs surpassed the threshold, suggesting sensitivity to all ALK inhibitors (Figure 26). Lorlatinib exhibited the highest AUC z-score among the identified sensitivities. Once again, the AUC Cmax z-score (Figure 26) demonstrated concordance with the AUC z-score in identifying the drugs that exceeded the threshold level.

In the case of patient P2_ BRAF_V600E who had previously undergone treatment with a combination of dabrafinib and trametinib, dabrafenib was identified as a hit above the threshold (Figure 26). Additionally, Vemurafenib displayed a positive response above the threshold, while sorafenib, selitrectinib and trametinib fell below the threshold indicating lack of sensitivity to these drugs. The observation of additional alterations in the patient sample, which would have made resistance to BRAF and MEKK1/2 inhibitors more plausible, was not fully realized in this case. The AUC Cmax z-score analysis (Figure 27) revealed a notable distinction compared to the AUC z-score as vemurafenib did not exceed the threshold. Once again, it was evident that the patient's medical history was not adequately reflected in this particular case.

P5_BRAF V600E, another patient with a BRAF mutation sensitivity was observed for vemurafenib and selumetinib (Figure 26) which better aligned with the patient's clinical history as the patient had already received trametinib and dabrafenib treatment that led to progressions. The AUC Cmax z-score analysis (Figure 27) yielded identical results to the AUC z-score, indicating that there was no added value in implementing Cmax for this specific case.

In the case of patient P1_ KANK1:NTRK3, sensitivity to entrectinib was detected based on the AUC z-score (Figure 26) while larotrectinib and selitrectinib fell below the threshold. The AUC Cmax z-score analysis (Figure 27) yielded identical outcomes to the AUC z-score, with the

exception of selitrectinib, which could not be determined due to the absence of Cmax information.

Considering all the data together, it was observed that both the AUC z-score and AUC Cmax z-score did not appear to effectively predict the matching drugs in the PPT subgroup I samples or accurately represent the patient's clinical history compared to the DSS Cmax z-score.

4.6 Clinical follow up

Clinical follow up was conducted by sending a follow up letter (Supplementary Figure 17) and a follow up questionnaire (Supplementary Figure 18 and Supplementary Figure 19) to the treating physician of the patient enrolled in the INFORM study. This was done within 3-6 months of sharing the DSP outcomes for the respective patient samples. The questionnaire was designed in a way to maximize efficiency and minimize the time required for physicians to complete it. Additionally, sections of the questionnaire that could be pre-filled before sending were completed in advance. A total of 36 follow up enquiries were sent out and response was obtained in 42% (15/36) of the enquiries. The drugs identified through the DSP analysis as potential hits and reported in the weekly MTB were not administered to the patients in any of the 15 cases. Given the lack of collected clinical response data, this outcome did not provide an adequate foundation for further analysis. Consequently, this arm of data collection was discontinued.

4.7 DSS Cmax z-score analysis of primary patient tumor samples without a defined drug target match

As demonstrated by its performance in reflecting the clinical history of the PPT subgroup I samples, the DSS Cmax z-score was evaluated across all PPT samples, without a defined and proven drug-target relationship. Due to the absence of *in vivo* clinical response data for these samples, the assessment of DSS Cmax z-score performance was confined to the patient cohort classified based on diagnostic categories and drug classes (Supplementary Figure 3). The data set comprised a total of 68 PPT samples and a total number of 991 observations, with each observation corresponding to a single drug measurement for a given sample. The predominant trend within the data set indicated resistance (64%, n=631/991, Supplementary Figure 4) of the samples, defined as a DSS Cmax z-score value below 0.04, towards the drugs tested. Among the subset that demonstrated sensitivity (36%, n=360/991) the top five most common drugs (Figure 28) were navitoclax (7.5% 27/360), idasanutlin (6.9%, n=25/360), cytarabine (6.4%, n=23/360) and daunorubicin (5.3%, n=19/360). AMG-232, gemcitabine and selinexor shared a fifth place each accounting for 5% (n=18/360) of the observations. Notably, the most commonly encountered top five drugs belong to two distinct drug classes namely, the apoptotic modulators and conventional chemotherapeutics.

Application of the DSS Cmax z-score on patient samples without a defined drug target match resulted in the identification of at least one drug hit, in 83% (n=57/68) of patient samples. Additionally, for 77% (n=53/68) of patient samples, the DSS Cmax z-score identified a hit where NGS did not identify a priority score 1 (very high) or priority score 2 (high) target, demonstrating a clear added benefit of DSP in addition to NGS guided information.
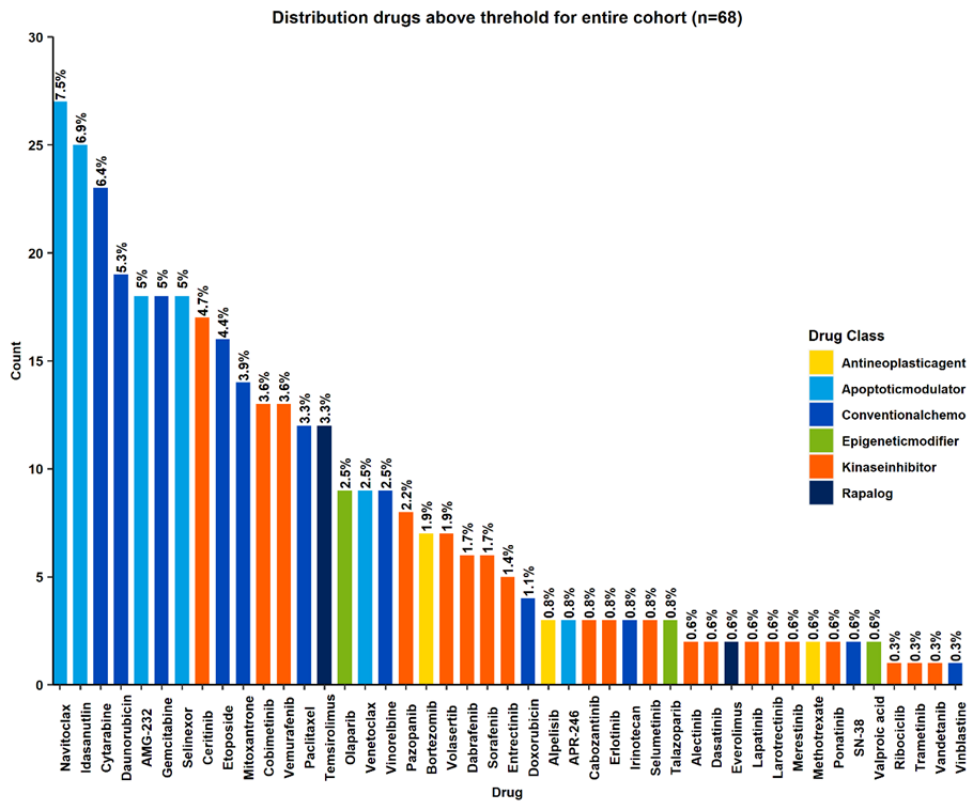
Figure 28. Drug distribution within the subset of observations showing sensitivity. A total of n=360/991 observations with DSS Cmax z-score values above 0.04.

The highest DSS Cmax z-score overall, was found among the group of rare tumors (diagnostic category "other"). The congenital mesoblastic nephroma sample showed the highest DSS Cmax z-score value of 5.1 for lapatinib the EGFR inhibitor. This was followed by entrectinib (DSS Cmax z-score 4.9) and venetoclax (DSS Cmax z-score 4.8) each occurring within distinct Wilms tumor samples and alextinib (DSS Cmax z-score 4.6) within an EWS sample.

4.7.1 Ewing sarcoma

The EWS samples (n=6) exhibited resistance (interpreted as DSS Cmax z-score below 0.04) to the majority of observations (71%, Figure 29a). Overall the EWS samples showed most sensitivity towards the apoptotic modulators (39%, n=11/28), followed by the conventional chemotherapeutics (32%, n=9/28) and kinase inhibitors (25%, n=7/28) (Figure 29b).

Figure 29. Summary of Ewing sarcoma (EWS) samples for the DSS Cmax z-score. (a) - Drug resistance and sensitivity trends for all ES patients and drugs. One observation represents one drug measurement for one sample. (b) - Drug distribution within the subset (n=28/97) of observations showing sensitivity (DSS Cmax z-score above 0.04). (c) - Overview of ESW primary patient tumor samples (n=6) classified by drug class using the DSS Cmax z-score (cut off 0.04). Drugs with DSS Cmax z-score below -3 had a clinically unattainable concentration.

Only one sample, I034_038_1T1_V2, demonstrated an in-class effect for the apoptotic modulators AMG-232, idasanutlin and selinexor targeting MDM2 and CRM1 (Figure 29c, Supplementary Figure 5). Based on the NGS results, this sample had an EZH2 overexpression.

Samples I063_020_1M1_V1, I034_038_1T1_V2 and I034_058_2T1_V1 exhibited higher sensitivity towards vemurafenib (Figure 29c, Supplementary Figure 5). These samples did not display any pattern in their molecular alterations compared to the non-sensitive samples. Notably, I034_058_2T1_V1 harbored a BRAF overexpression which could explain potentially its sensitivity towards vemurafenib. However, this alteration was not observed in the other two samples. Sample I063_020_1M1_V1 in addition to being sensitive to vemurafenib, demonstrated the highest sensitivity towards alectinib. Sample I013_026_4M1_V1 exhibited sensitivity towards volasertib. While there is no direct evidence in the literature linking sensitivity to vemurafenib, alectinib and/or volasertib in EWS, these drugs could be promising targets for further exploration.

It has been reported that chemotherapy, as the first-line treatment, effectively controlled EWS for many patients with localized disease. However, for relapsed patients, the prognosis was still dismal (49). Additionally, EWS did not have clear alterations, including mutations or amplification in the kinase domain. This was clearly reflected in the outcomes of DSP, where half of the tested drugs showed clinical unattainability (Figure 29) and drug resistance.

Functional screening provided valuable additional information that complemented NGS analysis. In the case of the mentioned samples, it revealed potential effectiveness in vemurafenib, volasertib, and alectinib sensitivities. This suggested the possibility of alternative treatment options for these patients, warranting further investigation.

4.7.2 Osteosarcoma

In the patient cohort of OSA (n=9), the samples showed high resistance to the majority of observations (75%, Figure 30a). Five out of the nine samples (I034_045_1M1_V1, I036_051_1M1_V1, I054_031_1M1_V1, I094_035_9M1_V1 and I133_009_1M2_V1) exhibited a very high level of resistance to all the listed drugs, while 2/5 samples (I036_051_1M1_V1, and I133_009_1M2_V1) exhibited resistance to all drugs tested (Figure 30c). Interestingly 4/5 samples shared a common molecular alteration background. These four samples presented with alterations involving the cell cycle regulation. Specifically, samples I034_045_1M1_V1, I094_035_9M1_V1 and I133_009_1M2_V1 displayed a CCNE1 amplification while sample I036_051_1M1_V1 exhibited a CDKN2A/B deletion and CCND3 amplification. Furthermore, sample I034_045_1M1_V1 also showed a MYC amplification, which has been previously associated with poor prognosis (50). Sample I036_051_1M1_V1 had a VEGFA amplification as well as FGFR1 and PDGFC overexpression contributing to a

worse prognosis as reflected in the DSP outcome. Sensitivity within the OSA cohort was displayed mainly for kinase inhibitors (43%) and conventional chemotherapeutics (36%) (Figure 30b).
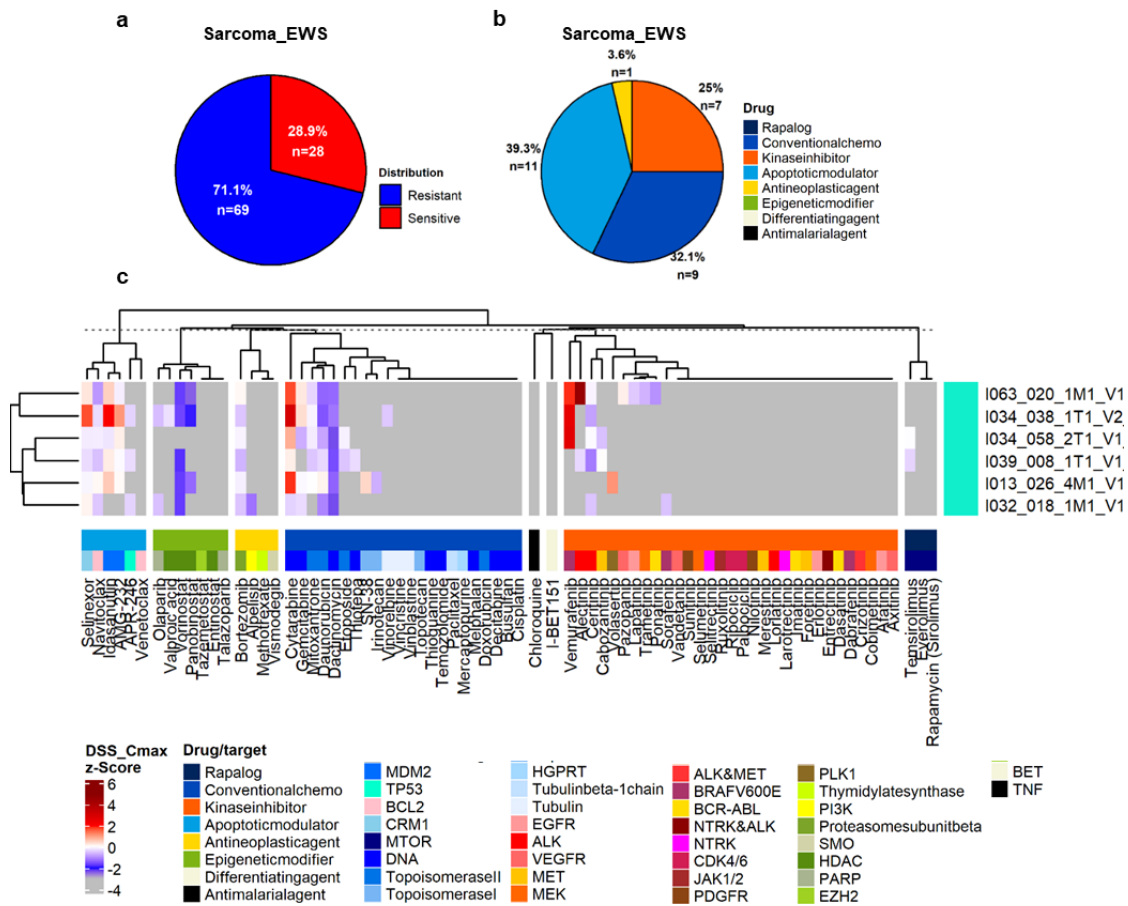

Figure 30. Summary of osteosarcoma (OSA) samples for the DSS Cmax z-score. (a) - Drug resistance and sensitivity trends for all OS patients and drugs. One observation represents one drug measurement for one sample. (b) - Drug distribution within the subset (n=28/110) of observations showing sensitivity (DSS Cmax z-score above 0.04). (c) - Overview of OSA primary patient tumor samples (n=9) classified by drug class using the DSS Cmax z-score (cut off 0.04). Drugs with DSS Cmax z-score below -3 had a clinically unattainable concentration.

Sample I063_021_9T1_V1 displayed the highest sensitivity (highest DSS Cmax z-score) to at least one drug within each tested drug class. An in-class effect was observed within the BRAF V600E inhibitors vemurafenib, dabrafenib and sorafenib (Figure 30c, Supplementary Figure 6), potentially attributed to the presence of the MYC amplification and overexpression identified in the NGS results for this sample. Additionally, the sample exhibited sensitivity towards volasertib, entrectinib, pazopanib and erlotinib. The presence of an ERBB4 mutation

could explain the sensitivity towards erlotinib. Furthermore, the sample demonstrated sensitivity towards olaparib which has been previously described in literature as OSA exhibited relatively high-level homologous recombination-deficient signatures, making it a target for PARP inhibitors such as olaparib (50). The antineoplastic agent bortezomib and the apoptotic modulator selinexor also showed positive responses in the DSP analysis.

Sample I133_012_1M1_V1 which exhibited a CCNE1 amplification and IGF1 overexpression demonstrated sensitivity towards temsirolimus (Figure 30c, Supplementary Figure 6). Although the molecular background of this sample did not indicate involvement in the PI3K/mTOR pathway, it has been described in literature that the IGF1 receptor, which promotes cell differentiation and proliferation, can interact with the PDGF receptor to produce mTOR in the PI3K pathway (50). Notably, this sample did not exhibit sensitivity towards any other drugs tested.

The poor prognostic outcome observed in patients who experienced relapse within this diagnostic category was evident in the results of the DSP analysis. Out of a total of nine patients, only one exhibited high sensitivity towards multiple drugs (Figure 30c, Supplementary Figure 6), while two patients displayed modest sensitivity towards a single drug. Although the literature lacks specific descriptions regarding these sensitivities within OSA, further investigation of these drugs could contribute to the identification of additional treatment possibilities.

4.7.3 Ependymoma

The EPN samples (n=6) exhibited a high level of resistance (74%, Figure 31a) towards most of the observations. Due to the presence of relapses, their prognosis is poor, and it has been reported that patients succumb to the disease within 8.7 – 24 months after several episodes of relapse (51). Prolonged survival is typically achieved through surgical interventions or radiation therapy. The samples showed most sensitivity towards the apoptotic modulators (40%) and conventional chemotherapeutics (30%) (Figure 31b).
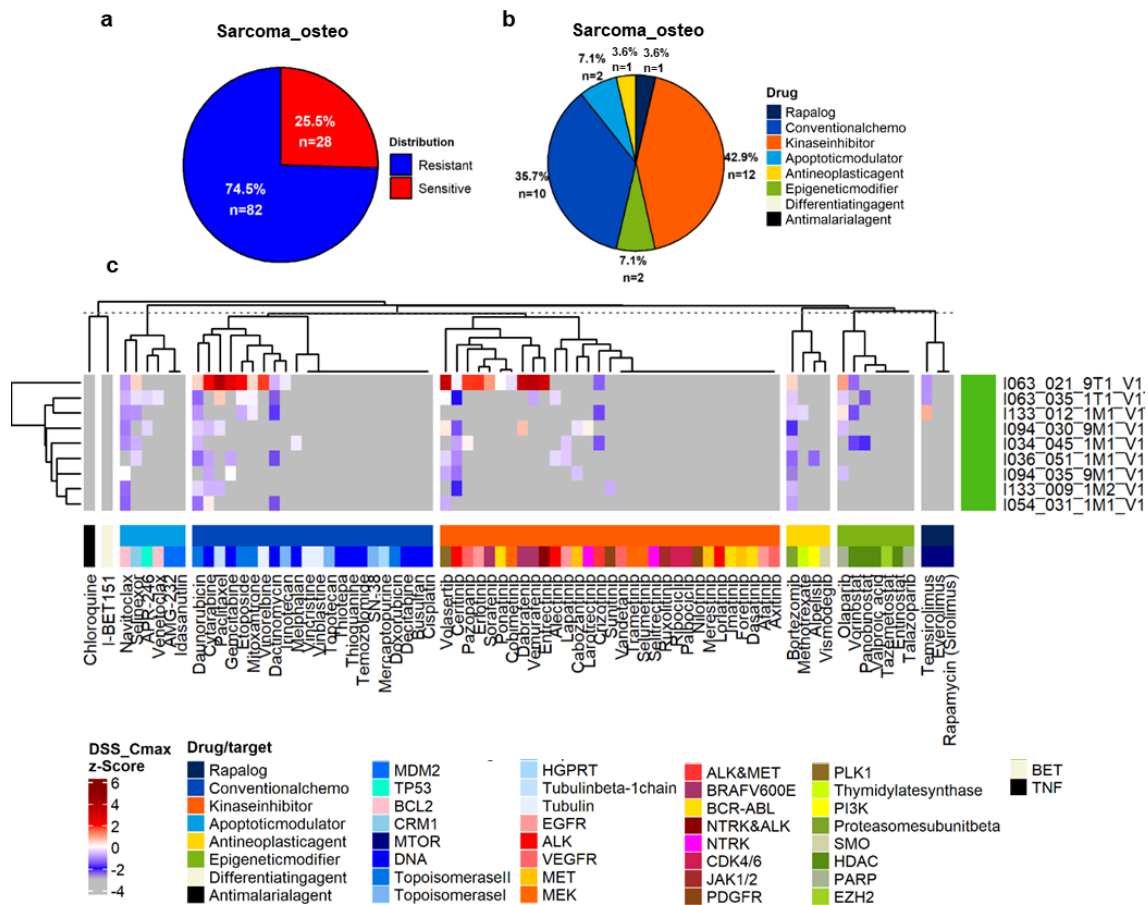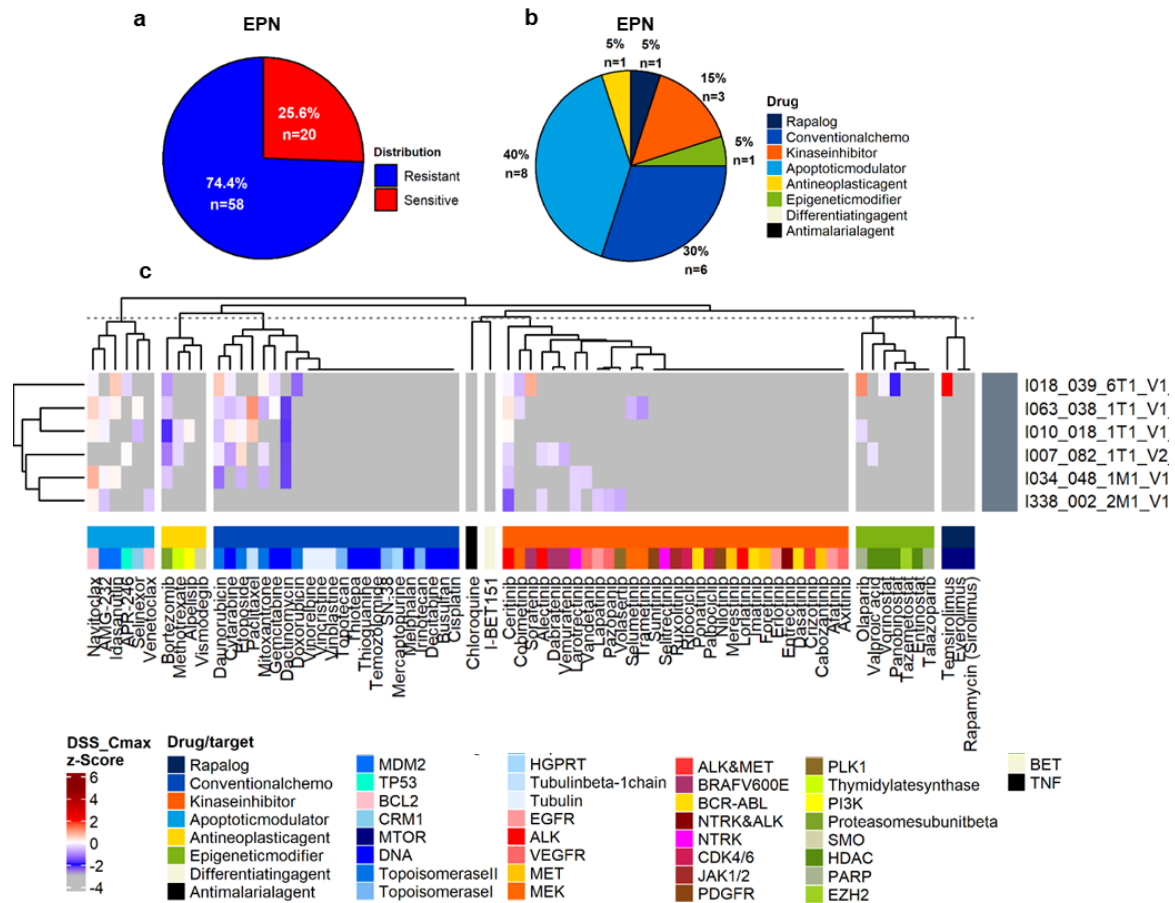
Figure 31. Summary of ependymoma (EPN) samples for the DSS Cmax z-score. (a) - Drug resistance and sensitivity trends for all EPN patients and drugs. One observation represents one drug measurement for one sample. (b) - Drug distribution within the subset (n=20/78) of observations showing sensitivity (DSS Cmax z-score above 0.04). (c) - Overview of EPN primary patient tumor samples (n=6) classified by drug class using the DSS Cmax z-score (cut off 0.04). Drugs with DSS Cmax z-score below -3 had a clinically unattainable concentration.

Out of the six samples, sample I018_039_6T1_V1, demonstrated sensitivity towards multiple drug classes with the highest sensitivity observed towards the rapalog temsirolimus (Figure 31c, Supplementary Figure 7), which targets the mTOR pathway. Clinical data on the efficacy of mTOR inhibitors in EPN has shown some response such as the treatment with sirolimus monotherapy which resulted in the best response rate and longest time before tumor progression. However, these responses did not translate into improved overall survival (52). Furthermore the sample exhibited sensitivity towards olaparib (Figure 31c, Supplementary Figure 7) which has been previously described in posterior fossa EPN (53). The tumor cells overexpressing EZHIP have shown sensitivity towards olaparib particularly when combined with radiotherapy (53). While the sample showed sensitivity towards idasanutlin and sorafenib

(Figure 31c, Supplementary Figure 7), there was limited information available in the literature regarding the use of these drugs within this diagnostic category.

The DSP outcome for this particular sample aligns with the drugs commonly mentioned in the literature, reflecting the potential of the metric DSS Cmax z-score in DSP outcomes.

4.7.4 Sarcoma other

Within the sarcoma_other group, n=11 samples with several types of sarcoma were included as they did not match the most common sarcoma subtypes (Figure 32). The samples showed resistance to the majority of observations (64%, Figure 33a). Interestingly, sensitivity of the samples was observed mainly for the apoptotic modulators (33%), conventional chemotherapeutics (33%) and kinase inhibitors (28%) (Figure 33b).
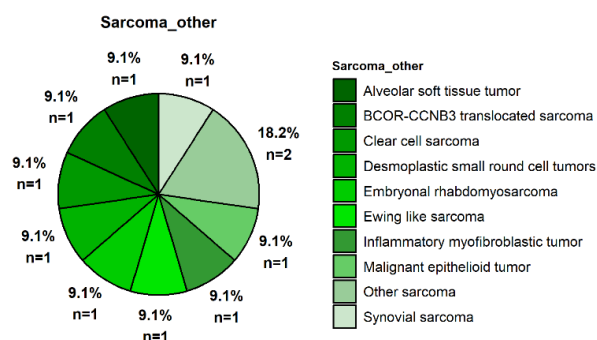
Figure 32. Summary of the ten sarcoma subtypes categorized within the "sarcoma_other" group.

Four out of the 11 samples, I045_006_0T1_V1, I137_013_1T1_V1, I036_038_9M1_V2 and I070_030_0T1_V2 showed resistance against all drugs tested (Figure 33c). Among the five samples I024_034_1M1_V1, I100_001_1T1_V1, I070_032_0T1_V1, I094_015_1M1_V1 and I045_005_0T1_V1 an in-class effect for the apoptotic modulators was observed (Figure 33c, Supplementary Figure 8). This could potentially be due to apoptotic priming which was not reflected in the NGS results. Samples I094_015_1M1_V1 and I045_005_0T1_V1 demonstrated a high sensitivity towards pazopanib (Figure 33c, Supplementary Figure 8), a multi target kinase inhibitor targeting VEGFR, PDGFR and c-KIT. A recent phase II clinical trial, which included pediatric and adult patients with advanced soft tissue sarcoma (excluding Ewing's sarcoma and rhabdomyosarcoma), showed enhanced efficacy of pazopanib when used in combination with conventional chemotherapy compared to chemotherapy alone (54). The primary outcome of the trial was to evaluate the rate of pathologic responses, evaluated through pathology review and defined as at least 90% non viable tumor. The trial found that 58.3% of patients treated with the addition of pazopanib treatment achieved the desired pathologic response, while only 22.2% of patients in the chemotherapy-only group reached this threshold. The trial did not report on survival outcomes due to the short duration of follow-up. It is noteworthy that I094_015_1M1_V1 exhibited PDGFR overexpression and sample

I045_005_0T1_V1 displayed overexpression of EPHB2. It has been reported in the literature that EPHB2 activates ephrin-B2, which in turn controls the endocytosis of VEGFR2 and VEGFR3, thereby influencing VEGFR2-dependent signaling pathways involved in tumor angiogenesis (55). This finding may explain the sensitivity of these two samples towards pazopanib.
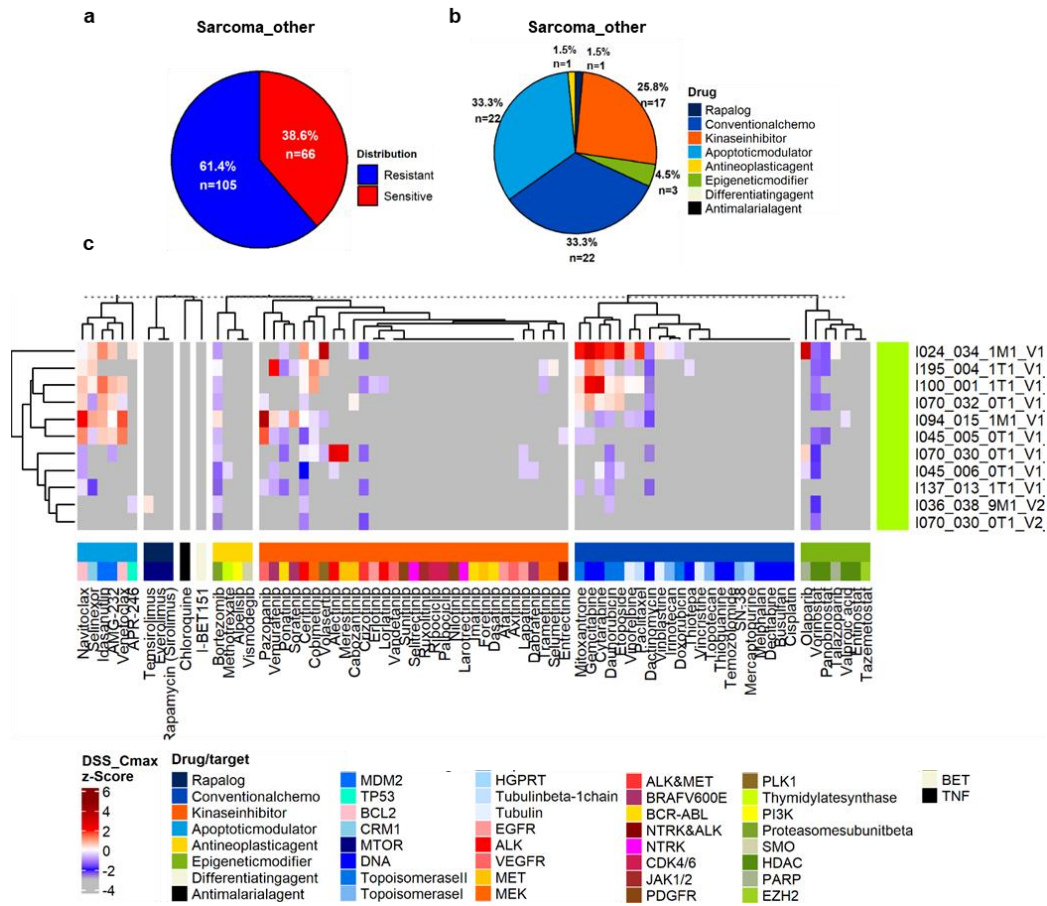
Figure 33. Summary of several sarcoma samples within the Sarcoma_other group for the DSS Cmax z-score. (a) - Drug resistance and sensitivity trends for all patients and drugs. One observation represents one drug measurement for one sample. (b) - Drug distribution within the subset (n=66/171) of observations showing sensitivity (DSS Cmax z-score above 0.04). (c) - Overview of Sarcoma other primary patient tumor samples (n=11) classified by drug class using the DSS Cmax z-score (cut off 0.04). Drugs with DSS Cmax z-score below -3 had a clinically unattainable concentration.

Sample I195_004_1T1_V1 exhibited sensitivity towards vemurafenib, cobimetinib and in lesser extend volasertib Figure 33c, Supplementary Figure 8). This sample carried an NF1 mutation which could potentially explain the sensitivity towards BRAF and MEK inhibitors that affect the RAS/MAPK pathway (56). Volasertib has been described in pre-clinical screens using NF1-null cell lines as well as mouse xenograft models to cause inhibition of tumor growth (57).

Sample I024_034_1M1_V1 exhibited strong sensitivity towards the kinase inhibitors volasertib and olaparib (Figure 33c, Supplementary Figure 8). Olaparib has been reported to demonstrate promising preliminary results in an adult clinical trial involving advanced soft tissue sarcoma in combination with radiotherapy (58). Furthermore, volasertib has received the Orphan Drug Designation from the FDA for the treatment of pediatric RMS and its effectiveness was also reflected in the sensitivity of this sample.

Sample I094_015_1M1_V1 exhibited sensitivity towards vemurafenib and sorafenib, and sample I100_001_1T1_V1 displayed sensitivity towards cobimetinib (Figure 33c, Supplementary Figure 8). Both showed sensitivity to BRAF and MEK inhibitors. However, no specific information could be found in the literature regarding this particular observation. Further investigation and research are needed to explore the potential significance and implications of the sensitivity of these samples to BRAF inhibitors and MEK inhibitors.

Samples I070_030_0T1_V1 and I070_030_0T1_V2 originated from the same patient and represented two different vial tissue samples submitted for screening. The first sample V1 was sensitive for alectinib, merestinib and olaparib (Figure 33c, Supplementary Figure 8). However, the second sample exhibited resistance to all drugs included in the screening. No existing evidence was found regarding the sensitivity of these samples to the mentioned drugs. Both samples carried a high priorty score (score 2) FGFR1:CAPRIN1 fusion and while the second sample did not display any effectiveness in response to the screened drugs, further exploration of the efficacy of alectinib, merestinib and olaparib could potentially lead to promising treatment.

4.7.5 Rhabdomyosarcoma

Within the RMS samples (n=6), 72% of the observations showed resistance (Figure 34a). Interestingly, sensitivity was shown within the kinase inhibitors (35%), apoptotic modulators (25%) and conventional chemotherapeutics (20%) (Figure 34b).

Figure 34. Summary of rhabdomyosarcoma (RMS) samples for the DSS Cmax z-score. (a) - Drug resistance and sensitivity trends for all patients and drugs. One observation represents one drug measurement for one sample. (b) - Drug distribution within the subset (n=20/71) of observations showing sensitivity (DSS Cmax z-score above 0.04). (c) - Overview of RMS primary patient tumor samples (n=6) classified by drug class using the DSS Cmax z-score (cut off 0.04). Drugs with DSS Cmax z-score below -3 had a clinically unattainable concentration.

Sample I003_011_9M1_V1 demonstrated high sensitivity towards alpelisib (Figure 34c, Supplementary Figure 9). The literature suggests that the presence of the ERBB3 alteration in these patients can activate the RAS/PI3K axis in RMS. Additionally, a study conducted on RMS cell lines has shown that inhibiting the PI3K/AKT pathway can induce cell death (59).

Sample I034_044_1T1_V1 exhibited a minor in-class effect for the apoptotic modulators AMG-232 and idasanutlin both targeting MDM2 (Figure 34c, Supplementary Figure 9). This observation was consistent with the NGS data, as the sample demonstrated MDM2 amplification/overexpression, which has been previously reported (60). However, the sample displayed the highest sensitivity towards the antineoplastic agent methotrexate. Although methotrexate has not been specifically described for the treatment of advanced pretreated RMS patients, it has shown a response in approximately 33% of previously untreated pediatric RMS patients (61).

I034_042_0T1_V1 exhibited sensitivity to the kinase inhibitor merestinib and a slight sensitivity to sorafenib (Figure 34c, Supplementary Figure 9). Additionally, there was a slight sensitivity to vemurafenib. Although the molecular alteration for this patient did not align with the outcomes observed in DSP, these findings could still provide valuable additional information for further investigation.

Sample I007_088_1T2_V1 exhibited sensitivity towards temsirolimus (Figure 34c, Supplementary Figure 9) and harbored an FGFR4 mutation which has been associated with the mTOR pathway (59). In a phase II clinical trial, temsirolimus was compared to bevacizumab in addition to conventional chemotherapy for the treatment of pediatric RMS.The patient group receiving temsirolimus demonstrated a longer PFS compared to the group receiving bevacizumab. Furthermore, the objective response rate was 47% for temsirolimus compared to 28% in bevacizumab (62).

4.7.6 High grade glioma

The HGG samples (n=8) exhibited resistance towards 74% of the obervations (Figure 35a). Sensitivity was displayed mostly for kinase inhibitors (43%) followed by apoptotic modulators (24%) and conventional chemotherapeutics (19%) (Figure 35b). Among the samples, three samples I105_036_0T1_V1, I338_007_2T1_V1 and I034_051_3T1_V1, displayed high resistance against all tested drugs.
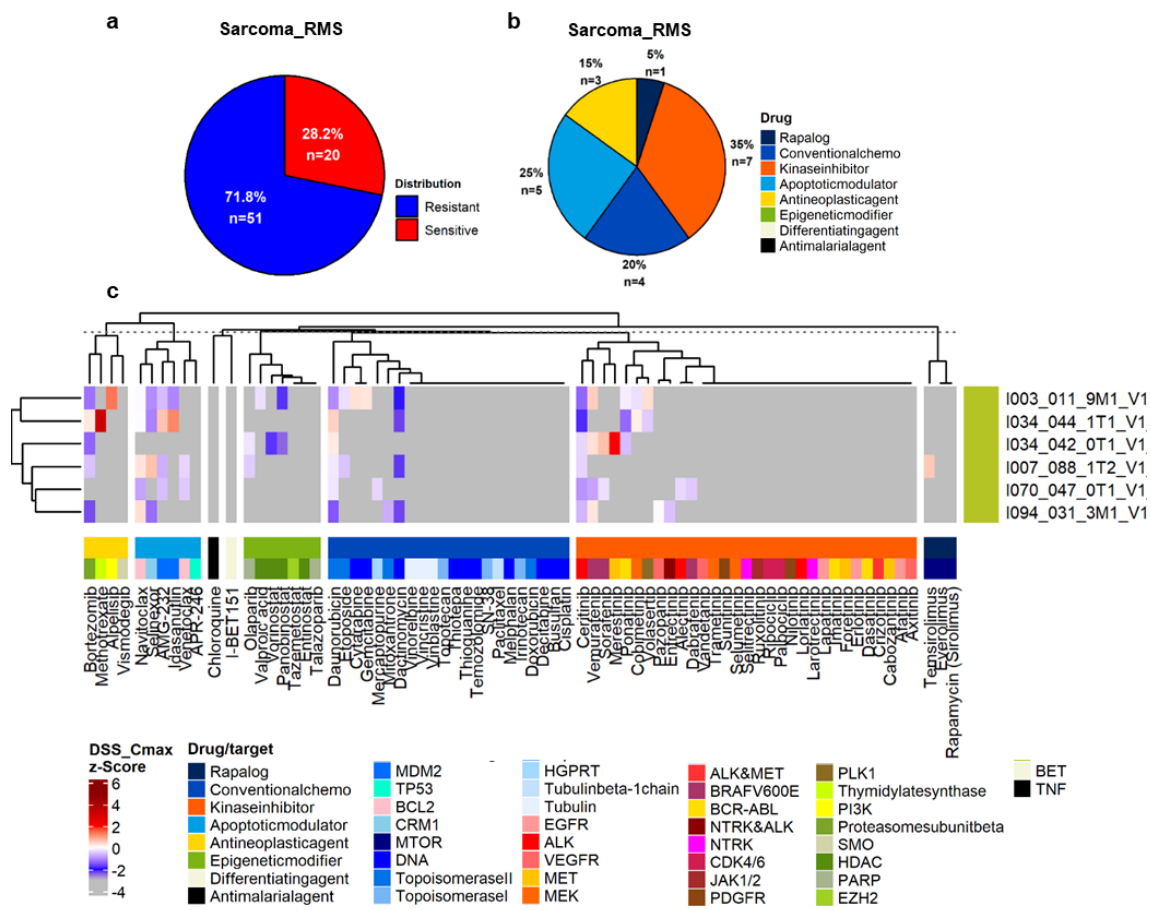
Figure 35. Summary of high grade glioma (HGG) samples for the DSS Cmax z-score. (a) - Drug resistance and sensitivity trends for all patients and drugs. One observation represents one drug measurement for one sample. (b) - Drug distribution within the subset (n=21/82) of observations showing sensitivity (DSS Cmax z-score above 0.04). (c) - Overview of HGG primary patient tumor samples (n=8) classified by drug class using the DSS Cmax z-score (cut off 0.04). Drugs with DSS Cmax z-score below -3 had a clinically unattainable concentration.

In sample I338_004_9T1_V1 sensitivity was observed for both rapalogs, temsirolimus and everolimus (Figure 35c, Supplementary Figure 10). Interestingly, the sample exhibited a genetic alteration, CSF1R overexpression, which has been reported to activate the AKT/mTOR pathway (63). This activation was clearly reflected in the DSP outcome. Additionally, this sample demonstrated sensitivity to dasatinib (Figure 35c, Supplementary Figure 10). A phase II clinical trial evaluated the efficacy of bevacizumab in combination with dasatinib compared to bevacizumab alone in patients with recurrent HGG or glioblastoma. The combination did not result in an improved PFS (64). Nonetheless, it is still noteworthy to consider dasatinib as a hit in this sample, providing additional information for consideration in treatment.

Sample I105_017_1T1_V1 exhibited sensitivity towards temsirolimus (Figure 35c, Supplementary Figure 10). In a study involving six children and young adults with PDGFRA-driven gliomas who were treated with a combination of dasatinib and everolimus, the median OS was reported to be 8.5 months (65). This highlights the potential of rapalogs in improving targeted therapy in HGG. Additionally, the sample demonstrated sensitivity to pazopanib, supporting the alignment between the DSP results and the molecular characteristics of the sample, as the sample harbored a PDGFRA gain.

4.7.7 Other tumors

Six rare tumors were classified in the group of other tumors (Figure 36). Resistance was shown for approximately 67% (Figure 37a) of the observations and sensitivity was shown mainly for kinase inhibitors (56%) and conventional chemotherapeutics (24%) (Figure 37b).
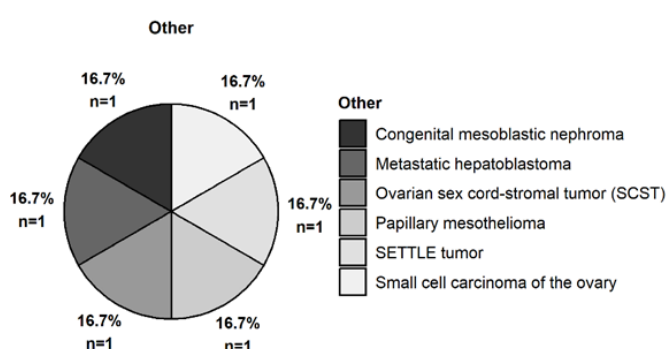
Figure 36. Summary of the six tumor subtypes categorized within the "other" tumors group.

Sample I036_024_1T1_V1, a congenital mesoblastic nephroma sample, exhibited sensitivity to the two apoptotic modulators navitoclax and idasanutlin (Figure 37c, Supplementary Figure 11). Additionally, it exhibited sensitivity towards several kinase inhibitors including lapatinib, dasatinib, vandetanib, erlotinib, cobimetinib and vemurafenib(Figure 37c, Supplementary Figure 11), with the highest sensitivity observed for lapatinib. Remarkably, the high activity of lapatinib was also the highest among the entire cohort, which is consistent with the NGS data since sample I036_024_1T1_V1 is the only sample in the cohort harboring an EGFR:EGFR fusion (priority score 1). This also explains the sensitivity towards erlotinib. While vandetanib has been reported to target EGFR to some extent, it is not as selective as the aforementioned drugs. The sensitivity of this sample to these kinase inhibitors provides an additional layer of information on top of the NGS data, warranting further investigation.

The ovarian sex cord-stromal tumor (SCST) sample I165_002_2T1_V1 exhibited sensitivity towards entrectinib and larotrectinib (Figure 37c, Supplementary Figure 11). The Small cell carcinoma of the ovary sample, I007_089_1T1_V1, displayed sensitivity to sorafenib and

cobimetinib (Figure 37c, Supplementary Figure 11). Both samples lacked any molecular analysis indications for this sensitivity.
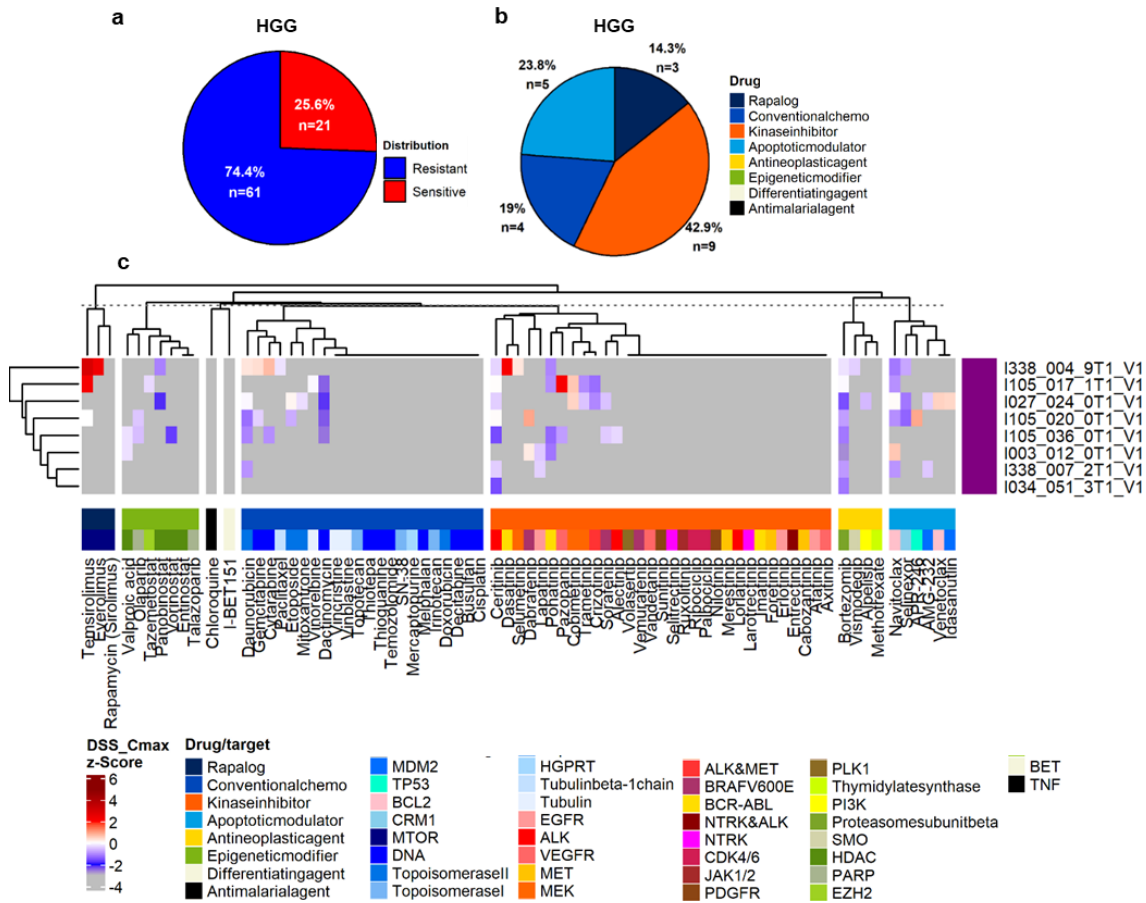

Figure 37. Summary of several rare tumors for the DSS Cmax z-score. (a) -Drug resistance and sensitivity trends for all patients and drugs. One observation represents one drug measurement for one sample. (b) - Drug distribution within the subset (n=25/75) of observations showing sensitivity (DSS Cmax z-score above 0.04). (c) - Overview of several rare tumor samples (n=6) classified by drug class using the DSS Cmax z-score (cut off 0.04). Drugs with DSS Cmax z-score below -3 had a clinically unattainable concentration.

4.7.8 Low grade glioma

The two LGG samples showed resistance towards 76% (Figure 38a) of the observations. Sensitivity was shown to kinase inhibitors (43%) and rapalogs (43%) (Figure 38b). The two LGG samples exhibited similarity in their sensitivity to the rapalogs. I007_094_9T1_V1 demonstrated sensitivity to temsirolimus and everolimus (Figure 38c, Supplementary Figure 12) while I123_042_3T1_V1 showed sensitivity only to temsirolimus (Figure 38c,

Supplementary Figure 12). Hyperactivation of the downstream mTOR pathway is frequently observed in LGG. In a small sized single center study, everolimus was investigated in 10 chemo and radiation naïve mTOR positive LGG patients (66). Among them, 7 patients had stable disease and one showed partial response. The two remaining patients experienced progressive disease. Sample I007_094_9T1_V1 harbored an overexpression of PRKCA. This alteration may explain the sensitivity of this sample to both rapalogs. In contrast, I123_042_3T1_V1 did not harbor any mTOR related pathway, yet showed sensitivity to temsirolimus. Both samples carried a high-priority alteration (score 1 KANK1:NTRK3 fusion and BRAF V600E mutation). However, neither sample exhibited sensitivity to the corresponding targeted drug. While both samples displayed sensitivity to vemurafenib, only I123_042_3T1_V1 harbored a BRAF V600E mutation.

Figure 38. Summary of low grade glioma (LGG) samples for the DSS Cmax z-score. (a) -Drug resistance and sensitivity trends for all patients and drugs. One observation represents one drug measurement for one sample. (b) - Drug distribution within the subset (n=7/29) of observations showing sensitivity (DSS Cmax z-score above 0.04). (c) - Overview of LGG primary patient tumor samples (n=2) classified by drug class using the DSS Cmax z-score (cut off 0.04). Drugs with DSS Cmax z-score below -3 had a clinically unattainable concentration.

4.7.9 Neuroblastoma

The NBL samples (n=4) showed resistance towards 38% of the observations (Figure 39a). The samples exhibited evident sensitivity primarily towards conventional chemo (44%) and apoptotic modulators (33%) (Figure 39b).
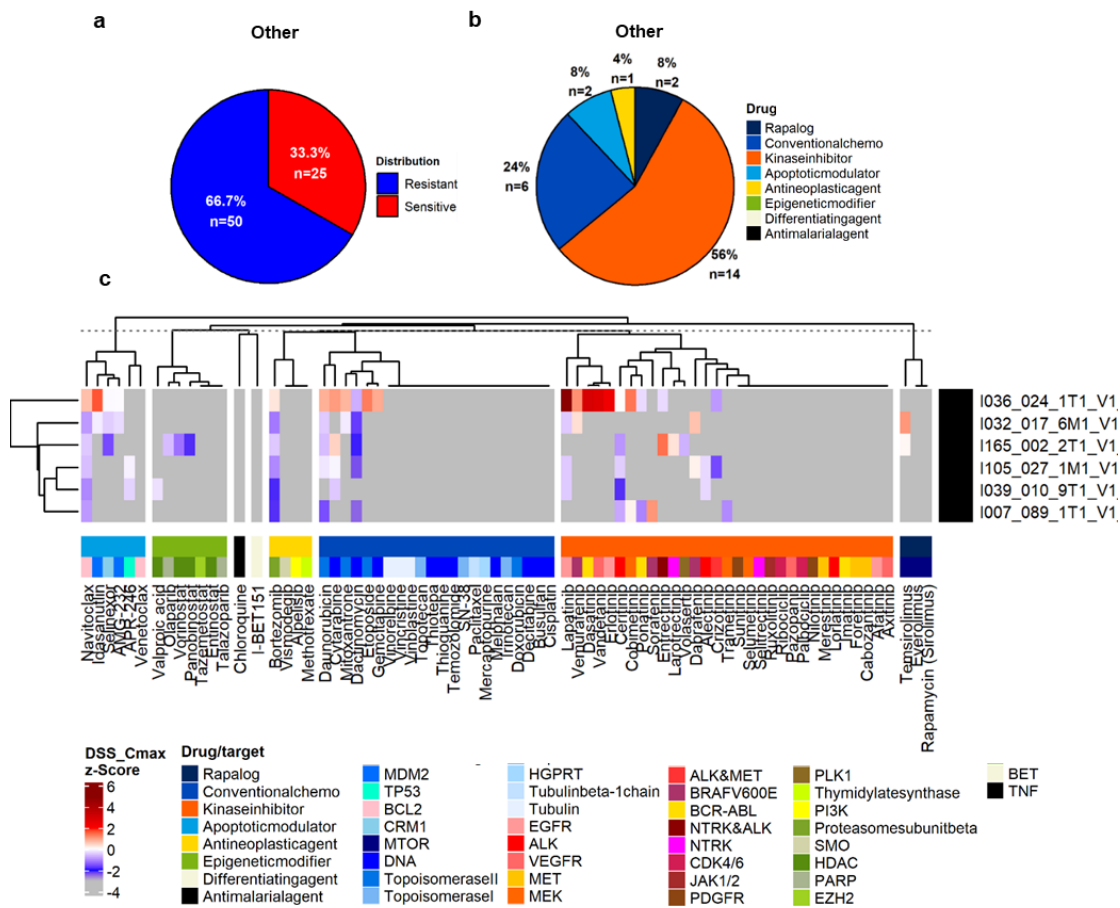

Figure 39. Summary of neuroblastoma (NBL) samples for the DSS Cmax z-score. (a) -Drug resistance and sensitivity trends for all patients and drugs. One observation represents one drug measurement for one sample. (b) - Drug distribution within the subset (n=52/83) of observations showing sensitivity (DSS Cmax z-score above 0.04). (c) - Overview of NBL primary patient tumor samples (n=4) classified by drug class using the DSS Cmax z-score (cut off 0.04). Drugs with DSS Cmax z-score below -3 had a clinically unattainable concentration.

Samples I124_020_3M1_V1 and I195_006_1T1_V1 exhibited sensitivity to both PARP inhibitors olaparib and talazoparib (Figure 39c, Supplementary Figure 13). PARP inhibitors have demonstrated potential in neuroblastoma treatment, particularly in cases characterized by MYCN amplification. MYCN plays a significant role in the development and progression of

neuroblastoma. In MYCN amplified NBL cell line models olaparib and talazoparib have been observed to enhance cell death (67). Both patient samples harbor MYCN amplification. Furthermore, in a first trial of olaparib monotherapy in pediatric patients with solid tumors, preliminary results have indicated promising antitumor responses. Two (2/15) partial responses have been reported in patients with Wilms tumor and NBL (68).

Sample I124_020_3M1_V1 exhibited additional sensitivity to the following kinase inhibitors: lapatinib, ceritinib and entrectinib (Figure 39c, Supplementary Figure 13). Although some data has been reported regarding the efficacy of these drugs in NBL, further research is necessary to fully comprehend their potential in treating NBL. This is because the clinical trials including ceritinib (NCT01742286) and entrectinib (NCT02650401) specifically include patients with certain alterations that are not present in this particular sample. As for lapatinib, its description is limited to pre-clinical data, indicating its potential as a combination partner in NBL (69). The observed synergy was attributed to the inhibition of the ABCB1 efflux transporter, which happens to be overexpressed in NBL-resistant cells. The results obtained from DSP analysis could serve as an additional motivation to explore the effects of these drugs in NBL more extensively.

Sample I034_047_1M1_V1 exhibited additional sensitivity to boritzomib, ceritinib and olaparib (Figure 39c, Supplementary Figure 13). As previously mentioned, these two drugs (ceritinib and olaparib) have been described in relation to NBL, but in the context of specific molecular alterations that were not present in this particular sample. This suggests that there might be an effect for certain samples even in the absence of these alterations. Further evaluation is required to investigate the underlying mechanisms responsible for this phenomenon and determine the basis for their effectiveness.

4.7.10 Wilms tumors

The six Wilms tumor samples showed resistance towards 53% (Figure 40a) of the observations. The highest sensitivity was shown for the conventional chemotherapeutics (38%), apoptotic modulators (27%) and kinase inhibitors (25%) (Figure 40b).
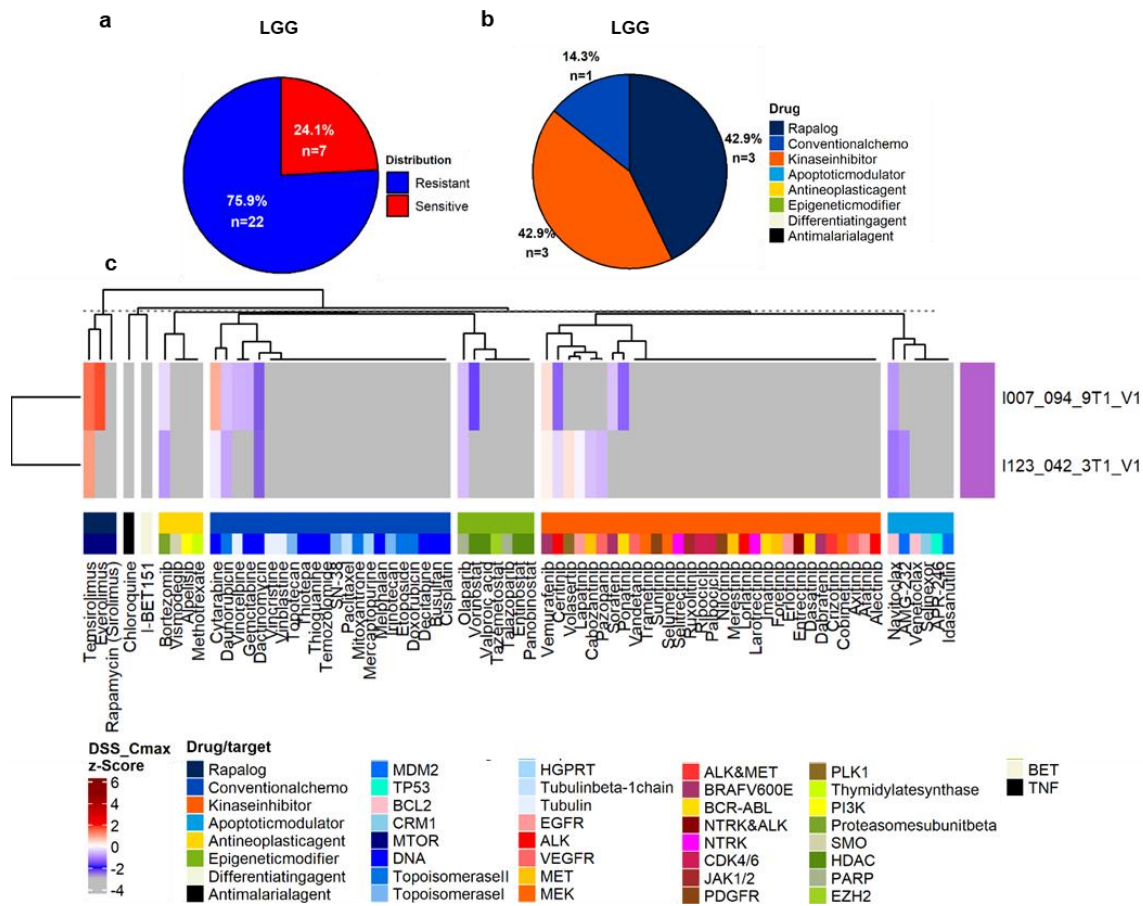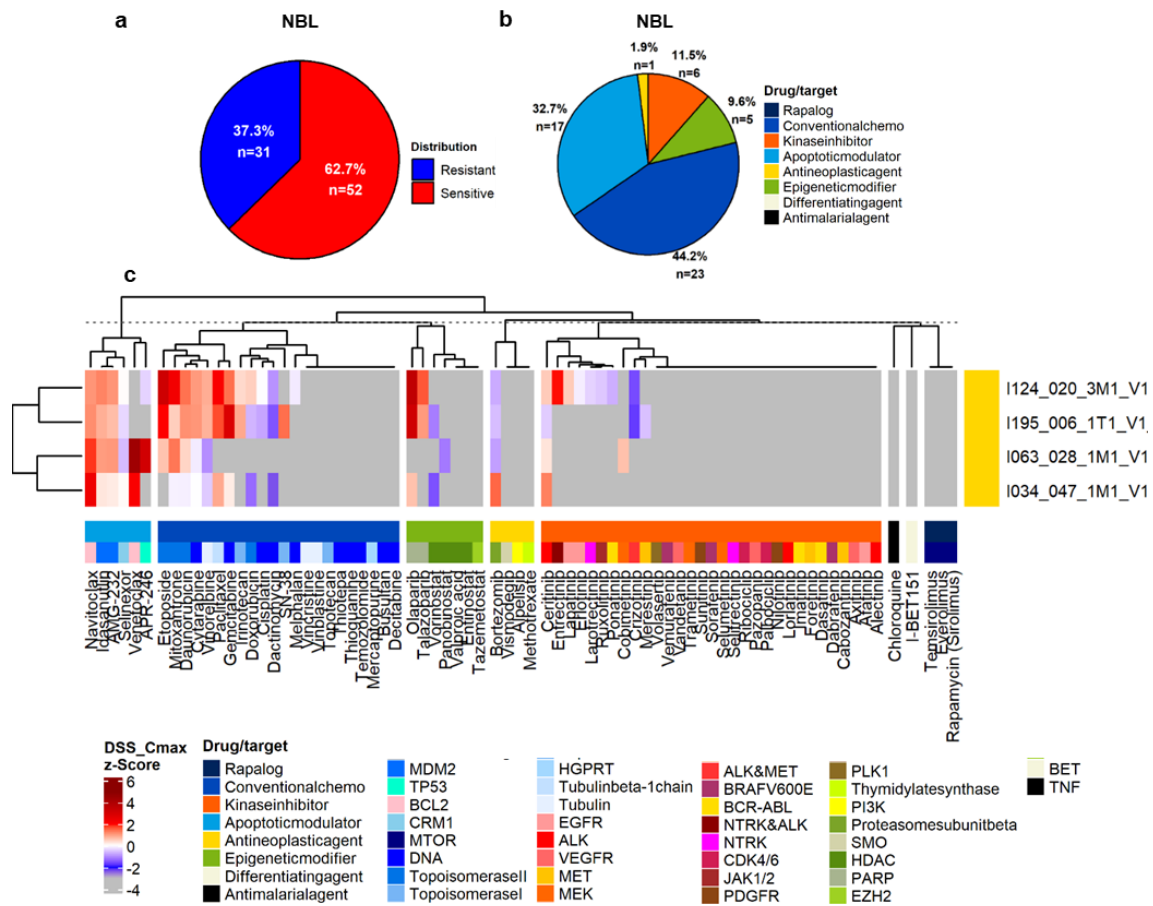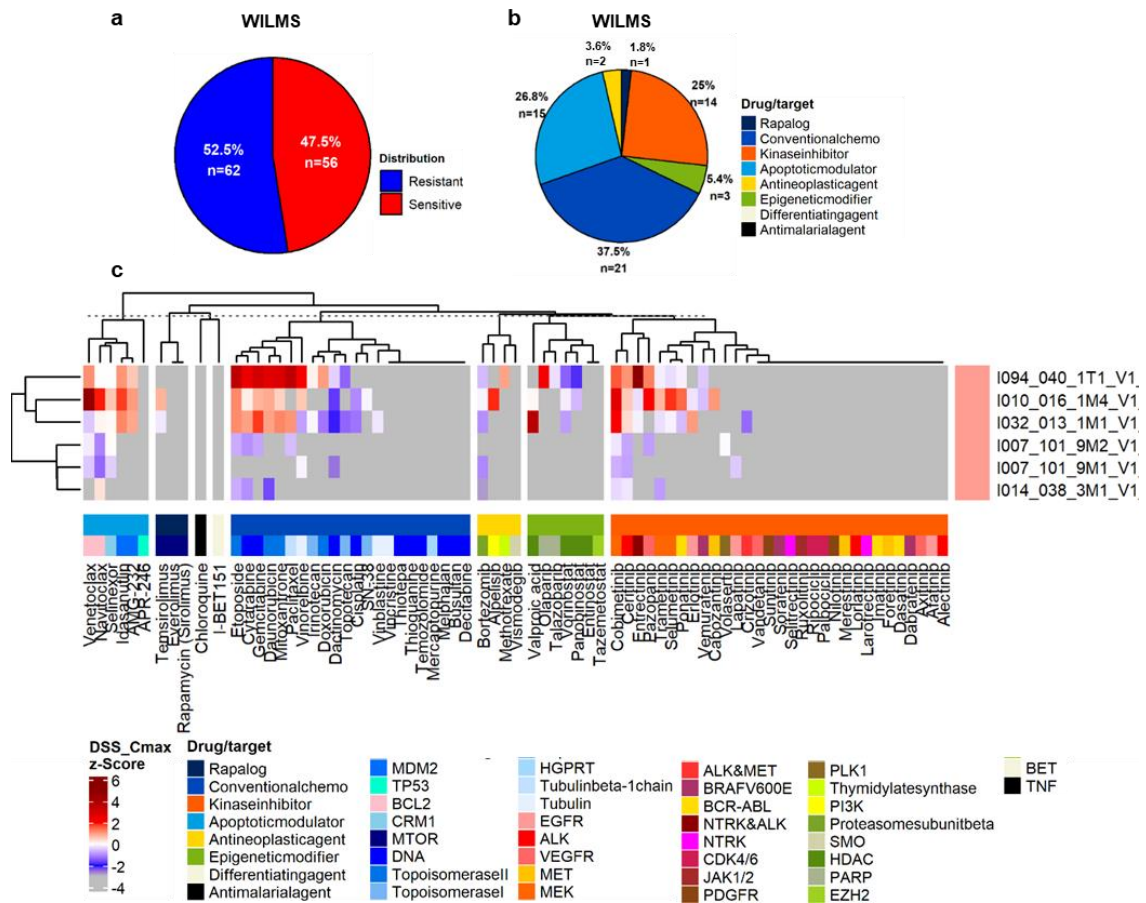
Figure 40. Summary of Wilms tumor samples for the DSS Cmax z-score. (a) -Drug resistance and sensitivity trends for all patients and drugs. One observation represents one drug measurement for one sample. (b) - Drug distribution within the subset (n=56/118) of observations showing sensitivity (DSS Cmax z-score above 0.04). (c) - Overview of Wilms primary patient tumor samples (n=6) classified by drug class using the DSS Cmax z-score (cut off 0.04). Drugs with DSS Cmax z-score below -3 had a clinically unattainable concentration.

Sample I007_101_9M1_V1, exhibited resistance to all drugs (Figure 40c, Supplementary Figure 14). Sample I007_101_9M2_V1 originated from different metastatic sites of the same patient. The DSP analysis revealed a striking similarity for these samples, although sample I007_101_9M2_V1 showed a slight sensitivity towards selinexor (DSS Cmax z-score 0.07, Supplementary Figure 14). The molecular basis for the observed resistance in these samples remains unclear. Further investigation is required to elucidate the molecular mechanisms underlying the resistance phenotype in these cases.

The remaining three samples exhibited an in-class effect in response to the apoptotic modulators. I010_016_1M4_V1 demonstrated the most striking in class effect, displaying sensitivity to navitoclax, AMG-232, idasanutlin, selinexor and particularly high sensitivity to venetoclax (Figure 40c, Supplementary Figure 14). This drug response pattern was consistent

with the NGS outcomes, which revealed overexpression of BCL2 and XPO1 in the sample. Sample I094_040_1T1_V1 exhibited sensitivity to AMG-232, idasanutlin and navitoclax (Figure 40c, Supplementary Figure 14) and sample I032_013_1M1_V1 displayed sensitivity to idasanutlin, AMG-232, navitoclax and selinexor (Figure 40c, Supplementary Figure 14). This sample harbored overexpression of BRD3, which is a member of the BET protein family which suggests a potential priming effect on the cells towards apoptosis.

Sample I094_040_1T1_V1 demonstrated sensitivity to multiple kinase inhibitors including cobimetinib, pazopanib, ceritinib and the highest sensitivity observed towards entrectinib (Figure 40c, Supplementary Figure 14). In addition to the kinase inhibitors, it also exhibited sensitivity to the epigenetic modifier olaparib (Figure 40c, Supplementary Figure 14). In a first trial of olaparib monotherapy in children with solid tumors, preliminary results have been found in antitumor responses. Two (2/15) partial responses have been reported in patients with Wilms tumor and NBL (68). No evidence of sensitivity was found in Wilms tumors towards the other drugs, indicating the presence of new potential areas that warrant further investigation.

Sample I010_016_1M4_V1 exhibited sensitivity to multiple kinase inhibitors as well, including pazopanib, cabozantinib, ceritinib, cobimetinib, trametinib, ponatinib and selumetinib (Figure 40c, Supplementary Figure 14), indicating an in-class effect for MEK inhibitors. In literature a case study involving the use of cabozantinib in a patient with multiple relapsed WILMS tumor reported a partial response lasting for 2 years (70). It is important to note that the genetic alterations observed in that particular case study, MYCN and MAX overexpressions do not correspond to the alterations found in the present patient's sample. Nonetheless, it is intriguing that this sample demonstrated an in-class effect for the MEK inhibitors. No information was found regarding the efficacy of the other drugs in Wilms tumors, suggesting new potential areas to be explored in the context of Wilms tumors.

Sample I032_013_1M1_V1 displayed sensitivity to the kinase inhibitors cobimetinib and erlotinib and to the epigenetic modifier valproic acid (Figure 40c, Supplementary Figure 14). However, there is currently no published information available regarding the use of these drugs in the context of Wilms tumors. Whenever information was found, it was specific to targeting certain alterations that the patient did not possess. This highlights the additional value of drug screening beyond known genetic alterations. In this case, the drug screening approach identified potential efficacy of cobimetinib, erlotinib, and valproic acid in the absence of the corresponding target alterations, emphasizing the importance of exploring broader drug response patterns in Wilms tumors.

4.7.11 Medulloblastoma

The MED (n=1) and MED SHH (n=2) samples showed 45% and 42% resistance towards the observations (Figure 41a). Both groups showed sensitivity mostly towards the apoptotic modulators (MED: 44%, MED SHH: 43%) and conventional chemotherapeutics (MED: 44%, MED_SHH: 50%) (Figure 41b).
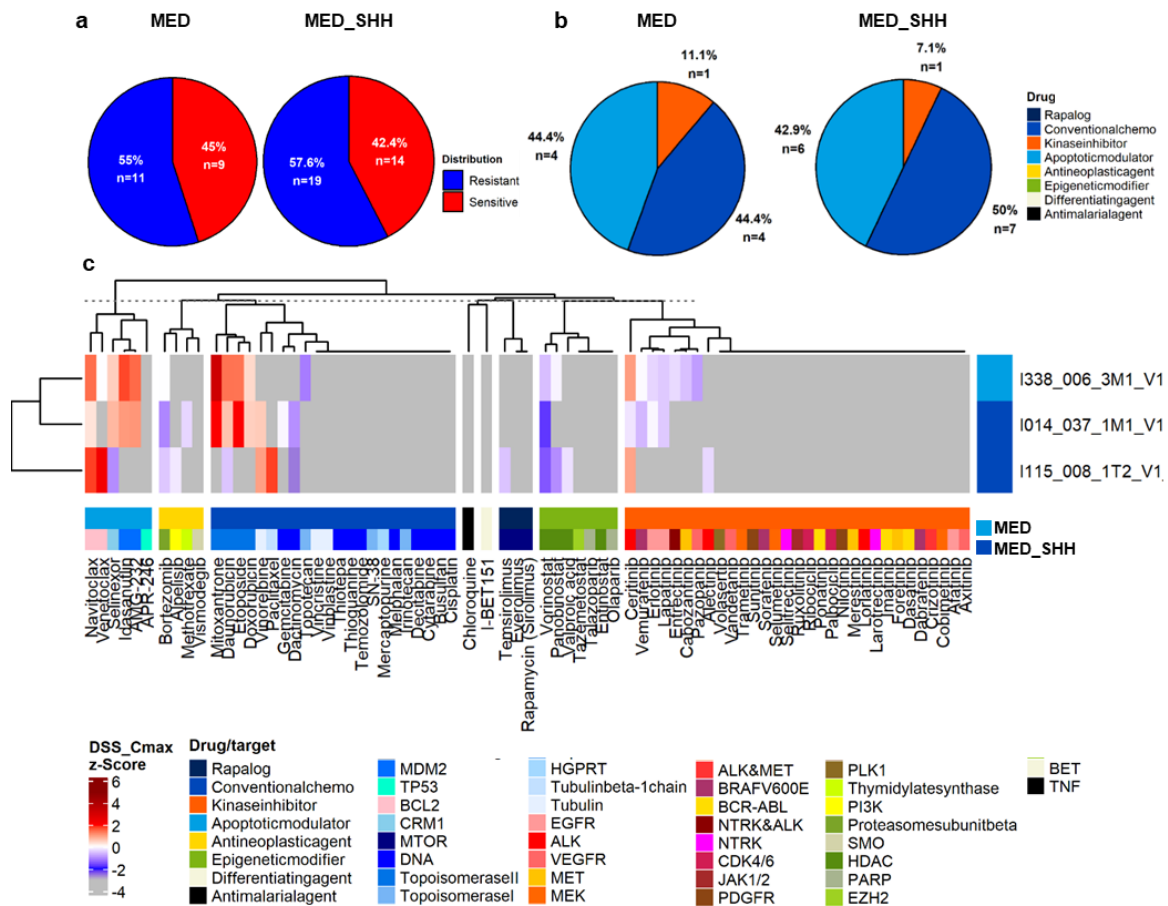
Figure 41. Summary of medulloblastoma (MED) and sonic hedgehog medulloblastoma (MED SHH) samples for the DSS Cmax z-score. (a) -Drug resistance and sensitivity trends for all patients and drugs. One observation represents one drug measurement for one sample. (b) - Drug distribution within the subset (MED: n=9/20, MED SHH: 14/33) of observations showing sensitivity (DSS Cmax z-score above 0.04). (c) - Overview of MED and MED SHH primary patient tumor samples (n=3) classified by drug class using the DSS Cmax z-score (cut off 0.04). Drugs with DSS Cmax z-score below -3 had a clinically unattainable concentration.

The MED sample I338_006_3M1_V1 demonstrated an in-class effect for the apoptotic modulators navitoclax, AMG-232, idasanutlin and selinexor (Figure 41c, Supplementary Figure 15). The potential of navitoclax and venetoclax was evaluated in pre-clinical cell lines and primary patient material of MED yielding promising results (71). This sample exhibited overexpression of BCL2L2 (BCL-w), a BCL2 family member, which suggests an increased sensitivity towards this group of drugs. Additionally, it showed sensitivity to the kinase inhibitor ceritinib. However, no available information could be found regarding the use of ceritinib specifically in the context of MED.

Samples I014_037_1M1_V1 and I115_008_1T2_V1 are both MED SHH samples but exhibited distinct sensitivity profiles without overlap (Figure 41c, Supplementary Figure 15). I014_037_1M1_V1_DS1 demonstrated sensitivity towards AMG-232, idasanutlin, selinexor and navitoclax indicating an in-class effect for the apoptotic modulators. Remarkably, this sample harbored a very high (priority score 1) PTEN mutation, which is not targetable but has been associated with resistance towards standard-of-care therapy and certain targeted treatments (72). Interestingly, this sample displayed the least sensitivity to all drug classes except for two conventional chemotherapy drugs.

Sample I115_008_1T2_V1 exhibited sensitivity towards nevitoclax and venetoclax and in lesser extent to one kinase inhibitor, ceritinib.

4.7.12 Rhabdoid tumor

There was only one RT sample in the cohort which showed resistance to 42% of the drugs (Figure 42a). Sensitivity was shown mainly for the kinase inhibitors (36%), conventional chemotherapeutics (29%) and apoptotic modulators (21%) (Figure 42b). Sample I036_028_1M1_V1 showed the highest sensitivity for sorafenib followed by temsorolimus and ribociclib (Figure 42c, Supplementary Figure 16). Additinally the sample showed sensitivity to three apoptotic modulators, idasanutlin selinexor and AMG-232. The molecular analysis did not offer an explanation for the drug sensitivity, suggesting the need to explore new targets within this diagnostic category.
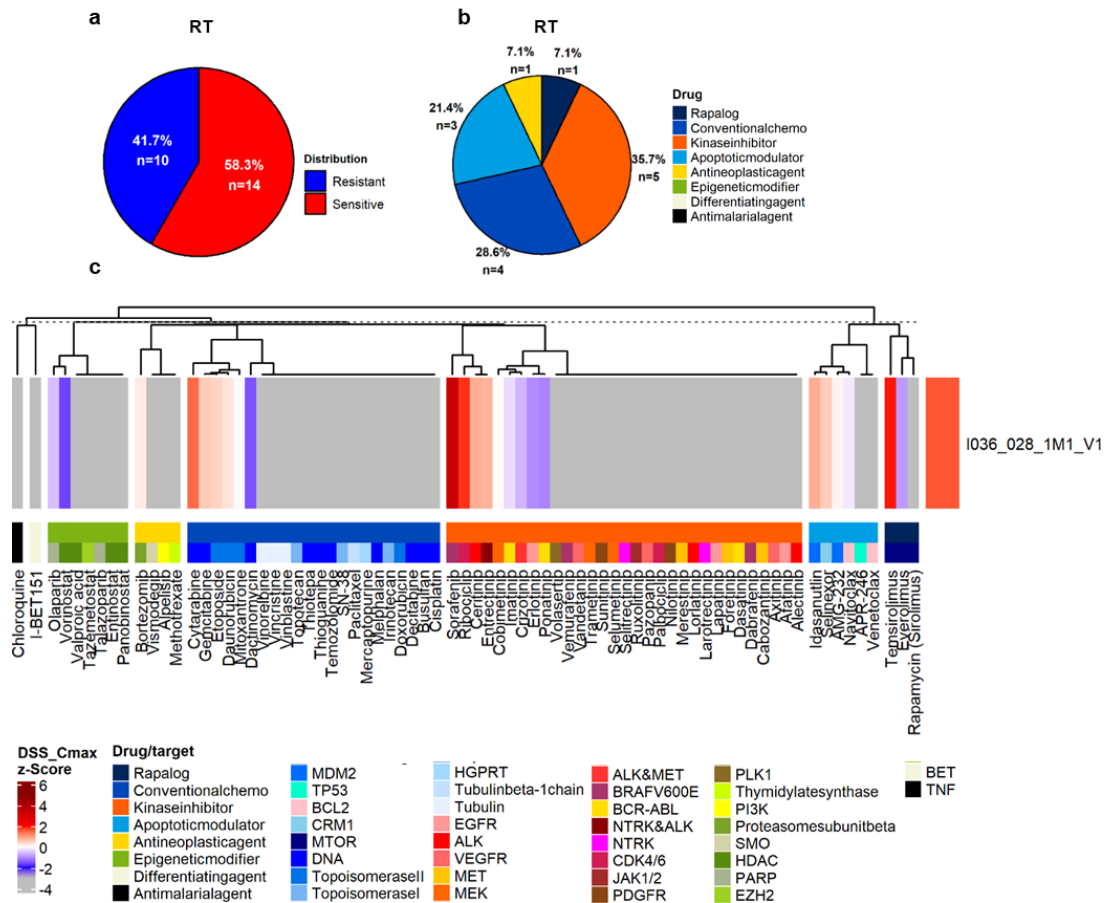
Figure 42. Summary of the rhabdoid tumor (RT) sample for the DSS Cmax z-score. (a) -Drug resistance and sensitivity trends for all patients and drugs. One observation represents one drug measurement for one sample. (b) - Drug distribution within the subset (14/24) of observations showing sensitivity (DSS Cmax z-score above 0.04). (c) - Overview of RT primary patient tumor sample (n=1) classified by drug class using the DSS Cmax z-score (cut off 0.04). Drugs with DSS Cmax z-score below -3 had a clinically unattainable concentration.

To sum up, when combining all samples within a diagnostic category along with their respective measured drugs, where each observation represented one measured drug of a given sample, the majority of diagnostic categories demonstrated resistance, accounting for approximately 61% to 76% of the observations. However NBL samples, reflected the lowest resistance rate at 37%, Wilms tumors at 53%, and MED tumors at 55% of the observations.

DSP provided valuable additional insights that served to either complement the outcomes from the NGS molecular analysis, adding new information and necessitating further investigation or aligned with the NGS molecular analysis confirming a sample's sensitivity or resistance characteristics.

In RMS, EWS, LGG, and NBL, several samples exhibited sensitivity to specific drugs without a clear indication from the NGS molecular analysis. For instance, within the ES cohort, sensitivity was observed to drugs like vemurafenib, alectinib, and volasertib. Among the LGG samples, both (n=2) samples displayed sensitivity to the rapalogs, whereas one exhibited sensitivity without any corresponding molecular alteration from the NGS analysis. Notably, in NBL, certain samples demonstrated sensitivity aligned with literature within NBL, despite lacking the molecular alterations commonly associated with such sensitivity as described in the respective existing literature.

In OSA, RMS, HGG, one sample of the rare tumors (congenital mesoblastic nephroma), NBL, MED and EPN a consistent alignment between DSP and the results of NGS molecular analysis were observed. For example, 5/9 samples in OSA showed resistance to most of the drugs which was corresponding to the NGS molecular analysis where several molecular alterations associated with resistance were found. In two HGG samples sensitivity towards the rapalogs was evident and one of the two samples additionally showed sensitivity towards pazopanib which all were associated with the molecular alteration of the samples provided by the NGS molecular analysis. Similarly, in the congenital mesoblastic nephroma sample, notable sensitivity to lapatinib (highest within the entire cohort) was observed. This sample harbored the EGFR:EGFR fusion which only occurred once within the entire cohort. In NBL two samples showed sensitivity to the PARP inhibitors which was also captured by the NGS molecular analysis. Moreover, in the MED samples sensitivity towards navitoclax and venetoclax aligned with what has been reported in literature. In EPN most samples were very resistant which is in line with the poor prognosis of relapsed cases withint this diagnostic category.

Within the group of other rare sarcoma samples (sarcoma_other) and Wilms tumors two compelling patient cases emerged, each involving the collection of two samples per patient case. The rare sarcoma samples procured during the same operation from the same tumor, yielded contrasting responses. Notably, the NGS molecular analysis highlighted a similarity in the high priority (priority score 2) alteration between the two samples. This DSP result underscores the potential influence of tumor heterogeneity within a single tumor when different samples are obtained.

The two Wilms tumor patient samples, originating from the same patient but from different metastatic sites yielded distinct outcomes. One sample exhibited slight sensitivity to selinexor, while the other remained fully resistant to all drugs.

4.8 DSS Cmax z-score distribution across diagnostic categories and its variation in different drug classes

After investigating the DSS Cmax z-score for each diagnostic category, the distribution of the score was compared across all diagnostic categories including all observations. Furthermore, the distribution was also investigated within the distinct drug classes to identify potential patterns across the diagnostic categories.

In terms of comparing the distribution of the DSS Cmax z-score across the different diagnostic categories including all observations, the widest distribution was identified in Wilms tumors with a range of -2.8 to 4.9 (difference (Δminimum-maximum): 7.7, median: -0.04). This trend was closely followed by the 'other' rare tumor group, exhibiting a range of 2.4 to 5.1 (difference: 7.5, median: -0.3), EWS with a range from -2.4 to 4.6, (difference: 7.1, median: -0.28) and NBL with a range of -2.3 to 4.4 (difference: 6.8, median: 0.56) as shown in Figure 43 and Supplementary Table 3.

Figure 43. DSS Cmax z-score distribution across the diagnostic categories. One dot represents one drug measurement for one sample. Red dot represents the mean.

It becomes apparent that while there are slight variations in the DSS Cmax z-score distribution among the different diagnostic categories, the overall distribution shape remains consistent. The EWS, EPN, OSA, RMS, HGG and LGG exhibited some outliers; however, the majority of observations (each representing a single drug measurement for one sample) were concentrated within the range of DSS Cmax z-scores from -1 to 0. Furthermore, no diagnostic category displayed a distinct separation from all the other categories.

When examining the DSS Cmax z-score distribution exclusively among the antineoplastic agents across the diagnostic categories the widest distribution was observed for RMS with a range of -2.3 to 3.3 (difference: 5.6, median: -0.50) as shown in Figure 44 and Supplementary Table 4. Following this the Wilms tumors displayed a range varying from -2.8 to 1.9 (difference: 4.7, median: -0.56). The remaining categories exhibited a consistent distribution shape with some outliers, however concentrating primarily within the range of DSS Cmax z-scores between -1 and 0. None of the diagnostic categories exhibited a distinct separation from the others.

Figure 44. DSS Cmax z-score distribution of the antineoplastic agents across the diagnostic categories. One dot represents one drug measured for one sample. Red dot represents the mean.

The same analysis was done for the apoptotic modulators revealing the widest distribution for the Wilms tumors ranging from -1.3 to 4.8 (difference: 6.1, median: 0.24) and NBL varying from -0.6 and 4.4 (difference: 5, median: 1.06) (Figure 45, Supplementary Table 5). Notably, the NBL, MED and MED SHH samples seemed to show a slight separation from the other categories with mean DSS Cmax z-scores of 1.09, 1.05 and 0.91. Conversely, the LGG samples also showed a slight separation displaying a distribution which was concentrated and centered on a mean DSS Cmax z-score of -1.04. In NBL and MED_SHH venetoclax was the highest outlier and selinexor the lowest.

Figure 45. DSS Cmax z-score distribution of the apoptotic modulators across the diagnostic categories. One dot represents one drug measurement for one sample. Red dot represents the mean.

For the conventional chemotherapeutics the distribution of the DSS Cmax z-score showed a wider distribution across all diagnostic categories as seen in Supplementary Table 6. The lowest difference was observed for RMS, with a difference of 2.8. The most pronounced distribution was displayed for OSA varying from -2.4 to 4.1 (difference: 6.4, median: -0.41) (Figure 46, Supplementary Table 6). This was followed by the distribution in Wilms tumors varying from -2.6 to 3.7 (difference: 6.2, median: 0.08). The MED sample showed a slight separatation from the other categories with a DSS Cmax z-score mean of 1.07. However, no clear pattern could be identified.

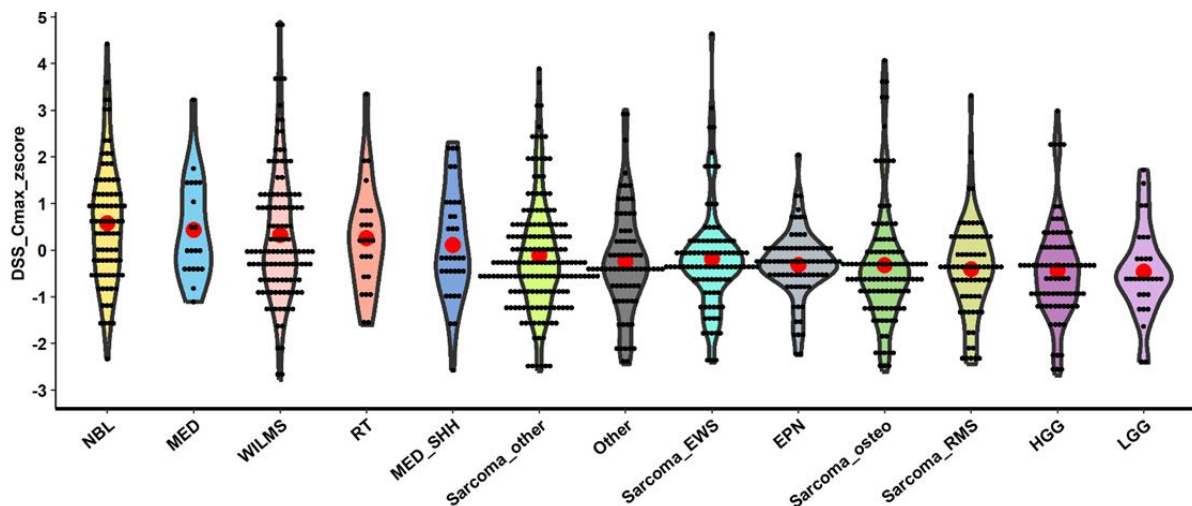Figure 46. DSS Cmax z-score distribution of the conventional chemotherapeutics across the diagnostic categories. One dot represents one drug measurement for one sample. Red dot represents the mean.

Within drug class epigenetic modifiers, the widest variability in distribution was identified for the Wilms tumors varying from -2.1 to 3.7 (difference: 5.9, median: -0.23), as well as the rare sarcoma tumor category (sarcoma_other) varying from -2.4 to 3.2 (difference: 5.5, median: -1.29) and NBL displaying a distribution range of -1.5 to 3.6 (difference: 5.1, median: 0.86) as shown in Figure 47 and Supplementary Table 7. For the sarcoma_other and Wilms category the distribution can be primarily attributed to the presence of outliers, while the majority of samples were concentrated at notably lower DSS Cmax z-scores. NBL was slightly separated from the remaining categories, evidenced by a mean DSS Cmax z-score of 0.8, while the remaining categories displayed mean values between 0 and -1.4. The outlier within the NBL category was observed for olaparib.
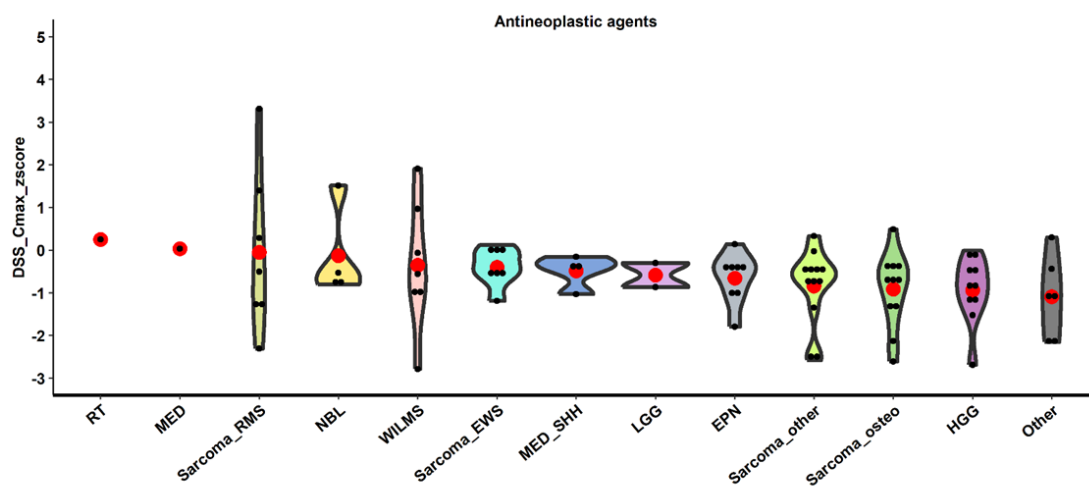

Figure 47. DSS Cmax z-score distribution of the epigenetic modifiers across the diagnostic categories. One dot represents one drug measurement for one sample. Red dot represents the mean.

The kinase inhibitors showed an exceptionally broad distribution in comparison to all other drug classes and diagnostic categories (Supplementary Table 8), particularly for the rare tumors group (other) with a DSS Cmax z-score range varying from -0.2 to 5.1 (difference: 7.2, median: -0.28). This was followed by the Wilms tumors with a distribution varying from -1.3 to 4.9 (difference: 6.2, median: -0.09) (Figure 48, Supplementary Table 8). While the majority of observations were centered around zero each diagnostic category exhibited distinct outliers with DSS Cmax z-score values of 2 and higher. Only MED SHH, MED, EPN, and LGG displayed concentrated observations around zero without pronounced high outliers. This was most striking in the case of the LGG category, while the other three categories had a single outlier each, albeit less prominent than those in the remaining categories.
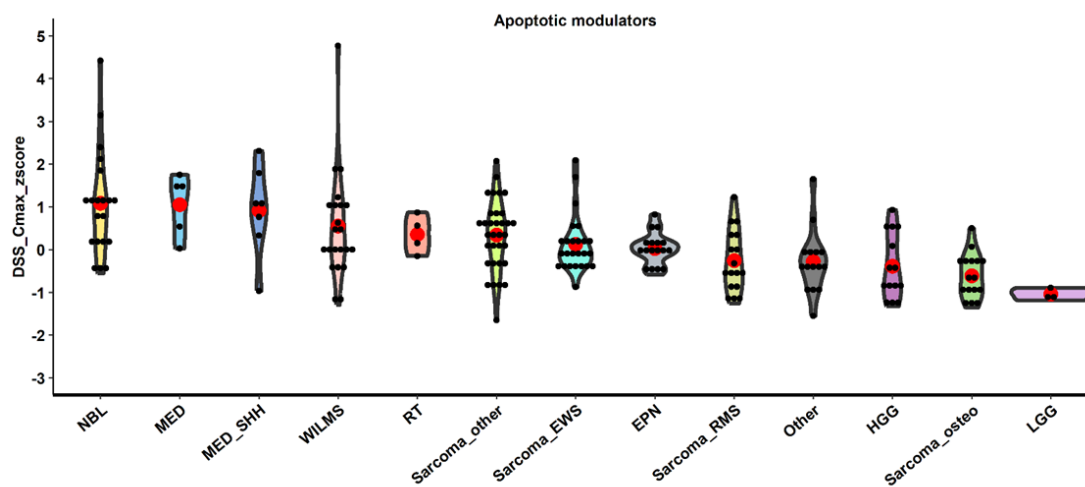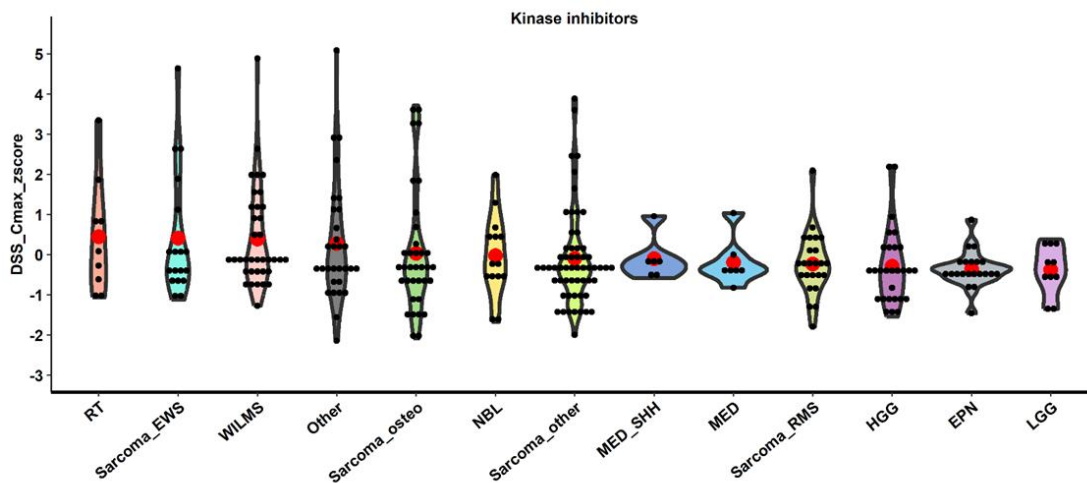

Figure 48. DSS Cmax z-score distribution of the kinase inhibitors across the diagnostic categories. One dot represents one drug measurement for one sample. Red dot represents the mean.

The only drug class that faced exclusion across entire diagnostic categories during the application of the DSS Cmax z-score filtering process were the rapalogs. This exclusion was a consequence of either a negative IC50 C5 or Cmax IC50 value or an IC50 which could not be determined. The diagnostic categories affected by this exclusion were NBL and MED (n=1). It's important to note that the rapalog group was smaller, comprised of three drugs, compared to the other larger drug classes. The broadest distribution was observed for HGG varying from 0.04 to 3 (difference: 2.95, median: 2.28) followed by the RT sample varying from -0.85 to 1.96 (difference: 2.81, median: 0.56) as shown in Figure 49 and Supplementary Table 9. A clear separation was observed for the HGG and LGG category, each with a DSS Cmax z-score mean value of 1.89 and 1.40 respectively, setting them apart from the other categories. The outlier in HGG was observed for temsirolimus while in LGG the highest DSS Cmax z-score was observed for everolimus.
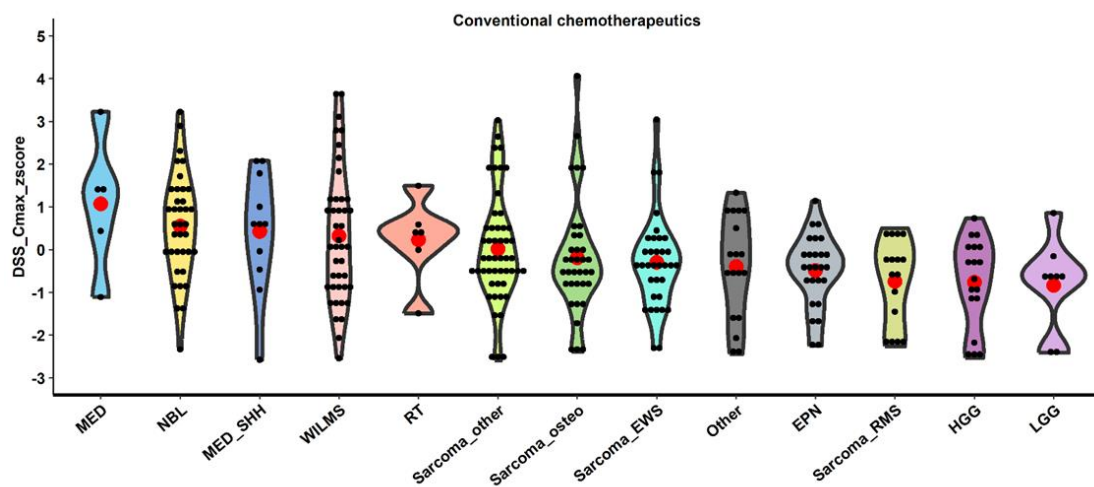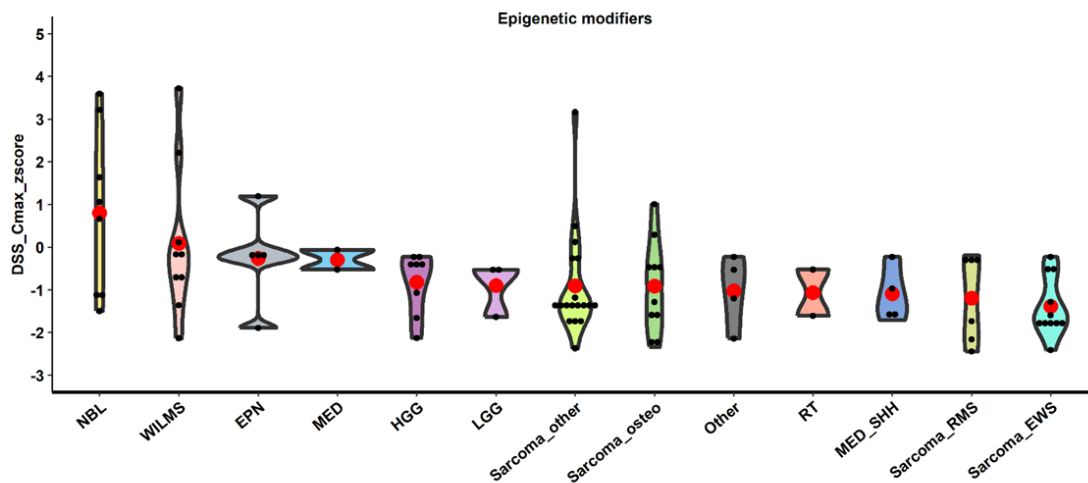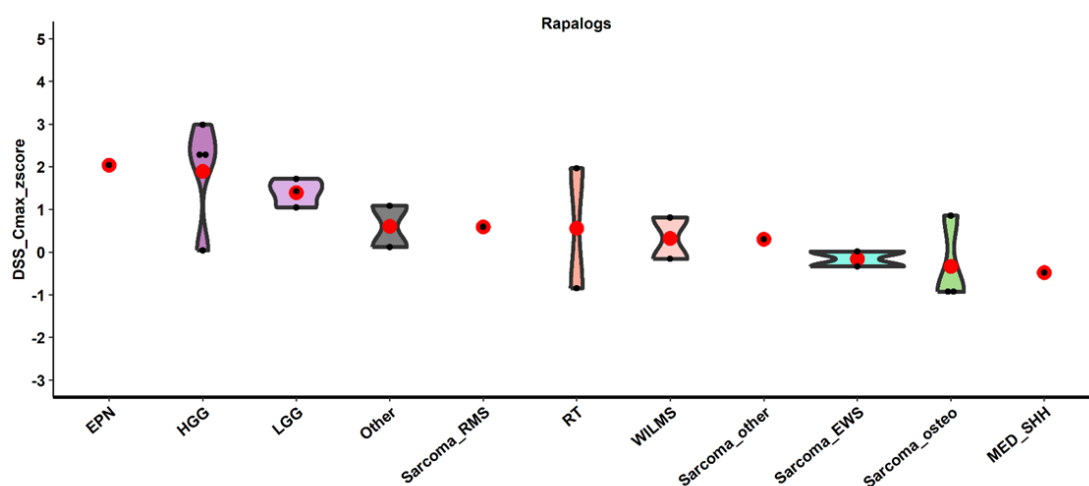

Figure 49. DSS Cmax z-score distribution of the rapalogs across the diagnostic categories. One dot represents one drug measurement for one sample. Red dot represents the mean.

For the majority of drug classes the distribution of the DSS Cmax z-score did not exhibit a pattern or a distinct separation across the diagnostic categories. However, slight differences were observed in the apoptotic modulators. Within this drug class the NBL, MED and MED SHH observations showed higher mean and median DSS Cmax z-score values compared to the other diagnostic categories, particularly in contrast to LGG which had the lowst mean and median values. Within the epigenetic modifiers, NBL showed a slight separation from the other diagnostic categories exhibiting the highest mean and median DSS Cmax z-score values. The most prominent separation between the diagnostic categories was observed within the rapalogs. Where HGG and LGG showed the highest mean and median DSS Cmax z-score values.

5 Discussion

Precision medicine driven only by genomics fails to identify high-evidence targets in 90% of patients which consequently leads to a lack in finding treatment options in most of the patient cases. To address this challenge, integration of approaches providing complementary information to genomics is essential to increase the accuracy of treatment prediction for all patients.

Therefore, in this study I aimed to improve the drug response prediction in high risk relapsed pediatric patients included in the INFORM study, by integrating functional drug screening parameters and pharmacological parameters in addition to the genomic information. By improving the drug respone prediction I intended to select effective treatments and ultimately improve patient outcomes, advancing the level of care provided to this population with dismal prognosis. To accomplish this, the DSS Cmax z-score, a novel DSP metric was developed that combines a functional drug screening parameter (DSS) with a pharmacological parameter (Cmax). This metric was investigated on five patient samples with a clinically proven drug target relationship (PPT subgroup I samples) by investigating if the patient treatment history was reflected in the DSP outcome. The metric was also applied on 68 patient samples without a clinically proven drug target match. In this cohort the outcome of applying the DSS Cmax z-score was only described, as information on the clinical outcome was not available.

5.1 Pharmacokinetic data base

I have selected nine PK parameters of 74 oncology drugs, focusing on the pediatric population (44). Pediatric data was available for 65% of the drugs (44). Adult data was reported for the remaining 35%. In general, pediatric PK parameters are comparable to adult PK parameters (44,73), except for children of three years of age or younger. This group of infants and young children accounts for approximately 3% of patients in phase I studies (44,74,75). In this age group the hepatic and renal functions are different from older children and adults, resulting in a different PK profile. In a study investigating 25 targeted drugs, it was revealed that the pediatric phase II dose (RP2D) ranged from 90 – 130% of the body surface area (BSA) adjusted adult dose, indicating that BSA-adjusted adult doses may approximate pediatric dosing within this given range. While it is clear that adult PK data cannot be converted into pediatric data in every and all age groups, for children of 3 years and above, the pediatric RP2D dose could be approximated from the adult PK profile especially in targeted therapy. Thus, by using adult PK data to estimate pediatric RP2D, the development of pediatric studies could be significantly accelerated (44).

The 'Guideline on the role of pharmacokinetics in the development of medicinal products in the pediatric population' as issued by the European Medicines Agency (EMA), underscores the importance of reporting specific pharmacokinetic parameters, namely AUC, Cmax, Cmin, Cl, T1/2, and PPB during clinical trials (44,76). However, there is a variability in the frequency to which these parameters are reported on in the literature. While the Cmax and AUC are commonly available for most drugs, the reporting of Ctrough and Css is less frequent (44). Nonetheless, these parameters, specifically Ctrough and Css, could play a crucial role in pre-clinical and translational studies. When combined with Cmax, Ctrough can establish a concentration range window, minimizing the risk of both over- and underestimations of a drug's therapeutic response. This combination also contributes to a decrease of false positives and false negatives within DSP experiments. Cmax, as a single PK parameter, can serve as an upper limit in experiments, preventing potential clinically not meaningful as well as off-target effects and pre-clinical administration of clinically unattainable drug concentrations. Among all the PK parameters, Css stands out as the parameter best reflecting a drug's concentration in patients undergoing continuous treatment (44).

With this pediatric PK database, I have successfully generated and published the first resource that summarizes pediatric PK data and physicochemical information for oncology drugs. My aim was to use the PK data for integration with PD data, while also providing a comprehensive database to the scientific community, which can help guide preclinical research towards a clinical approach that takes drug concentration into consideration at the outset. This data base serves as a valuable resource to help increase the success rate in pediatric drug development and drug repurposing pipelines.

5.2 Pharmacodynamic parameter DSS z-score performance in PPT samples with a defined drug target match

Upon investigating the best performing PD parameter, the data indicated that the DSS z-score performed best and effectively selected the matching drugs in PPT subgroup I samples, with a clinically proven drug target relationship. However the score was not able to fully reflect the patient's treatment history which was provided for 3/5 patients in subgroup I.

The DSS as originally published by Yadav et al. (26) has been applied in several adult studies as a metric to determine *ex vivo* drug response (27,77). None of these studies implemented pharmacokinetic parameters in the drug hit selection. Malani et al., prospectively investigated the DSS implementation in DSP on AML patients and found an objective response for 58% of the cases (27). Swords et al. applied an adapted form of the DSS on 12 adult AML patients

which were treated either according to DSP results or not. They showed that patients who were treated according to the DSP results showed significantly higher clinical responses compared to the group not treated according to DSP results.

The results of these two studies differ from my results, where the DSS z-score tested in a retrospective manner could not reflect the patient's treatment history fully in the three patient cases investigated. It is essential to acknowledge several differences such as sample size, DSS algorithm calculation, and the definition of a drug hit which could lead to the differences in outcomes between my study and that of Malani et al. (27) and Swords et al. (77).

In my study, I have used five patient samples (PPT subgroup I samples) with a clinically proven drug target-relationship, and retrospectively evaluated them based on treatment history which was available for 3/5 patients. Conversely, Malani et al. examined 37 AML patients and Swords et al. examined 12 AML patients prospectively evaluating objective response through an n=1 case study approach (27,77).

Furthermore, Malani et al. applied the DSS as originally published by Yadav et al., without integrating pharmacokinetic implementation or adapting the algorithm. Their assessment of DSS for drug hit selection involved a comparison with healthy bone marrow and peripheral blood tissue to test a drug's toxicity. Swords et al. slightly changed the Yadav algorithm but also applied the comparison to healthy bone marrow. To define the drug hit cutoff, Malani et al. used the 95th percentile of the DSS distribution across all drugs and all patient cases. Swords et al. did not use any additional hit selection step. In my study, I calculated the DSS using an in-house automated pipeline (29), based on the work of ElHarouni et al. (47). ElHarouni et al. reported that the DSS calculation was derived from the method of Yadav et al. with some modifications (47). However, they did not elaborate on the specific adaptations nor the specific use of DSS version (DSS1, DSS2, or DSS3) in their paper. The only difference they noted was the change from a 4P model initially used by Yadav et al. to a 5PL model (47). In this study I assessed the DSS and determined a drug hit by deriving z-scores to compare drug effectiveness across the entire database. I have not tested the outcome with any healthy controls. To determine a drug hit, I performed a ROC analysis using PCC models and applied the obtained cutoff on the PPT subgroup I samples. Each of these aspects could have caused the discrepancy in my results as compared to Malani et al. (27) and Swords et al.'s (77) findings.

Finally, when applying a prospective approach using the DSS in DSP and including a bigger sample size, it is reasonable to expect more reliable outcomes. Nevertheless, my approach offers additional value from a methodological background as it determines cutoff values based

on PCC models which are then applied on PPT samples. PCC models are homogenous and therefore, the determined cutoff based on the matched and non-matched drugs is expected to be higher compared to a heterogeneous sample mixture such as in the PPT samples (29). By making the PD parameter approach more rigorous in identifying drug hits in PPT samples, it should reduce the occurrence of false positives. This should prevent the administration of drugs to patients that might not have any treatment benefit while still exposing them to potential side effects. What all three studies concur on is the need for larger sample sizes and clinical trials to investigate the added benefit of DSP in clinical outcome prediction.

5.3 Pharmacodynamic pharmacokinetic parameter DSS Cmax z-score performance in PPT samples with a defined drug target match

I have integrated the pharmacokinetic parameter Cmax together with the best performing PD parameter DSS which resulted in the DSS Cmax z-score. When tested in PPT subgroup I samples (with a clinically proven drug target relationship), the score led to the exclusion of several drugs that, based on the experimental setup within this study, were potentially false positives, as they could not have been achieved at a clinically relevant dose in the patient. Additionally the DSS Cmax z-score was able to reflect the clinical treatment (prior to analysis) history in PPT subgroup I samples.

My findings are comparable with the results obtained by the TARGET (28) and INFORM (29)study. TARGET and INFORM obtained promising results in DSP outcomes when taking the Cmax as an additional parameter into account in predicting the drug response. It should be noted that different algorithms and hit filtering steps were applied compared to my approach. Although INFORM used a DSS-based approached, they adjusted the score by using healthy controls (bone marrow, non-malignant astrocytes and fibroblasts) and taking the drug's toxicity into account (29). TARGET used the AUC and IC50 to define drug hits. Initially, both studies looked at different pharmacodynamic parameters, however a common feature in PK implementation was the comparison of the IC50 with Cmax (28,29). Additionally, the retrospective approach and smaller sample size is also a common factor between my study and the TARGET and INFORM study. Both studies were able to retrospectively correlate the DSP findings with the clinical outcome in either 3 (INFORM) (29) or 4 (TARGET) (28) patient cases. It should be mentioned that compared to my study, these two studies had more detailed clinical information of the patients. In my study, the treatment history prior to study inclusion was only available for 3 patient cases.

What differentiates my approach from the TARGET and INFORM studies is that I focused on a single comprehensive parameter that informs about a patient's response and automatically excludes unattainable drugs from the final outcome. Although all three approaches apply different algorithms and their correlation of the clinical outcome to the DSP outcome is based on retrospective observation, the results could potentially indicate that the patient's clinical history can be reflected in a small sample size, regardless of the algorithm chosen when PK is integrated in the drug hit selection.

5.4 Description of DSS Cmax z-score in PPT samples without a defined drug target match

Application of the DSS Cmax z-score on patient samples without a defined drug target match nor patient treatment history information, resulted in the identification of at least one drug hit, in 83% (n=57/68) of patient samples. This result is similar to the TARGET study where drug hits were identified for 76% (n=13/17) of patients (28) and to the INFORM study where drug hits were identified for 72% (n=47/65) of the patients (29). Additionally, for 77% (53/68) of patients, the DSP metric DSS Cmax z-score found a hit where NGS did not identify a priority score 1 (very high) or priority score 2 (high) target, demonstrating an added benefit of DSP on top of the NGS guided information. Comparable findings were observed in the INFORM study where in 80% of cases, their DSP pipeline has shown added benefit next to the NGS information. Interestingly, all three studies have used different algorithms to identify drug hits, yet had approximately the same fraction of hits overall. What my study has in common with the TARGET and INFORM studies is the investigation of each drug over the entire patient cohort to define true outliers/drug hits. This was also previously reported by Fallahi et al. whom stated that AUC related parameters have indeed proven to be robust as response measures, when compared for one drug over the entire tested cohort (24). It is remarkable that by using different algorithms the DSP demonstrates the ability to detect drug hits even in the absence of high priority actionable targets identified by NGS. Whether the drug hits identified by DSP are truly effective in the patient remains to be seen as it still depends on the critical significance of clinical follow-up data to train the algorithms.

5.5   Limitations

This study has several limitations that need to be addressed in order to form the basis of improvement for future research.

Firstly, although I have included *ex vivo* data for 68 PPT samples, I did not have any clinical patient response data of these samples. The importance of clinical data outcomes in developing drug response prediction algorithms cannot be disregarded. In an attempt to gather the clinical outcome of patients included in the INFORM DSP pipeline, a clinical patient follow up was carried out by sending treating physicians a questionnaire enquiring about the clinical state of the patient and whether any of the DSP determined hits were applied clinically. Unfortunately, the response rate of physicians was relatively low and among the group that did respond, the DSP hits were not applied in clinical treatment for a variety of reasons. Without a clinical validation data set my approach to draw clear conclusions about the performance and most importantly, clinical benefit of this newly introduced PD-PK parameter DSS Cmax z-score was limited. Additionally, published data including clinical outcome details are not available, particularly those that publish their raw data in an experimental setting that aligns with my research methods. Thus, I have chosen to describe the outcome of DSS Cmax z-score application overall.

This highlights two key points, (I) the DSP outcomes can only be validated if these are implemented in a clinical trial setting including standardized outcome reporting, and (II) the importance of including raw data in publications so that other scientists in the field can use these to validate their own hypotheses and algorithms.

Secondly, *ex vivo* drug screening is in general more applicable for testing drug resistance rather than drug effectiveness in the patient. The reason for this is that despite applying pharmacokinetics and 3D cell culture models to mimic the clinical situation, the experiment involves a constant tumor cell-drug interaction for 72 hours and viability is tested at a single time point. If cells are considered resistant after such a constant drug exposure approach, there is a high chance that no effect will occur in the patient either. Especially because in the in patient situation numerous physiological factors influence the interaction between cells and drugs. Indeed, measuring effectiveness *ex vivo* can lead to overestimation of the effect, which may not translate accurately to clinical patient conditions. Although organs on a chip and microfluidic devices add the dynamic and PK aspects to the experiment as shown by Komen et al. (21), it currently remains time and cost intensive, making it impractical for systemic implementation in a clinical setting.

Thirdly, I have applied the ROC analysis on the entire drug library to determine the effectiveness and cutoff of the parameters investigated without an indication of the tumor cell content of the samples. Ideally the cutoff value should be determined for every drug class separately as the different drugs cannot be considered equal in their performance. The conventional chemotherapeutics are nonspecific and target dividing cells (healthy cells included), making them generally toxic. Targeted therapy however, targets cancer cells and/or specific molecular alterations in cells. This also underscores the significance of accurately determining or estimating the proportion of tumor cells within the sample. As drug classes have different mechanisms of action, treating them equally could lead to inaccurate representation of the drug effectiveness. Acknowledging this point, in my project, applying a drug class-based approach is challenging due to the limited sample size and the absence of clinical outcome information. Ideally assignment should be based on a large data set including clinical outcome information for each patient covering all drugs in the library.

In summary, the majority of limitations could be addressed for if clinical outcome information was available. Knowledge about the patient's clinical outcome allows for flexibility in assigning different weights to the parameters incorporated in DSP algorithms. Ultimately, this could significantly enhance the precision and adaptability of the approach.

6 Conclusion

The aim of my study was to integrate functional drug screening parameters together with pharmacological parameters and genomic information to improve the drug response prediction in high risk pediatric patients enrolled in the INFORM study. This aim was driven by four predefined objectives, which have been successfully achieved, either in their entirety or to a substantial degree given the available resources.

Objective 1. Building the distinct data bases nesccesary for this study

The PK data base was successfully generated for 74 oncology drugs and nine pharmacokinetic parameters focusing on the pediatric population. This data base served as the basis for selecting the Cmax as the primary PK parameter of interest in this study to be integrated with the best performing PD parameter from the functional screening. Additionally, this data base was published in the journal of Clinical Pharmacology & Therapeutics to serve as a valuable resource for the scientific community. Through publicly providing this data base to the community my aim was to facilitate the early integration of physiological conditions in pre-clinical research and increase the success rate of clinical translation.

The PD data base obtained from cell culture experiments on seven PCC models and 68 PPT samples was generated and data was successfully compiled in a processable manner to facilitate data analysis.

Objective 2. Analyzing the performance of PD parameters in the PCC models and PPT samples with a defined drug taget match.

Application of the ROC analysis on the PCC models, identified the DSS z-score as best performing PD parameter able to predict the matching drugs. The determined cutoff from the ROC analysis was implemented on the PPT subgroup I samples, with a defined drug target match. The DSS z-score could select the matching drugs however it could not fully capture the patient's clinical treatment history. Furthermore, the drugs that surpassed the cutoff and demonstrated potential efficacy, had an IC50 value higher than the Cmax. Thus, integrating PK parameter Cmax with PD parameter DSS in this study served as a promising filtering step to identify clinically attainable drug candidates.

Objective 3. Mathematical integration of the best performing PD parameter with the PK parameter of interest.

By mathematically combining the Cmax with the DSS, a novel drug response metric, the DSS Cmax z-score, was successfully obtained. The metric was applied on the PCC models to

access its predictive value and establish a cutoff value for application on the PPT subgroup I samples. Notably, DSS Cmax z-score successfully captured the patient's clinical treatment history and reduced the number of false positive drug hits, ensuring that only clinically attainable drugs at effective doses during the experiment were taken into account.

Objective 4. Application of the PD-PK parameter to the PPT without a defined drug target match.

Although obtaining the clinical follow up information of the PPT samples for validation of the DSS Cmax z-score in the patient cohort without a defined drug target match was not achieved, was able to effectively describe the outcomes of this metric within this patient cohort. For 83% of the patients at least one drug hit was identified by DSP. Furthermore, the DSS Cmax z-score successfully identified a drug hit for 77% (n=53/68) of patients, in cases where NGS did not identify a priority score 1 (very high) or priority score 2 (high) target, highlighting a clear benefit of DSP alongside NGS guided information. Additionally, within observations showing sensitivity the top five drugs most frequently identified as a drug hit were navitoclax, idasanutlin, cytarabine, daunorubicin, AMG-232, gemcitabine and selinexor where the latter three drugs shared a fifth place each. These drugs belong to two distinct drug classes: the apoptotic modulators and conventional chemotherapeutics.

The principal finding in this dissertation underscores that applying the DSS Cmax z-score is a promising approach to improve drug response prediction using a single metric, in heavily pre-treated, high risk, relapsed pediatric patients. However I have also shown that an unmet need lies in the availability of clinical follow up data to effectively train DSP algorithms and improve their predictive power. This is crucial to advance the DSS Cmax z-score and enable its application in prospective interventional clinical trials, unlocking its true clinical potential in providing patient tailored therapies from the bench to their bedside.

6.1 Future perspective

In precision oncology and translational research, it is essential to strike a balance between aspects involving different processes and stakeholders. While having highly accurate methods is of importance, it is equally important for these methods to be practical in the clinical setting, considering for it to be time and cost effective. Without taking this into consideration, the potential treatment might not reach the patients in the first place. The mean PFS of patients with aggressive tumors is approximately four months (1), which places substantial pressure on deciding on the next treatment option in a timely manner for this patient group with dismal prognosis. Though there are promising techniques like microfluidic devices which can mimic PK profiles and make the experiment more dynamic, their current limitation lies in high costs and low throughput in drug screening.

In conclusion, as clinical follow up data becomes more consistently available in the future, the focus should be placed on synergistically integrating several disciplines to mathematically model a combination of parameters. These parameter could include the tumor heterogeneity, the tumor microenvironment, tumor cell-drug pharmacodynamic parameters, physiochemical characteristics of drugs, pharmacokinetics of the drugs, genomics and DSP. *Ex vivo* drug response translation into a clinical efficacy, is complex and calls for collaboration of a multidisciplinary team composed of biologists, physicians, pharmacists, imaging experts, pharmacokinetic modeling experts, mathematicians and cell culture and *ex vivo* drug screening experts. Only in this way, we can advance our understanding and refine our strategies to improve patient outcomes.

7   Supplementary material

7.1   Supplementary figures
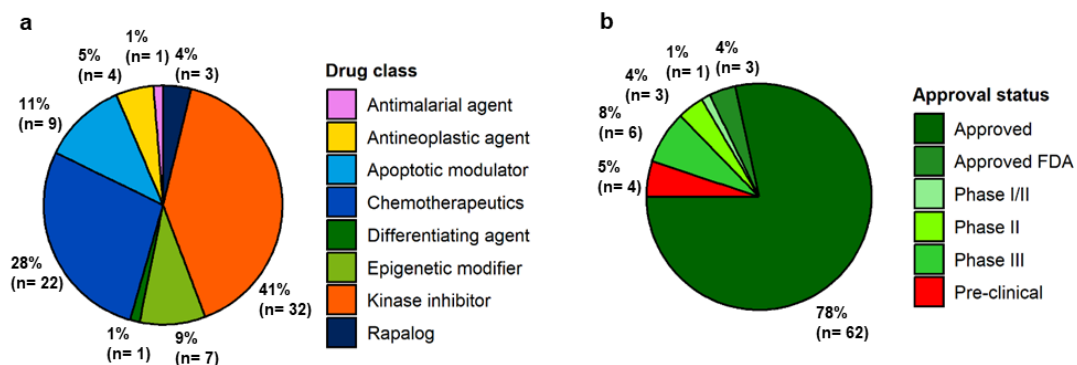
Supplementary Figure 1. INdividualized Therapy FOr Relapsed Malignancies in Childhood (INFORM) core drug library composition n=79 drugs. Overview of drug class (a) and overview of approval status (b). FDA: Food and Drug Administration. Originally published by Jamaladdin et al. (44).
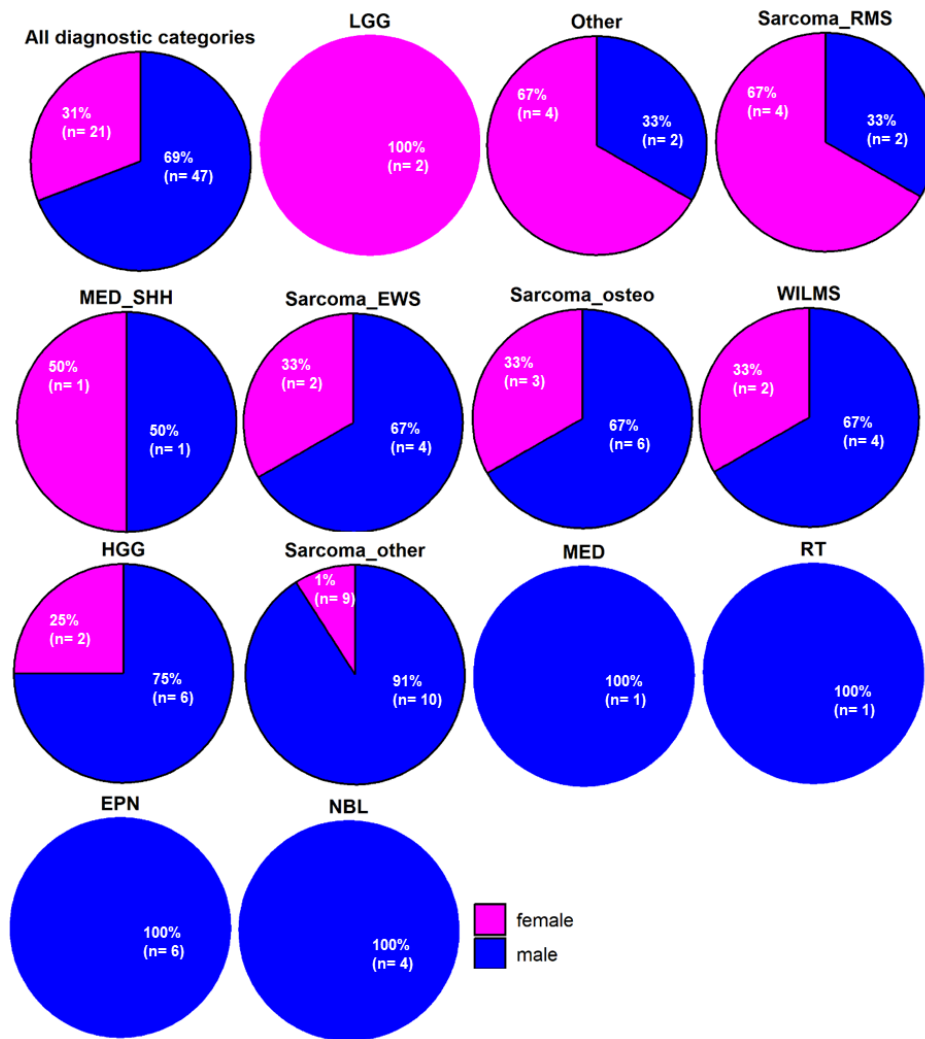
Supplementary Figure 2. Gender distribution (n=68) across all diagnostic categories and by specific diagnostic category.
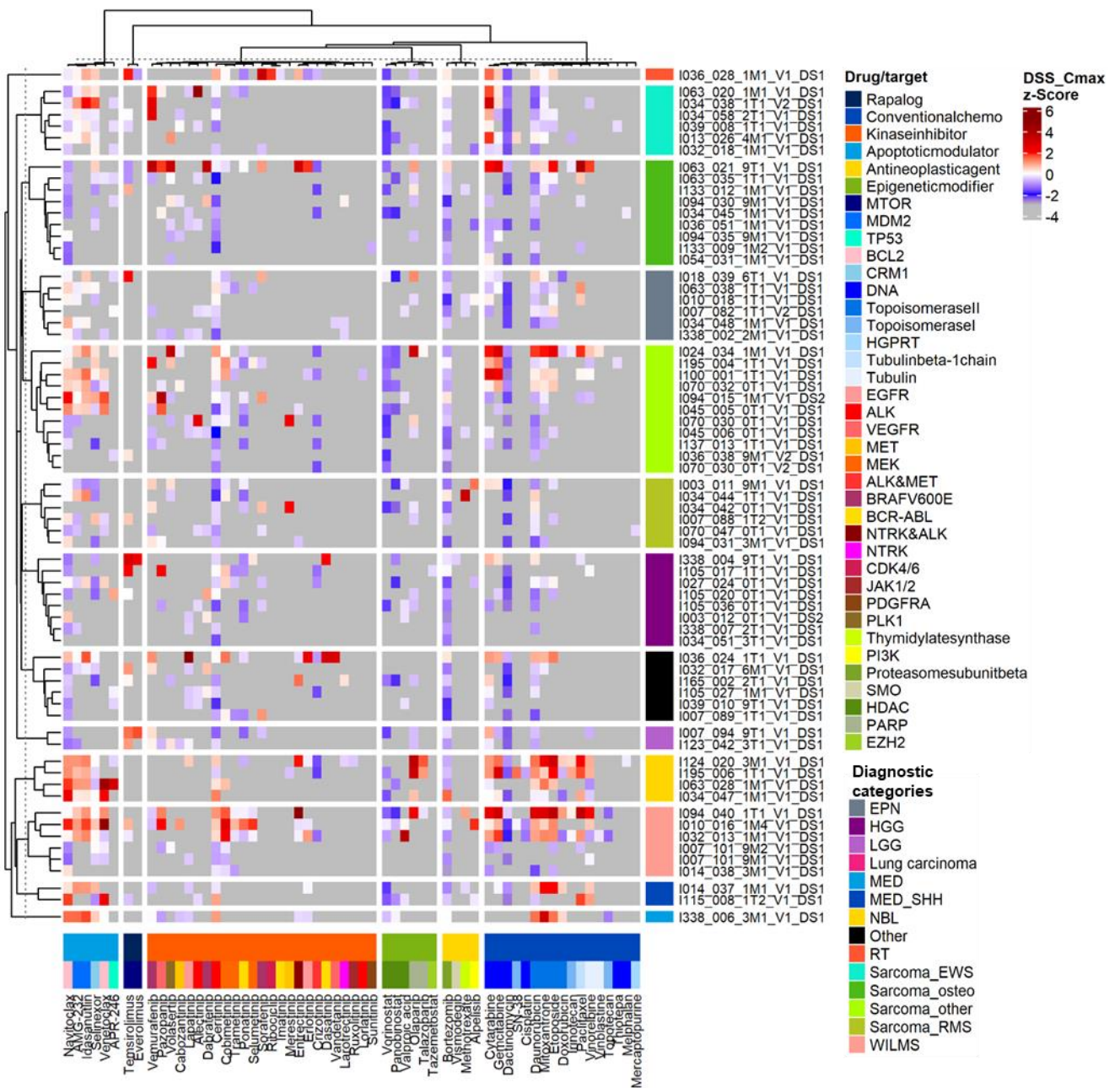
Supplementary Figure 3. Overview of all primary patient tumor samples (n=68) classified according to diagnostic categories and drug class using the DSS Cmax z-score (cut off 0.04). Drugs with DSS Cmax z-score below -3 had a clinically unattainable concentration.

PPT samples n=68
one observation represents one drug of one sample (n=991)

36.3%
n=360

63.7%
n=631

Distribution
■ Resistant
■ Sensitive
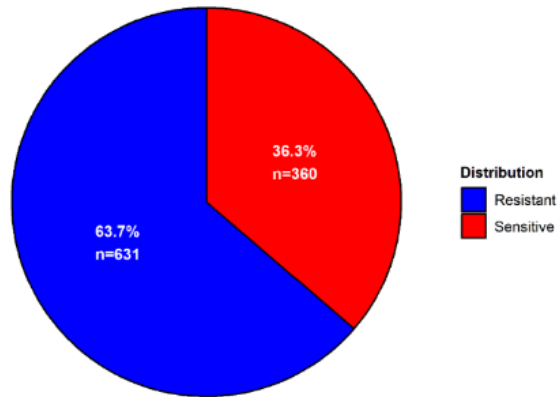
Supplementary Figure 4. Drug resistance and sensitivity trends within the primary patient tumor (PPT) samples (n=68) comprising 991 observations, where one observation represents one drug measurement for one sample. Sensitive is defined as a DSS Cmax z-score above 0.04
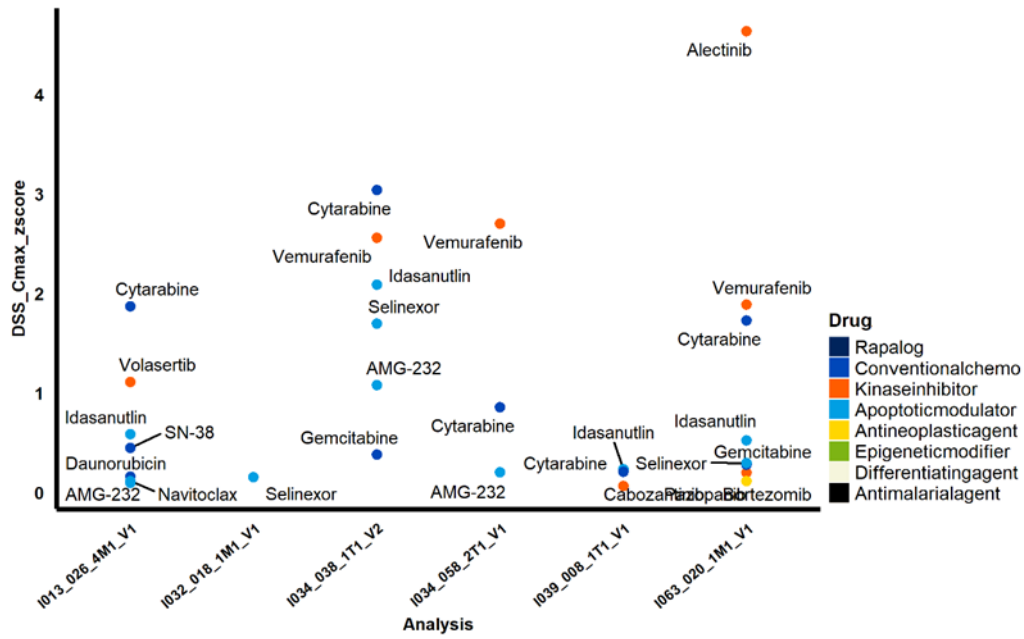
Supplementary Figure 5. Drug sensitivity (DSS Cmax z-score above 0.04) overview across the Ewing sarcoma (EWS) samples.
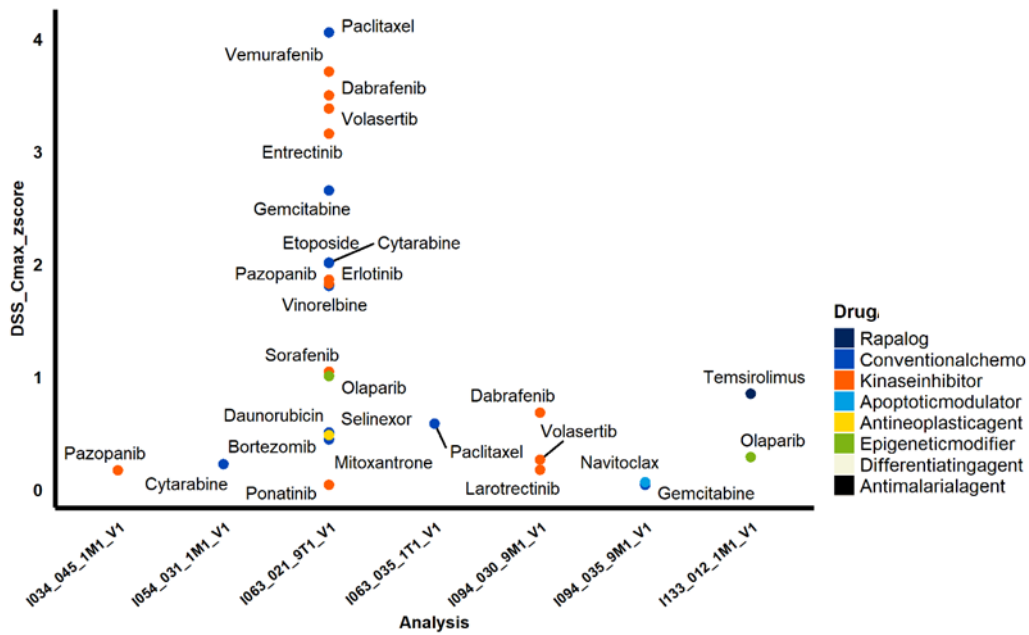
Supplementary Figure 6. Drug sensitivity (DSS Cmax z-score above 0.04) overview across the osteosarcoma (OSA) samples.
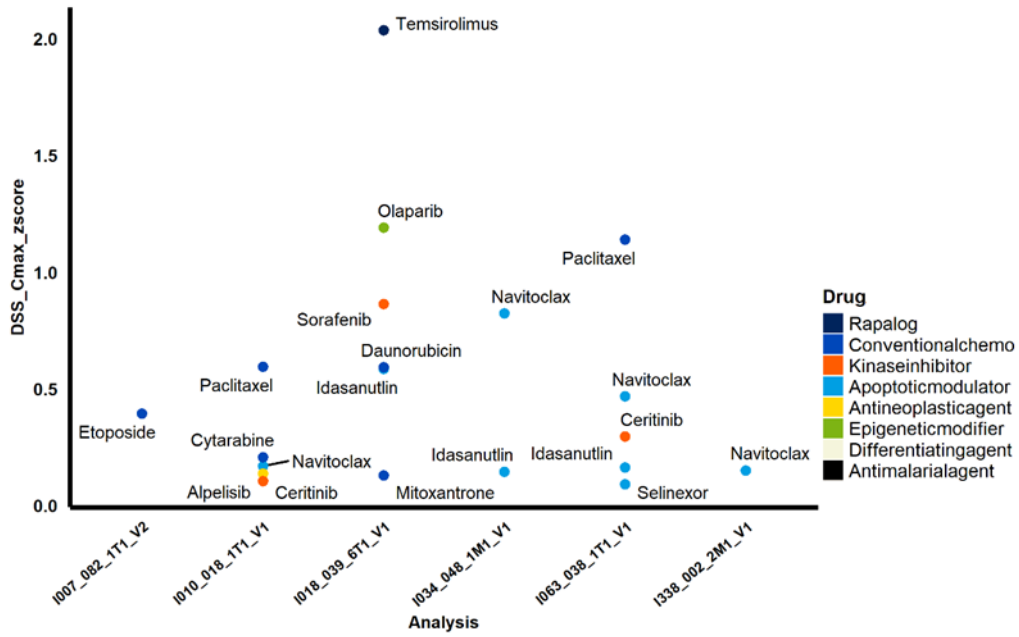
Supplementary Figure 7. Drug sensitivity (DSS Cmax z-score above 0.04) overview across the ependymoma (EPN) samples.
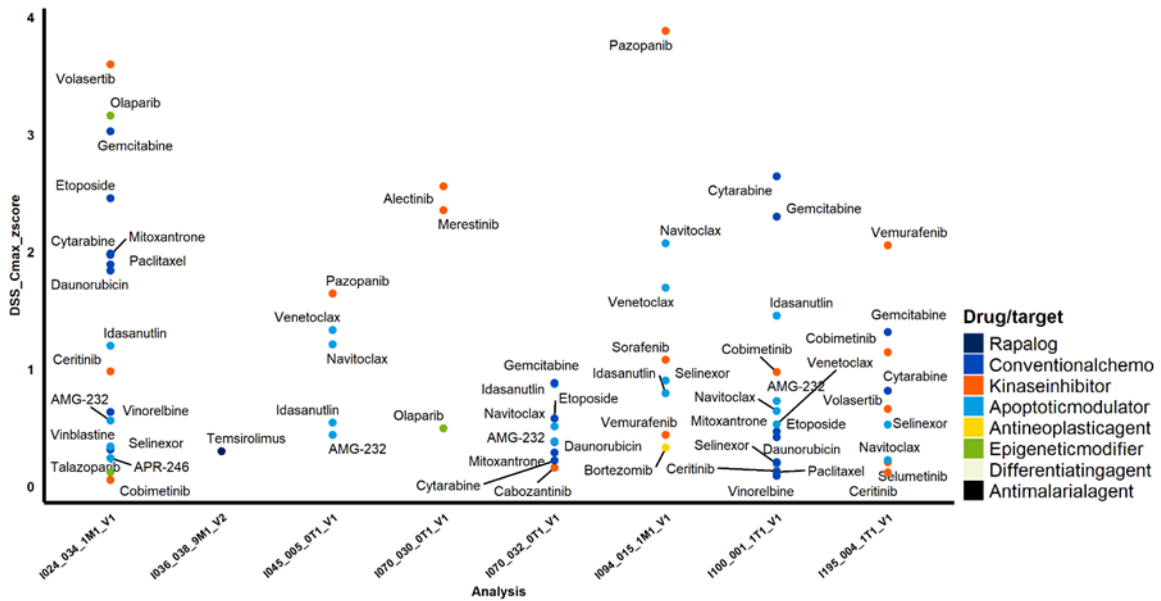
Supplementary Figure 8. Drug sensitivity (DSS Cmax z-score above 0.04) overview across the group of other sarcoma (Sarcoma_other) samples.
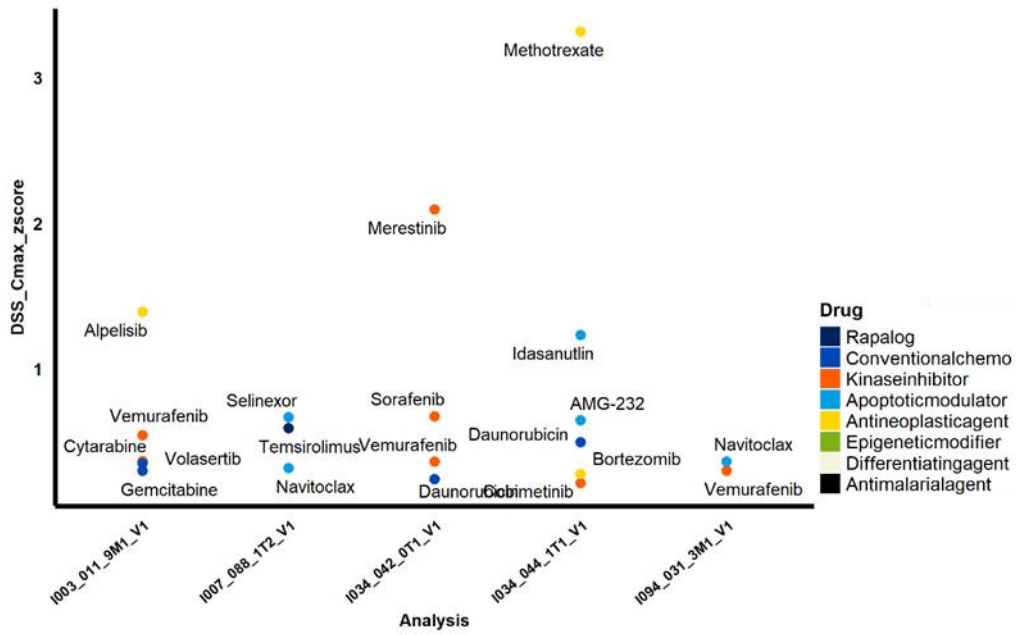
Supplementary Figure 9. Drug sensitivity (DSS Cmax z-score above 0.04) overview across the group of rhabdomyosarcoma (RMS) samples.
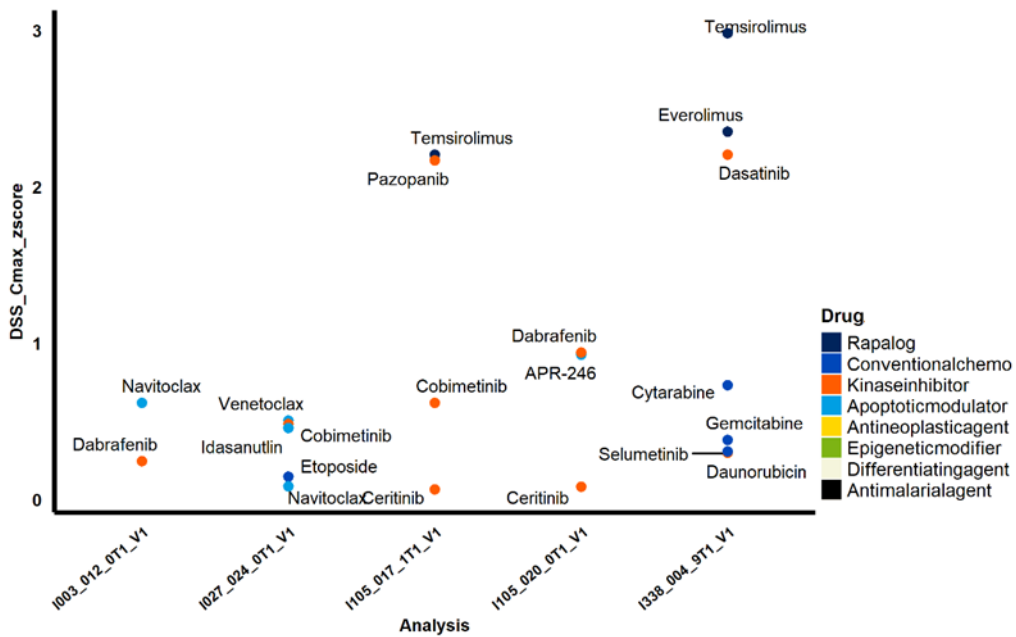
Supplementary Figure 10. Drug sensitivity (DSS Cmax z-score above 0.04) overview across the group of high grade glioma (HGG) samples.
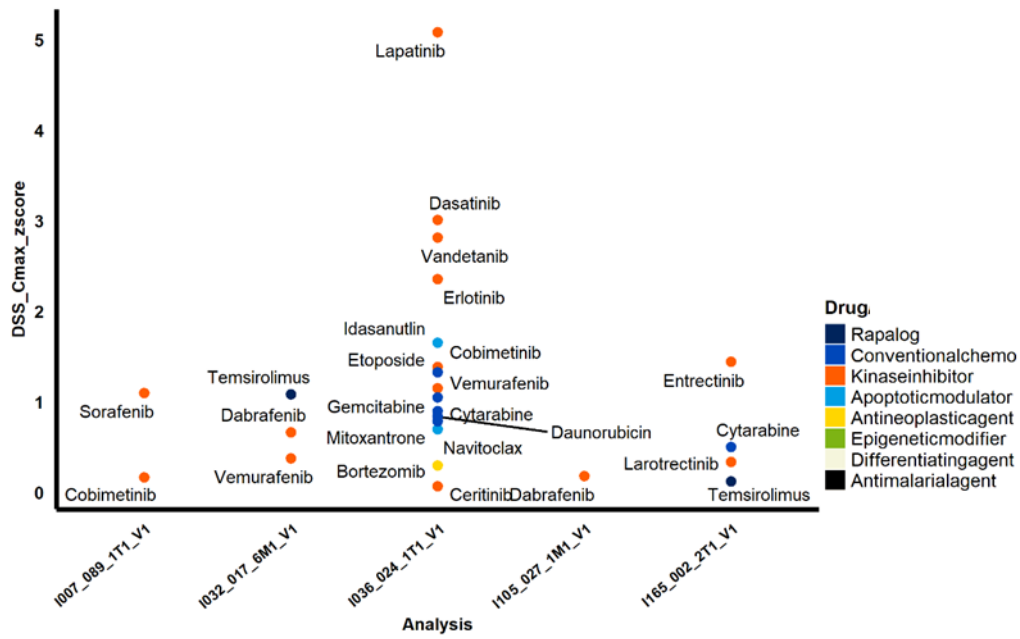
Supplementary Figure 11. Drug sensitivity (DSS Cmax z-score above 0.04) overview across the group of patients with several rare tumors (other).
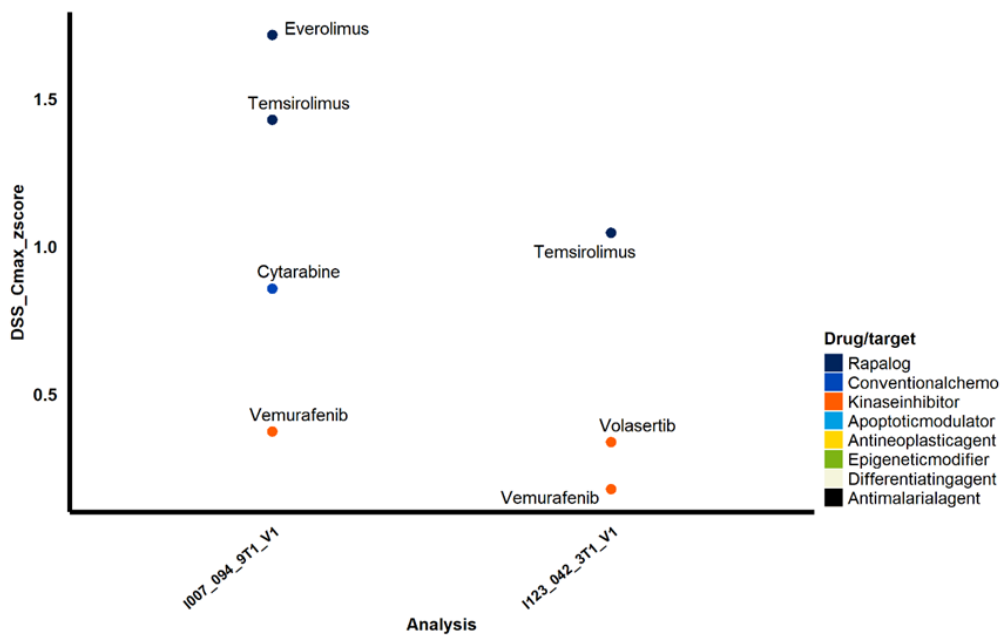
Supplementary Figure 12. Drug sensitivity (DSS Cmax z-score above 0.04) overview across the group of low grade glioma (LGG) samples.
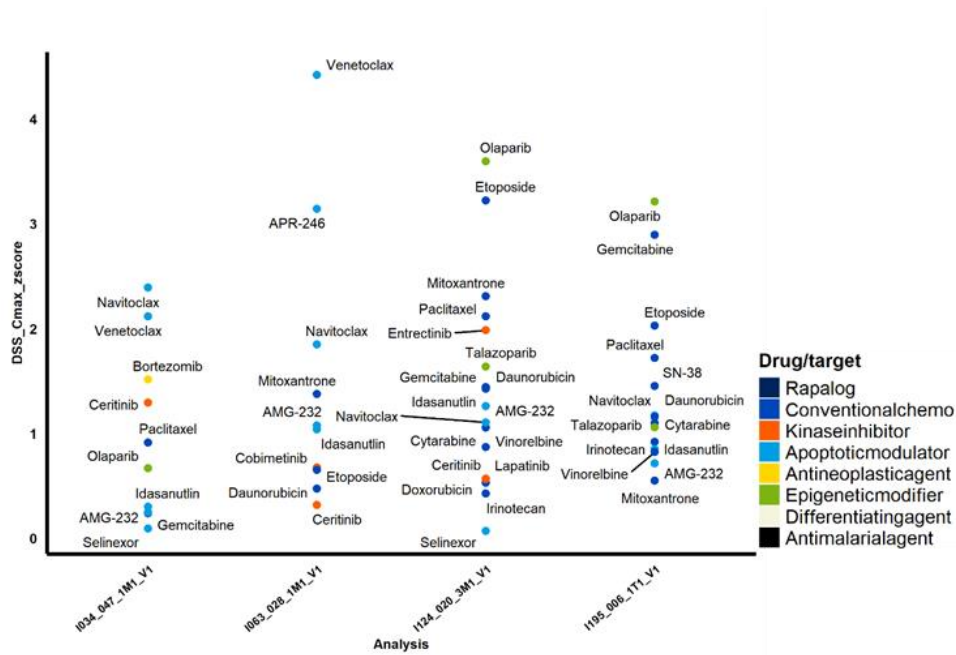
Supplementary Figure 13. Drug sensitivity (DSS Cmax z-score above 0.04) overview across the group of neuroblastoma (NBL) samples.
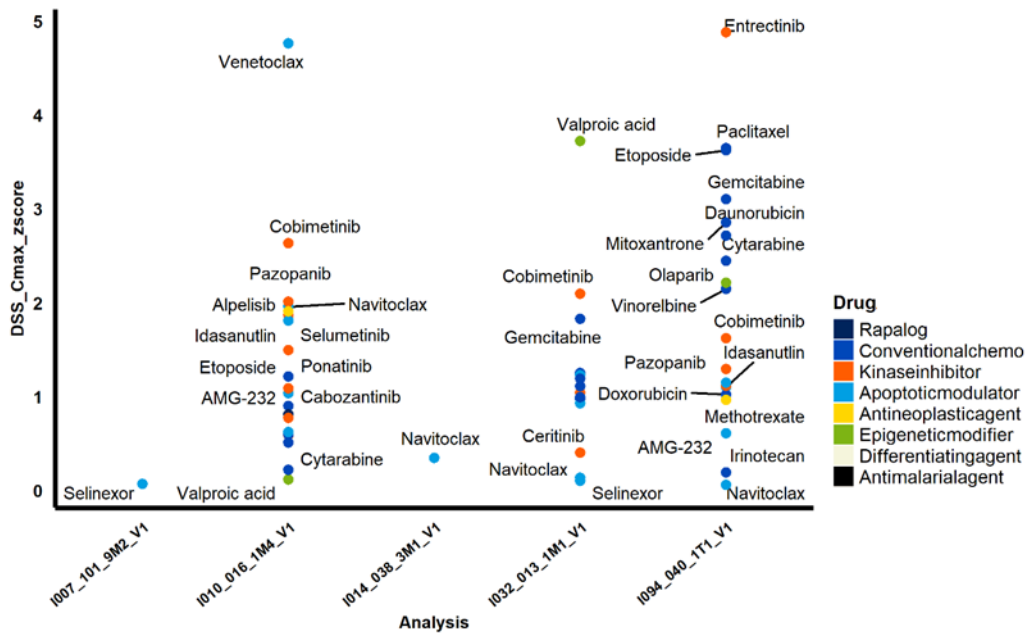
Supplementary Figure 14. Drug sensitivity (DSS Cmax z-score above 0.04) overview across the group of WILMS tumor samples.
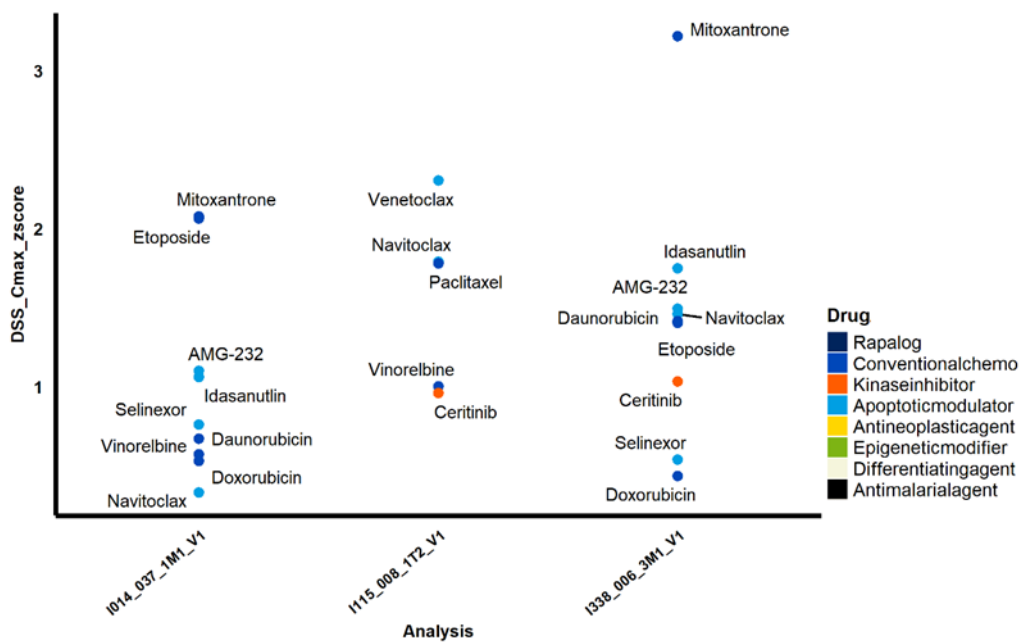
Supplementary Figure 15. Drug sensitivity (DSS Cmax z-score above 0.04) overview across the group of medulloblastoma (MED, I338_006_3M1_V1) and the sonic hedgehoc medulloblastoma (MED_SHH) samples.
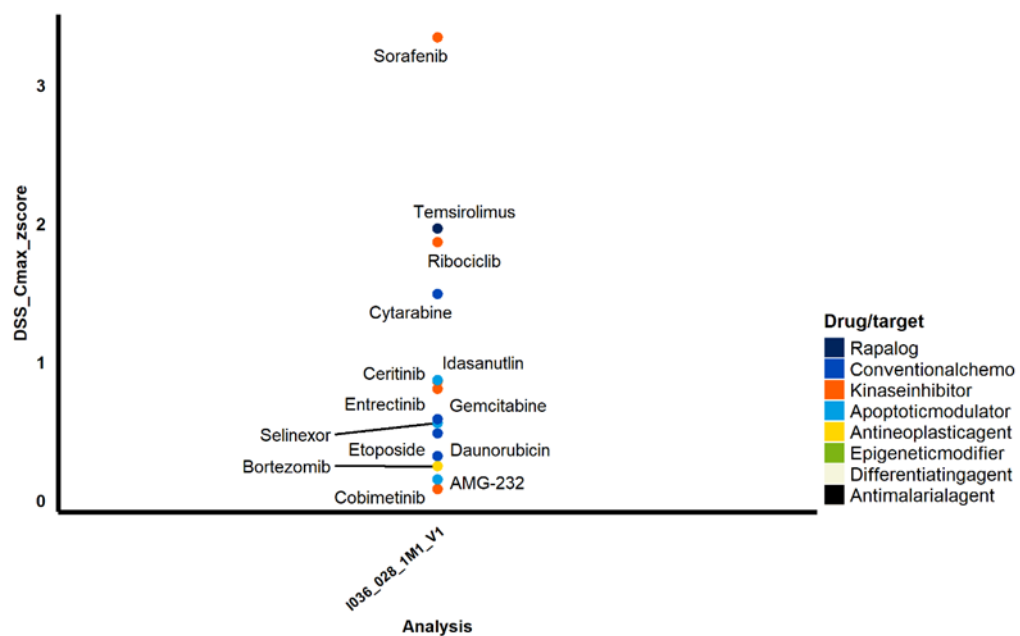
Supplementary Figure 16. Drug sensitivity (DSS Cmax z-score above 0.04) overview for the rhabdoid tumor (RT) sample.

PD Dr. Till Milde | KiTZ Heidelberg | INF 430 | D-69120 Heidelberg | Germany

Address

KiTZ
Hopp Children's Cancer Center
Heidelberg

German Cancer Research Center (DKFZ)
Heidelberg University Hospital
Heidelberg University

PD Dr. med. Till Milde
Head Targeted Therapies
Senior Pediatric Oncologist and
Hematologist
Group leader

Hopp Children's Cancer Center
Heidelberg (KiTZ)
Im Neuenheimer Feld 430
D-69120 Heidelberg
Germany

T: +49 6221 56-37429
t.milde@kitz-heidelberg.de
www.kitz-heidelberg.de

Heidelberg, MM DD, YYYY

INFORM DSP clinical follow-up questionnaire

Dear Dr. xxx

Thank you for sending the fresh vital tissue of INFORM patient IXXX_XXX to the Translational Drug Screening Unit (TDSU). The drug sensitivity profiling (DSP) for your patient has been successfully completed and was discussed during the INFORM board meeting on the DD of MM-YYYY. The DSP results showed that the tumor tissue of your patient was most sensitive to DRUG DRUG.

Up until now more than 50 patients have been screened successfully in the DSP pilot phase. We now aim at the systemic evaluation of these analyses in form of a clinical follow-up. In particular, we want to evaluate the translation of DSP results into clinical management of the patient.

We kindly ask you to fill out the attached short follow-up form. You can either fill it out in "Word" or print out and write on the hard-copy. Please return the Word-file or scan of the hard-copy by email, or the hard-copy by mail. All addresses are indicated on the questionnaire.

The data contributed by you will be used to improve the predictive value of the DSPs, improving therapeutic options for pediatric patients.

With the greatest thanks from the TDSU and INFORM teams,

PD Dr. Till Milde   Nora Jamaladdin   Prof. Dr. Olaf Witt

Directorate

Prof. Dr. med. Andreas Kulozik, PhD
Director Clinical Pediatric Oncology
Head of Department of Pediatric Oncology,
Hematology and Immunology,
Heidelberg University Hospital

Prof. Dr. med. Olaf Witt
Director Translational Pediatric Oncology
Head of Department, CCU Pediatric
Oncology,
German Cancer Research Center (DKFZ)
Head of KiTZ Clinical Trial Unit and Brain
Tumors, Department of Pediatric Oncology,
Hematology and Immunology
Heidelberg University Hospital

Prof. Dr. med. Stefan M. Pfister
Director Preclinical Pediatric Oncology
Division Head "Pediatric Neurooncology",
German Cancer Research Center (DKFZ)
Consultant Pediatric Oncologist,
Heidelberg University Hospital

Supplementary Figure 17. INFORM drug sensitivity profiling (DSP) clinical follow up letter template.

INFORM Drug sensitivity profiling (DSP)
Follow-up questionnaire

With this form our aim is to evaluate the patient follow-up information in a systematic manner. Thank you for your much-appreciated contribution.

To be filled out by INFORM/TDSU:

Patient ID: *I000-000*   **Date of Birth:** *yyyy*   **Diagnosis:**

Treating physician (TP):   **Phone nr. TP:**   **e-mail TP:**

Documentalist: **Phone nr. :**   **e-mail:**

Results DSP

Tumor board: Date: *yyyy-MM-dd*   **QC screen:**   **Drug hits:**

To be filled out by the treating physician:

1. **What anti-cancer drug treatment did the patient receive prior to the INFORM biopsy (consider only 3–6 months before biopsy)?**
   Please specify number and names of drug(s) (or name of chemotherapy protocol and block/cycle):

2. **Did you use the results from the INFORM DSP during clinical decision making?**
   ☐ Yes   ☐ No, please continue to **question 8**

If the answer to question 2 was 'no' please do <u>not</u> answer questions 3-7 and continue to question 8

3. **What drug treatment provided by the DSP did you apply?**
   Please specify number and names of drug(s):

4. **Duration of treatment based on DSP:**
   ☐ 0-1 month   ☐ 2-3 months   ☐ 4-6 months   ☐Other: months

5. **Reason for discontinuation of treatment based on DSP:**
   ☐ Toxicity   ☐ Tumor progression (clinical or by imaging)   ☐ Death   ☐ Complete remission
   ☐ Patient´s/guardian´s choice   ☐ other: _____

6. **Was the patient included in a clinical trial based on the DSP results?**
   ☐ No   ☐ Yes: Phase ☐I ☐II ☐I/II ☐III

   Name of trial if available: _____ NCT/EudraCT nr:: _____Name of drug(s) applied:_____

7. **What was the best response to the DSP based treatment according to local or reference radiology assessment?**
   ☐ SD (stable disease)   ☐ PD (Progressive disease)
   ☐ PR (partial response)   ☐ CR (complete response)   ☐ ND (not determined)

Drug Sensitivity Profiling – INFORM Patient Follow-Up
INFORM DSP FU form Version 1.0, from 2.3.2021

Supplementary Figure 18. INFORM drug sensitivity profiling (DSP) clinical follow up questionnaire (page 1).

8. **What was the reason for not using the DSP results? (multiple answers possible)**
   - ☐ Poor quality of the DSP screen
   - ☐ DSP is still in pilot phase
   - ☐ The results did not match the NGS results
   - ☐ Other treatment already initiated at time of DSP results information
   - ☐ Patient´s/guardian´s choice
   - ☐ Other reason, if possible please specify:

   Please return to:

   Scan by email: n.jamaladdin@kitz-heidelberg.de

   OR

   Hard-copy by mail:

   TDSU
   c/o Nora Jamaladdin
   CCU Pediatric Oncology B310
   German Cancer Research Center (DKFZ)
   Im Neuenheimer Feld 280
   69120 Heidelberg / Germany

   Thank you! – The INFORM-TDSU team

Drug Sensitivity Profiling – INFORM Patient Follow-Up
INFORM DSP FU form Version 1.0, from 2.3.2021

Supplementary Figure 19. INFORM drug sensitivity profiling (DSP) clinical follow up questionnaire (page 2).

7.2 Supplementary tables

Supplementary Table 1. Blood-Brain Barrier (BBB) Score calculated based on seven physiochemical properties of each drug molecule to predict the probability of BBB penetration. Score represents the chance of a molecule to be a central nervous system active molecule which would penetrate the BBB. Score: 0-2 (extremely low predictive chance to be CNS active), 2-3 (very low predictive chance to be CNS active), 3-4 (low predictive chance to be CNS active), 4-5 (intermediate predictive chance to be CNS active) and 5-6 (high predictive chance to be CNS active).

Generic name	BBB Score	Chance (%)
Afatinib	2.52	12.8
Alectinib	3.74	21.9
Alpelisib	2.29	12.8
AMG-232	3.32	21.9
APR-246	3.91	21.9
Axitinib	2.65	12.8
Bortezomib	1.82	0
Busulfan	2.6	12.8
Cabozantinib	1.99	0
Ceritinib	2.27	12.8
Chloroquine	5.51	90.3
Cisplatin	1.99	0
Cobimetinib	4.34	54.5
Crizotinib	3.65	21.9
Cytarabine	1.39	0
Dabrafenib	1.47	0
Dactinomycin	0.82	0
Dasatinib	1.73	0
Daunorubicin	1.39	0
Decitabine	1.29	0
Doxorubicin	1.35	0
Entinostat	2.03	12.8
Entrectinib	1.75	0

(Continued on the following page)

Generic name	BBB Score	Chance (%)
Erdafitinib	2.77	12.8
Erlotinib	3.25	21.9
Etoposide	1.27	0
Everolimus	0.34	0
Foretinib	1.04	0
Gemcitabine	1.84	0
Idasanutlin	2.49	12.8
Imatinib	1.9	0
Irinotecan	2.12	12.8
Lapatinib	1.73	0
Larotrectinib	2.19	12.8
Lorlatinib	2.61	12.8
Melphalan	4.41	54.5
Mercaptopurine	2.27	12.8
Merestinib	0.8	0
Methotrexate	1.31	0
Mitoxantrone	2.15	12.8
Navitoclax	1.31	0
Nilotinib	1.79	0
Olaparib	3.32	21.9
Paclitaxel	0.69	0
Palbociclib	2.17	12.8
Panobinostat	2.51	12.8
Pazopanib	0.99	0
Rapamycin (Sirolimus)	0.34	0
Ribociclib	2.58	12.8
Selumetinib	2.49	12.8
SN-38	2.44	12.8
Sorafenib	2.06	12.8

(Continued on the following page)

Generic name	BBB Score	Chance (%)
Sunitinib	3.21	21.9
Talazoparib	2.34	12.8
Tazemetostat	3.11	21.9
Temozolomide	2.22	12.8
Temsirolimus	0.34	0
Thioguanine	1.98	0
Thiotepa	3.84	21.9
Topotecan	2.74	12.8
Trametinib	2.47	12.8
Valproicacid	4.09	54.5
Vandetanib	4.26	54.5
Vemurafenib	2.35	12.8
Venetoclax	0.48	0
Vinblastine	1.19	0
Vincristine	1.19	0
Vinorelbine	1.19	0
Vismodegib	3.7	21.9
Volasertib	2.17	12.8
Vorinostat	2.72	12.8

Supplementary Table 2. Overview of the number of drugs excluded due to IC50, IC50 C5 distance and Cmax IC50 distance. C5: highest concentration measured, Cmax: maximum plasma concentration, neg: negative.

Analysis	Total nr drugs	PK missing	IC50 missing	IC50 – C5 negative	Cmax - IC50 negative	Matching drug excluded	Matching drug name	Reason
P1_KANK1:NTRK3							Larotrectinib	No IC50
	76	6/76	17/76	25/59	34/53	3/3	Entrectinib	IC50 – C5 neg
							Selitrectinib	No IC50 No Cmax
P2_BRAF mix							Trametinib	IC50 – C5 neg Cmax - IC50 neg
	76	6/76	37/76	16/39	29/33	5/5	Dabrafenib	No IC50
							Selumetinib	Cmax - IC50 neg
							Sorafenib	No IC50
							Vemurafenib	IC50 – C5 neg
P3_LRRFIP1:ALK							Alectinib	No IC50
	76	6/76	22/76	31/54	36/48	4/5	Lorlatinib	IC50 – C5 neg Cmax - IC50 neg
							Crizotinib	Cmax - IC50 neg
							Entrectinib	IC50 – C5 neg
P4_ALK R1275Q							Crizotinib	Cmax - IC50 neg
	76	6/76	31/76	9/45	22/39	4/5	Lorlatinib	No IC50
							Alectinib	IC50 – C5 neg
							Entrectinib	IC50 – C5 neg
P5_BRAF V600E							Trametinib	IC50 – C5 neg Cmax - IC50 neg
	76	6/76	11/76	24/65	41/53	4/5	Selumetinib	Cmax - IC50 neg
							Dabrafenib	IC50 – C5 neg
							Sorafenib	IC50 – C5 neg

Supplementary Table 3. DSS Cmax z-score distribution of all drug classes across the tumor diagnostic categories. The minimum, maximum, mean, median and difference (Δmin-max) of DSS Cmax z-score per diagnostic category. The data comprises all patient samples for each diagnostic category, with individual drug measurements combined.

Diagnostic category	Minimum	Maximum	Difference (Δmin-max)	Mean	Median
WILMS	-2.78	4.88	7.67	0.33	-0.04
Other	-2.45	5.08	7.53	-0.16	-0.30
Sarcoma_EWS	-2.42	4.64	7.05	-0.18	-0.28
NBL	-2.33	4.42	6.75	0.58	0.56
Sarcoma_osteo	-2.61	4.06	6.67	-0.32	-0.52
Sarcoma_other	-2.60	3.88	6.48	-0.11	-0.28
Sarcoma_RMS	-2.45	3.32	5.76	-0.40	-0.32
HGG	-2.69	2.98	5.67	-0.44	-0.44
RT	-1.61	3.34	4.95	0.25	0.20
MED_SHH	-2.57	2.30	4.88	0.11	-0.16
MED	-1.11	3.22	4.33	0.44	0.03
EPN	-2.25	2.04	4.28	-0.31	-0.31
LGG	-2.41	1.72	4.13	-0.46	-0.53

Supplementary Table 4. DSS Cmax z-score distribution of the antineoplastic agents across the tumor diagnostic categories. The minimum, maximum, mean, median and difference (Δmin-max) DSS Cmax z-score per diagnostic category. The data comprises all patient samples for each diagnostic category, with individual drug measurements combined.

Diagnostic category	Minimum	Maximum	Difference (Δmin-max)	Mean	Median
Sarcoma_RMS	-2.31	3.32	5.62	-0.05	-0.50
WILMS	-2.78	1.91	4.69	-0.36	-0.56
Sarcoma_osteo	-2.61	0.48	3.09	-0.92	-0.67
Sarcoma_other	-2.58	0.33	2.91	-0.84	-0.60
HGG	-2.69	-0.01	2.67	-0.94	-0.83
Other	-2.15	0.30	2.45	-1.09	-1.08
NBL	-0.80	1.51	2.32	-0.13	-0.61
EPN	-1.80	0.14	1.93	-0.66	-0.47
Sarcoma_EWS	-1.19	0.12	1.31	-0.40	-0.46
MED_SHH	-1.03	-0.16	0.87	-0.49	-0.38
LGG	-0.87	-0.30	0.57	-0.59	-0.59
MED	0.03	0.03	0.00	0.03	0.03
RT	0.25	0.25	0.00	0.25	0.25

Supplementary Table 5. DSS Cmax z-score distribution of the apoptotic modulators across the tumor diagnostic categories. The minimum, maximum, mean, median and difference (Δmin-max) DSS Cmax z-score per diagnostic category. The data comprises all patient samples for each diagnostic category, with individual drug measurements combined.

Diagnostic category	Minimum	Maximum	Difference (Δmin-max)	Mean	Median
WILMS	-1.29	4.76	6.06	0.55	0.24
NBL	-0.56	4.42	4.97	1.09	1.06
Sarcoma_other	-1.65	2.07	3.72	0.34	0.44
MED_SHH	-0.97	2.30	3.27	0.91	1.06
Other	-1.55	1.65	3.20	-0.28	-0.34
Sarcoma_EWS	-0.88	2.09	2.96	0.13	-0.05
Sarcoma_RMS	-1.26	1.23	2.49	-0.26	-0.43
HGG	-1.33	0.93	2.26	-0.39	-0.59
Sarcoma_osteo	-1.36	0.50	1.86	-0.61	-0.66
MED	0.02	1.75	1.73	1.05	1.46
EPN	-0.58	0.82	1.40	0.02	0.00
RT	-0.15	0.87	1.02	0.36	0.35
LGG	-1.19	-0.89	0.29	-1.04	-1.03

Supplementary Table 6. DSS Cmax z-score distribution of the conventional chemotherapeutics across the tumor diagnostic categories. The minimum, maximum, mean, median and difference (∆min-max) DSS Cmax z-score per diagnostic category. The data comprises all patient samples for each diagnostic category, with individual drug measurements combined.

Diagnostic category	Minimum	Maximum	Difference (∆min-max)	Mean	Median
Sarcoma_osteo	-2.38	4.06	6.44	-0.19	-0.41
WILMS	-2.55	3.65	6.19	0.32	0.08
Sarcoma_other	-2.60	3.03	5.62	0.02	-0.15
NBL	-2.33	3.22	5.56	0.55	0.55
Sarcoma_EWS	-2.31	3.04	5.35	-0.30	-0.31
MED_SHH	-2.57	2.08	4.65	0.42	0.57
MED	-1.11	3.22	4.33	1.07	1.40
Other	-2.45	1.33	3.77	-0.39	-0.30
EPN	-2.25	1.14	3.39	-0.49	-0.32
LGG	-2.41	0.86	3.27	-0.83	-0.66
HGG	-2.54	0.73	3.27	-0.76	-0.53
RT	-1.49	1.49	2.98	0.23	0.40
Sarcoma_RMS	-2.26	0.50	2.76	-0.74	-0.40

Supplementary Table 7. DSS Cmax z-score distribution of the epigenetic modifiers across the tumor diagnostic categories. The minimum, maximum, mean, median and difference (∆min-max) DSS Cmax z-score per diagnostic category. The data comprises all patient samples for each diagnostic category, with individual drug measurements combined.

Diagnostic category	Minimum	Maximum	Difference (∆min-max)	Mean	Median
WILMS	-2.14	3.72	5.86	0.09	-0.23
Sarcoma_other	-2.37	3.16	5.53	-0.91	-1.29
NBL	-1.50	3.60	5.09	0.80	0.86
Sarcoma_osteo	-2.34	1.01	3.35	-0.91	-0.91
EPN	-1.89	1.19	3.08	-0.26	-0.23
Sarcoma_RMS	-2.45	-0.20	2.25	-1.20	-1.07
Sarcoma_EWS	-2.42	-0.23	2.19	-1.38	-1.66
Other	-2.14	-0.23	1.91	-1.03	-0.87
HGG	-2.13	-0.23	1.90	-0.83	-0.49
MED_SHH	-1.71	-0.23	1.48	-1.09	-1.21
LGG	-1.63	-0.53	1.10	-0.90	-0.53
RT	-1.61	-0.53	1.08	-1.07	-1.07
MED	-0.53	-0.06	0.46	-0.30	-0.30

Supplementary Table 8. DSS Cmax z-score distribution of the kinase inhibitors across the tumor diagnostic categories. The minimum, maximum, mean, median and difference (Δmin-max) DSS Cmax z-score per diagnostic category. The data comprises all patient samples for each diagnostic category, with individual drug measurements combined.

Diagnostic category	Minimum	Maximum	Difference (Δmin-max)	Mean	Median
Other	-2.15	5.08	7.23	0.28	-0.28
WILMS	-1.27	4.88	6.16	0.39	-0.09
Sarcoma_other	-2.00	3.88	5.88	-0.10	-0.36
Sarcoma_osteo	-2.08	3.71	5.79	0.03	-0.30
Sarcoma_EWS	-1.13	4.64	5.76	0.41	-0.18
RT	-1.07	3.34	4.41	0.45	0.08
Sarcoma_RMS	-1.80	2.09	3.89	-0.23	-0.31
HGG	-1.55	2.21	3.75	-0.29	-0.41
NBL	-1.67	1.98	3.66	-0.02	-0.23
EPN	-1.46	0.86	2.33	-0.37	-0.35
MED	-0.82	1.03	1.86	-0.19	-0.32
LGG	-1.35	0.37	1.72	-0.38	-0.40
MED_SHH	-0.59	0.96	1.54	-0.10	-0.25

Supplementary Table 9. DSS Cmax z-score distribution of the rapalogs across the tumor diagnostic categories. The minimum, maximum, mean, median and difference (Δmin-max) DSS Cmax z-score per diagnostic category. The data comprises all patient samples for each diagnostic category, with individual drug measurements combined.

Diagnostic category	Minimum	Maximum	Difference (Δmin-max)	Mean	Median
HGG	0.04	2.98	2.95	1.89	2.28
RT	-0.85	1.96	2.81	0.56	0.56
Sarcoma_osteo	-0.94	0.85	1.79	-0.34	-0.92
WILMS	-0.16	0.81	0.97	0.32	0.32
Other	0.12	1.08	0.96	0.60	0.60
LGG	1.04	1.72	0.67	1.40	1.43
Sarcoma_EWS	-0.34	0.02	0.35	-0.16	-0.16
EPN	2.04	2.04	0.00	2.04	2.04
MED_SHH	-0.48	-0.48	0.00	-0.48	-0.48
Sarcoma_RMS	0.59	0.59	0.00	0.59	0.59
Sarcoma_other	0.30	0.30	0.00	0.30	0.30

8   References

1.   van Tilburg CM, Pfaff E, Pajtler KW, Langenberg KPS, Fiesel P, Jones BC, et al. The Pediatric Precision Oncology INFORM Registry: Clinical Outcome and Benefit for Patients with Very High-Evidence Targets. Cancer Discov. 2021 Nov;11(11):2764–79.

2.   O'Dwyer PJ, Gray RJ, Flaherty KT, Chen AP, Li S, Wang V, et al. The NCI-MATCH trial: lessons for precision oncology. Nat Med. 2023 Jun 15;29(6):1349–57.

3.   Napoli GC, Figg WD, Chau CH. Functional Drug Screening in the Era of Precision Medicine. Front Med (Lausanne). 2022;9:912641.

4.   Letai A. Functional precision cancer medicine-moving beyond pure genomics. Nat Med. 2017 Sep 8;23(9):1028–35.

5.   Allen CE, Laetsch TW, Mody R, Irwin MS, Lim MS, Adamson PC, et al. Target and Agent Prioritization for the Children's Oncology Group-National Cancer Institute Pediatric MATCH Trial. J Natl Cancer Inst. 2017 May 1;109(5).

6.   Wong M, Mayoh C, Lau LMS, Khuong-Quang DA, Pinese M, Kumar A, et al. Whole genome, transcriptome and methylome profiling enhances actionable target discovery in high-risk pediatric cancer. Nat Med. 2020 Feb;26(11):1742–53.

7.   Worst BC, van Tilburg CM, Balasubramanian GP, Fiesel P, Witt R, Freitag A, et al. Next-generation personalised medicine for high-risk paediatric cancer patients - The INFORM pilot study. Eur J Cancer. 2016 Sep;65:91–101.

8.   Lee J, Gillam L, Visvanathan K, Hansford JR, McCarthy MC. Clinical Utility of Precision Medicine in Pediatric Oncology: A Systematic Review. JCO Precis Oncol. 2021 Nov;(5):1088–102.

9.   Frismantas V, Dobay MP, Rinaldi A, Tchinda J, Dunn SH, Kunz J, et al. Ex vivo drug response profiling detects recurrent sensitivity patterns in drug-resistant acute lymphoblastic leukemia. Blood. 2017 Mar 16;129(11):e26–37.

10.   Pemovska T, Kontro M, Yadav B, Edgren H, Eldfors S, Szwajda A, et al. Individualized systems medicine strategy to tailor treatments for patients with chemorefractory acute myeloid leukemia. Cancer Discov. 2013 Dec;3(12):1416–29.

11.   WRIGHT JC, COBB JP, GUMPORT SL, GOLOMB FM, SAFADI D. Investigation of the relation between clinical and tissue-culture response to chemotherapeutic agents on human cancer. N Engl J Med. 1957 Dec 19;257(25):1207–11.

12.   van Renterghem AWJ, van de Haar J, Voest EE. Functional precision oncology using patient-derived assays: bridging genotype and phenotype. Nat Rev Clin Oncol. 2023 May;20(5):305–17.

13. Zanella ER, Grassi E, Trusolino L. Towards precision oncology with patient-derived xenografts. Nat Rev Clin Oncol. 2022 Nov;19(11):719–32.

14. Bingel C, Koeneke E, Ridinger J, Bittmann A, Sill M, Peterziel H, et al. Three-dimensional tumor cell growth stimulates autophagic flux and recapitulates chemotherapy resistance. Cell Death Dis. 2017 Aug 24;8(8):e3013.

15. Letai A, Bhola P, Welm AL. Functional precision oncology: Testing tumors with drugs to identify vulnerabilities and novel combinations. Cancer Cell. 2022 Jan 10;40(1):26–35.

16. Białkowska K, Komorowski P, Bryszewska M, Miłowska K. Spheroids as a Type of Three-Dimensional Cell Cultures-Examples of Methods of Preparation and the Most Important Application. Int J Mol Sci. 2020 Aug 28;21(17).

17. Sato T, Stange DE, Ferrante M, Vries RGJ, Van Es JH, Van den Brink S, et al. Long-term expansion of epithelial organoids from human colon, adenoma, adenocarcinoma, and Barrett's epithelium. Gastroenterology. 2011 Nov;141(5):1762–72.

18. Williams ST, Wells G, Conroy S, Gagg H, Allen R, Rominiyi O, et al. Precision oncology using ex vivo technology: a step towards individualised cancer care? Expert Rev Mol Med. 2022 Oct 3;24:e39.

19. Calandrini C, Schutgens F, Oka R, Margaritis T, Candelli T, Mathijsen L, et al. An organoid biobank for childhood kidney cancers that captures disease and tissue heterogeneity. Nat Commun. 2020 Mar 11;11(1):1310.

20. Verduin M, Hoeben A, De Ruysscher D, Vooijs M. Patient-Derived Cancer Organoids as Predictors of Treatment Response. Front Oncol. 2021;11:641980.

21. Komen J, Westerbeek EY, Kolkman RW, Roesthuis J, Lievens C, van den Berg A, et al. Controlled pharmacokinetic anti-cancer drug concentration profiles lead to growth inhibition of colorectal cancer cells in a microfluidic device. Lab Chip. 2020;20(17):3167–78.

22. Mazzocchi AR, Rajan SAP, Votanopoulos KI, Hall AR, Skardal A. In vitro patient-derived 3D mesothelioma tumor organoids facilitate patient-centric therapeutic screening. Sci Rep. 2018 Feb 13;8(1):2886.

23. Brooks EA, Galarza S, Gencoglu MF, Cornelison RC, Munson JM, Peyton SR. Applicability of drug response metrics for cancer studies using biomaterials. Philosophical Transactions of the Royal Society B: Biological Sciences. 2019 Aug 19;374(1779):20180226.

24. Fallahi-Sichani M, Honarnejad S, Heiser LM, Gray JW, Sorger PK. Metrics other than potency reveal systematic variation in responses to cancer drugs. Nat Chem Biol. 2013 Nov 8;9(11):708–14.

25. Hafner M, Niepel M, Sorger PK. Alternative drug sensitivity metrics improve preclinical cancer pharmacogenomics. Nat Biotechnol. 2017 Jun 7;35(6):500–2.

26. Yadav B, Pemovska T, Szwajda A, Kulesskiy E, Kontro M, Karjalainen R, et al. Quantitative scoring of differential drug sensitivity for individually optimized anticancer therapies. Sci Rep. 2014 Jun 5;4:5193.

27. Malani D, Kumar A, Brück O, Kontro M, Yadav B, Hellesøy M, et al. Implementing a Functional Precision Medicine Tumor Board for Acute Myeloid Leukemia. Cancer Discov. 2022 Feb;12(2):388–401.

28. Lau LMS, Mayoh C, Xie J, Barahona P, MacKenzie KL, Wong M, et al. In vitro and in vivo drug screens of tumor cells identify novel therapies for high-risk child cancer. EMBO Mol Med. 2022 Apr 7;14(4):e14608.

29. Peterziel H, Jamaladdin N, ElHarouni D, Gerloff XF, Herter S, Fiesel P, et al. Drug sensitivity profiling of 3D tumor tissue cultures in the pediatric precision oncology program INFORM. NPJ Precis Oncol. 2022 Dec 27;6(1):94.

30. Silva A, Silva MC, Sudalagunta P, Distler A, Jacobson T, Collins A, et al. An Ex Vivo Platform for the Prediction of Clinical Response in Multiple Myeloma. Cancer Res. 2017 Jun 15;77(12):3336–51.

31. Acanda De La Rocha AM, Fader M, Coats ER, Espinal PS, Berrios V, Saghira C, et al. Clinical Utility of Functional Precision Medicine in the Management of Recurrent/Relapsed Childhood Rhabdomyosarcoma. JCO Precis Oncol. 2021;5.

32. Mathonnet M, Vanderstraete M, Bounaix Morand du Puch C, Giraud S, Lautrette C, Ouaissi M, et al. ONCOGRAM: study protocol for the evaluation of therapeutic response and survival of metastatic colorectal cancer patients treated according to the guidelines of a chemosensitivity assay, the Oncogramme®. Trials. 2021 Aug 21;22(1):556.

33. Bounaix Morand du Puch C, Nouaille M, Giraud S, Labrunie A, Luce S, Preux PM, et al. Chemotherapy outcome predictive effectiveness by the Oncogramme: pilot trial on stage-IV colorectal cancer. J Transl Med. 2016 Dec 12;14(1):10.

34. LOHSE I, AZZAM DJ, AL-ALI H, VOLMAR CH, BROTHERS SP, INCE TA, et al. Ovarian Cancer Treatment Stratification Using *Ex Vivo* Drug Sensitivity Testing. Anticancer Res. 2019 Aug 31;39(8):4023–30.

35. Snijder B, Vladimer GI, Krall N, Miura K, Schmolke AS, Kornauth C, et al. Image-based ex-vivo drug screening for patients with aggressive haematological malignancies: interim results from a single-arm, open-label, pilot study. Lancet Haematol. 2017 Dec;4(12):e595–606.

36. Coffey DG, Cowan AJ, DeGraaff B, Martins TJ, Curley N, Green DJ, et al. High-Throughput Drug Screening and Multi-Omic Analysis to Guide Individualized Treatment for Multiple Myeloma. JCO Precis Oncol. 2021;5.

37. Shuford S, Lipinski L, Abad A, Smith AM, Rayner M, O'Donnell L, et al. Prospective prediction of clinical drug response in high-grade gliomas using an ex vivo 3D cell culture assay. Neurooncol Adv. 2021;3(1):vdab065.

38. Shuford S, Wilhelm C, Rayner M, Elrod A, Millard M, Mattingly C, et al. Prospective Validation of an Ex Vivo, Patient-Derived 3D Spheroid Model for Response Predictions in Newly Diagnosed Ovarian Cancer. Sci Rep. 2019 Aug 1;9(1):11153.

39. Jardim DL, Groves ES, Breitfeld PP, Kurzrock R. Factors associated with failure of oncology drugs in late-stage clinical development: A systematic review. Cancer Treat Rev. 2017 Jan;52:12–21.

40. Aldape K, Brindle KM, Chesler L, Chopra R, Gajjar A, Gilbert MR, et al. Challenges to curing primary brain tumours. Nat Rev Clin Oncol. 2019 Aug;16(8):509–20.

41. Vassal G, Houghton PJ, Pfister SM, Smith MA, Caron HN, Li XN, et al. International Consensus on Minimum Preclinical Testing Requirements for the Development of Innovative Therapies For Children and Adolescents with Cancer. Mol Cancer Ther. 2021 Aug;20(8):1462–8.

42. Grossman SA, Romo CG, Rudek MA, Supko J, Fisher J, Nabors LB, et al. Baseline requirements for novel agents being considered for phase II/III brain cancer efficacy trials: conclusions from the Adult Brain Tumor Consortium's first workshop on CNS drug delivery. Neuro Oncol. 2020 Oct 14;22(10):1422–4.

43. Begley CG, Ellis LM. Drug development: Raise standards for preclinical cancer research. Nature. 2012 Mar 28;483(7391):531–3.

44. Jamaladdin N, Sigaud R, Kocher D, Kolodziejczak AS, Nonnenbroich LF, Ecker J, et al. Key pharmacokinetic parameters of 74 pediatric anticancer drugs providing assistance in preclinical studies. Clin Pharmacol Ther. 2023 Jul 13;

45. Gupta M, Lee HJ, Barden CJ, Weaver DF. The Blood–Brain Barrier (BBB) Score. J Med Chem. 2019 Nov 14;62(21):9824–36.

46. Schmitt M, Pawlita M. High-throughput detection and multiplex identification of cell contaminations. Nucleic Acids Res. 2009 Oct;37(18):e119.

47. ElHarouni D, Berker Y, Peterziel H, Gopisetty A, Turunen L, Kreth S, et al. iTReX: Interactive exploration of mono- and combination therapy dose response profiling data. Pharmacol Res. 2022 Jan;175:105996.

48. Ahronian LG, Sennott EM, Van Allen EM, Wagle N, Kwak EL, Faris JE, et al. Clinical Acquired Resistance to RAF Inhibitor Combinations in BRAF-Mutant Colorectal Cancer through MAPK Pathway Alterations. Cancer Discov. 2015 Apr;5(4):358–67.

49. Zöllner SK, Amatruda JF, Bauer S, Collaud S, de Álava E, DuBois SG, et al. Ewing Sarcoma-Diagnosis, Treatment, Clinical Challenges and Future Perspectives. J Clin Med. 2021 Apr 14;10(8).

50. Hu Z, Wen S, Huo Z, Wang Q, Zhao J, Wang Z, et al. Current Status and Prospects of Targeted Therapy for Osteosarcoma. Cells. 2022 Nov 5;11(21).

51. Bowers DC, Rajaram V, Karajannis MA, Gardner SL, Su JMF, Baxter P, et al. Phase II study of everolimus for recurrent or progressive pediatric ependymoma. Neurooncol Adv. 2023;5(1):vdad011.

52. Adolph JE, Fleischhack G, Gaab C, Mikasch R, Mynarek M, Rutkowski S, et al. Systemic chemotherapy of pediatric recurrent ependymomas: results from the German HIT-REZ studies. J Neurooncol. 2021 Nov;155(2):193–202.

53. Han J, Yu M, Bai Y, Yu J, Jin F, Li C, et al. Elevated CXorf67 Expression in PFA Ependymomas Suppresses DNA Repair and Sensitizes to PARP Inhibitors. Cancer Cell. 2020 Dec 14;38(6):844-856.e7.

54. Weiss AR, Chen YL, Scharschmidt TJ, Chi YY, Tian J, Black JO, et al. Pathological response in children and adults with large unresected intermediate-grade or high-grade soft tissue sarcoma receiving preoperative chemoradiotherapy with or without pazopanib (ARST1321): a multicentre, randomised, open-label, phase 2 trial. Lancet Oncol. 2020 Aug;21(8):1110–22.

55. Arthur A, Gronthos S. Eph-Ephrin Signaling Mediates Cross-Talk Within the Bone Microenvironment. Front Cell Dev Biol. 2021 Feb 9;9.

56. Kiuru M, Busam KJ. The NF1 gene in tumor syndromes and melanoma. Lab Invest. 2017 Feb;97(2):146–57.

57. Guo J, Chaney KE, Choi K, Witek G, Patel A V, Xie H, et al. Polo-like kinase 1 as a therapeutic target for malignant peripheral nerve sheath tumors (MPNST) and schwannomas. Am J Cancer Res. 2020;10(3):856–69.

58. Sargos P, Sunyach MP, Ducassou A, Llacer C, Bellera CA, Michot A, et al. Preliminary results of a phase IB study of olaparib with concomitant radiotherapy in locally advanced/unresectable soft-tissue sarcoma from the French Sarcoma Group. Journal of Clinical Oncology. 2022 Jun 1;40(16_suppl):11522–11522.

59. Piazzi M, Bavelloni A, Cenni V, Salucci S, Bartoletti Stella A, Tomassini E, et al. Combined Treatment with PI3K Inhibitors BYL-719 and CAL-101 Is a Promising Antiproliferative Strategy in Human Rhabdomyosarcoma Cells. Molecules. 2022 Apr 24;27(9).

60. Hettmer S, Linardic CM, Kelsey A, Rudzinski ER, Vokuhl C, Selfe J, et al. Molecular testing of rhabdomyosarcoma in clinical trials to improve risk stratification and outcome: A consensus view from European paediatric Soft tissue sarcoma Study Group, Children's Oncology Group and Cooperative Weichteilsarkom-Studiengruppe. Eur J Cancer. 2022 Sep;172:367–86.

61. Pappo AS, Bowman LC, Furman WL, Rao BN, Kun LE, Jenkins JJ, et al. A phase II trial of high-dose methotrexate in previously untreated children and adolescents with high-risk unresectable or metastatic rhabdomyosarcoma. J Pediatr Hematol Oncol. 1997;19(5):438–42.

62. Mascarenhas L, Chi YY, Hingorani P, Anderson JR, Lyden ER, Rodeberg DA, et al. Randomized Phase II Trial of Bevacizumab or Temsirolimus in Combination With Chemotherapy for First Relapse Rhabdomyosarcoma: A Report From the Children's Oncology Group. J Clin Oncol. 2019 Nov 1;37(31):2866–74.

63. Murga-Zamalloa C, Rolland DCM, Polk A, Wolfe A, Dewar H, Chowdhury P, et al. Colony-Stimulating Factor 1 Receptor (CSF1R) Activates AKT/mTOR Signaling and Promotes T-Cell Lymphoma Viability. Clin Cancer Res. 2020 Feb 1;26(3):690–703.

64. Galanis E, Anderson SK, Twohy EL, Carrero XW, Dixon JG, Tran DD, et al. A phase 1 and randomized, placebo-controlled phase 2 trial of bevacizumab plus dasatinib in patients with recurrent glioblastoma: Alliance/North Central Cancer Treatment Group N0872. Cancer. 2019 Nov 1;125(21):3790–800.

65. Miklja Z, Yadav VN, Cartaxo RT, Siada R, Thomas CC, Cummings JR, et al. Everolimus improves the efficacy of dasatinib in PDGFRα-driven glioma. J Clin Invest. 2020 Oct 1;130(10):5313–25.

66. Cacchione A, Lodi M, Carai A, Miele E, Tartaglia M, Megaro G, et al. Upfront treatment with mTOR inhibitor everolimus in pediatric low-grade gliomas: A single-center experience. Int J Cancer. 2020 Dec 15;

67. King D, Li XD, Almeida GS, Kwok C, Gravells P, Harrison D, et al. MYCN expression induces replication stress and sensitivity to PARP inhibition in neuroblastoma. Oncotarget. 2020 Jun 9;11(23):2141–59.

68. Takagi M, Ogawa C, Iehara T, Aoki-Nogami Y, Ishibashi E, Imai M, et al. First phase 1 clinical study of olaparib in pediatric patients with refractory solid tumors. Cancer. 2022 Aug 1;128(15):2949–57.

69. Radic-Sarikas B, Halasz M, Huber KVM, Winter GE, Tsafou KP, Papamarkou T, et al. Lapatinib potentiates cytotoxicity of YM155 in neuroblastoma via inhibition of the ABCB1 efflux transporter. Sci Rep. 2017 Jun 8;7(1):3091.

70. Anderson B, Jasty-Rao R, Wu YM, Paul T, Robinson D, Mody RJ. Exceptional Response to Cabozantinib in a Patient With Multiply Relapsed Wilms Tumor. JCO Precis Oncol. 2018;2.

71. Westhoff MA, Schuler-Ortoli M, Zerrinius D, Hadzalic A, Schuster A, Strobel H, et al. Bcl-XL but Not Bcl-2 Is a Potential Target in Medulloblastoma Therapy. Pharmaceuticals (Basel). 2022 Jan 14;15(1).

72. Fischer T, Hartmann O, Reissland M, Prieto-Garcia C, Klann K, Pahor N, et al. PTEN mutant non-small cell lung cancer require ATM to suppress pro-apoptotic signalling and evade radiotherapy. Cell Biosci. 2022 Apr 27;12(1):50.

73. Paoletti X, Geoerger B, Doz F, Baruchel A, Lokiec F, Le Tourneau C. A comparative analysis of paediatric dose-finding trials of molecularly targeted agent with adults' trials. Eur J Cancer. 2013 Jul;49(10):2392–402.

74. Moreno L, Pearson ADJ, Paoletti X, Jimenez I, Geoerger B, Kearns PR, et al. Early phase clinical trials of anticancer agents in children and adolescents - an ITCC perspective. Nat Rev Clin Oncol. 2017 Aug;14(8):497–507.

75. Kearns GL, Abdel-Rahman SM, Alander SW, Blowey DL, Leeder JS, Kauffman RE. Developmental pharmacology--drug disposition, action, and therapy in infants and children. N Engl J Med. 2003 Sep 18;349(12):1157–67.

76. CHMP. Guideline on the guideline on the role of pharmacokinetics in the development of medicinal products in the pediatric population [Internet]. 2006 [cited 2023 Jan 4]. Available from: https://www.ema.europa.eu/en/documents/scientific-guideline/guideline-role-pharmacokinetics-development-medicinal-products-paediatric-population_en.pdf

77. Swords RT, Azzam D, Al-Ali H, Lohse I, Volmar CH, Watts JM, et al. Ex-vivo sensitivity profiling to guide clinical decision making in acute myeloid leukemia: A pilot study. Leuk Res. 2018 Jan;64:34–41.